5-3-2017

Investigating Differences in the Biomechanics of Goal Directed Movements of the Upper Extremity

Tanimu Deleon-Nwaha
tanimu.deleon-nwaha@uconn.edu

Investigating Differences in the Biomechanics of

Goal Directed Movements of the Upper Extremity

Tanimu Deleon-Nwaha, PhD

University of Connecticut, 2017

The Office of Naval Research (ONR) is interested in studying the biomechanics of upper extremity movement in a non-sea state environment. In this work, efforts to understand goal directed motor movement efficiency in the context of human performance is vital in modeling and predicting potential outcomes to shipboard naval damage control procedures, which becomes of particular importance with the introduction of women (who are of smaller anthropometries) on maritime vessels. This dissertation directly supports this Navy initiative and provides further insight into measuring goal directed end-effector (i.e., fingertip) biomechanics from an anthropometric perspective. The two objectives of this dissertation were to: 1) create a simple technique to quantify biomechanical information in an upper extremity goal directed movement task, and 2) validate the technique by assessing upper extremity movement patterns of right-hand dominant participants with respect to anthropometry. These objectives were accomplished by focusing on the kinematic analyses of study participants executing a goal-directed touching task on a touch-sensitive flat screen monitor. Upper extremity movements were measured, in-addition to, surface electromyography, and postural adjustments as a result of displacements in center of gravity (CoG). Additionally, the measurement technique in this dissertation uses motor control and anthropometric adaptation through learning as a means to exploit movement efficiency in performing a simple closed loop goal directed end-effector movement in an open and constrained space.

The results for 10 subjects show little variation in terminal touch points on the touchscreen; however, clear differences in angular displacement statistics were observed between subjects with anthropometric measurements greater than the 50^{th} percentile male and those less than the 50^{th} percentile male. Additionally, when participants were separated by gender, there were statistical differences between the genders in the open and constrained scenario performance across: kinematics, MVC, power spectral density, and total CoG displacement. As a result, design integration cannot be based on one singular dimension, which is commonly stature. The consideration needs to be based on the multi-dimensionality of the human physique. In the case of a goal directed pointing movement, arm length and shoulder breadth, in addition to stature, should be considered.

The true benefit of this method is that it can be ported to a maritime vessel and in-situ sea-state analysis can be conducted to compare and contrast the biomechanical adaptations that may occur. Results from this dissertation, coupled with the ONR research, will directly support a broader ONR initiative known as STAMPS (i.e., Simulation Toolset for Analysis of Mission, Personnel & Systems). The overarching goal of STAMPS is to simulate the major design of Naval vessels and the associated manpower and related cost variables, in order to model and optimize the trade spaces and human performance in platform design. The broad STAMPS initiative includes the development of detailed analysis tools, such as those presented in this dissertation, which will provide Navy decision makers with the information required to optimize and balance system and manning performance, as well as accurately predict total life-cycle costs. The technique herein can be expanded to comparing both upper-extremities in a sea state environment. Furthermore, the technique can focus more on reaction time assessments if the

need exists. The technique developed can not only assess design with respect to anthropometry, but the technique can be leveraged by clinicians for retraining the upper extremity after surgery. A pointing task is a simple movement that addresses an intent by the participant to move to a target. Pointing is a precursor to a more complex task like grasping, thus the technique herein can retrain a fundamental principal of movement. Lastly, the technique developed can also be expanded to upper extremity prosthetic assessments. The data yielded by the method provides a holistic view of an upper extremity movement. A comparison between a natural upper extremity and prosthetic upper extremity in a fundamental movement, such a pointing task, can aid clinicians in fine tuning the parameters necessary for more efficient human performance.

Investigating Differences in the Biomechanics of Goal Directed Movements of the Upper Extremity

Tanimu Deleon-Nwaha

B.S., Manhattan College, 2003

M.S., Manhattan College, 2006

A Dissertation

Submitted in Partial Fulfillment of the

Requirement for the Degree of

Doctor of Philosophy

at

The University of Connecticut

2017

APPROVAL PAGE
Doctor of Philosophy Dissertation

Investigating Differences in the Biomechanics of

Goal Directed Movements of the Upper Extremity

Presented by

Tanimu Deleon-Nwaha, M.S., B.S.

Major Advisor _____
Donald R. Peterson

Associate Advisor _____
Martin G. Cherniack

Associate Advisor _____
John C. Bennett

Associate Advisor _____
Lindsay J. DiStefano

Associate Advisor _____
Pouran D. Faghri

University of Connecticut
2017

Acknowledgments

This dissertation was funded by an Office of Naval Research (ONR) grant N000141512538. My deepest thanks goes to ONR code 34 for their support, and for understanding that the Warfighter is the most important asset on any maritime vessel. Thank you for the opportunity to learn and grow, and for supporting a concept as fundamental as human centered design.

First of all, I would like to express my deepest gratitude to my major advisor, Dr. Donald R. Peterson. Dr. P as he is known to many students, took a chance on me back in 2009, when the relationship with my then advisor was on the rocks. Dr. P welcomed me into his lab knowing full well that I worked fulltime. The one thing that Dr. P told me is that he would be a bumper to bump me back on course if I veered off. This approach forced me to think in ways that I was not accustomed. Further, thinking from that perspective fostered a great deal of creativity. I will be forever grateful for this life lesson.

I would also like to express my gratitude to my associate advisors, Dr. Martin Cherniack, Dr. John Bennett, Dr. Lindsay DiStefano, and Dr. Pouran Faghri. Their guidance and intellectual prowess afforded this dissertation world class oversight. Dr. Bennett showed me how to consider and manage uncertainty. Dr. DiStefano, provided insights on how to conceptualize the data and to make it applicable. Dr. Cherniack always pushed the level of thought to heights that I sometimes considered beyond my capabilities. Dr. Faghri was always thinking ahead, and she could help me navigate obstacles well before they ever manifested.

Additionally, all the folks that are never in the limelight, but who roll up their sleeves and get stuck in: Mr. Simon Kudernatsch, Dr. Takafumi Asaki, Dr. Joshua Spencer, Mr. Craig Haverly, and Mr. Tarek Tantawy for their support with the experiment. Mr. Kudernatsch assisted in piloting the experiments, and Solidworks validation for kinematic data. Most importantly, Mr. Kudernatsch's hospitality during my various travels to Texarkana to conduct this research is priceless. I will never forget the time my connection to Texarkana was cancelled in Dallas and Mr. Kudernatsch drove 6 hours plus roundtrip to pick me up – I have no words to do that deed justice, all I can say is I thank you from the bottom of my heart. Dr. Asaki,

provided assistance with data acquisition, data synchronization, and force plate validation. Dr. Asaki, would always go out of his way to help me with things that were very much beneath him. Without Mr. Kudernatsch and Dr. Asaki this dissertation would not have been possible. Dr. Spencer and Mr. Tantawy, provided Matlab tutorials and assistance in the early stages of data analysis. Without these lessons, the use of Matlab would not have been possible, and without Matlab, my efforts would have quadrupled. Mr. Haverly, assisted with C++ assistance and tutorials in the early stages of pilot studies. Without which, the touchscreen application may not have worked so well. I would also like to thank Mrs. Tammy Wojtusik for all her help in coordinating logistics, and encouragement. Additionally, I would like to thank my mentor and friend Dr. Brian Gilchrist for his pearls of wisdom.

Last but not least, I want to thank my biggest supporters and fans – my mother and brother. Ramat you are not only my brother, but you are my best friend. Momma always said, "She wanted to make sure there would always be someone I could count on when she passed from this world". I am ever so grateful that the person is you. Momma, you are not only my mother, you are my friend, and most importantly, you are my hero! As a single mother raising two boys, in a new land, must have been harder than I have ever appreciated - you are such a remarkable woman. Your extremely high level of education instilled the value of education and the success it has on this world. The strength you have shown me since I was a little lad is where I get my will to persevere. All the trials, illness, pains, disappointments, and you still carried on with a smile – thank you for the honor to have you as my mother.

Tanimu Deleon-Nwaha

May 2, 2017

Dedicate to my mother and brother.

List of Figures

List of Tables

1. Introduction

1.1Background and Significance

Biomechanics is a branch of science concerned with the internal and external forces which act on the human body and the resulting effects of said forces. One of these effects is displacement of the body via the neuromuscular system to affect movement of some kind; therefore, biomechanics is quintessential to human survival. Biomechanics, and the resulting effects, is required in almost everything human beings do daily. Kroemer (2006) said "Human capabilities are determined by: an individual's capacity for energy output, including physique, training, health, the characteristics of neuromuscular function, such as coordination of motion, and muscle strength". There are two general facets to biomechanics: kinematics, which encompasses the study of movement from a geometric perspective, and kinetics, which is concerned with the forces acting on the mechanism that allows movement to occur. Delving deeper into the kinematic parameters of biomechanics, motor control and learning are an essential aspect with respect to human goal directed movement. Motor control is the study of the nature and cause of movement, while motor learning is the acquisition and/or modification of movement (Shumway-Cook and Woollacott, 2001). This dissertation focused on a study to measure the kinematics of an upper extremity movement and the biomechanics of postural adjustments to account for the upper extremity movement as a result of center of gravity (CoG) shifts in a non-sea state environment within earth's gravity. Furthermore, the measurement technique leverages motor control and anthropometric adaptation

through learning as a means to exploit movement efficiency in performing a simple closed loop goal directed pointing task in an open and constrained space.

Learning is defined by two predominant aspects: non-associative and associative. Non-associative aspects encompass habituation and sensitization, where habituation is the response to a non-painful stimulus due to the repetitive nature of the stimulus. Sensitization, on the other hand, is exhibiting more of a response due to a threatening or dangerous stimulus (Kupfermann, 1991). Associative forms of learning couples one concept with another concept. A good example of associative learning is classical conditioning, which teaches pairing of two stimuli that do not have a prior connection. The model takes a weak stimulus, or the conditioned stimulus, and associates it with another stronger unconditioned stimulus. A classic example is Pavlov's dog, where Pavlov associated the ring of a bell with the awarding of food for a dog. Whenever the researcher rang a bell, the dog would start to salivate in anticipation of getting something to eat. Another type of associative learning is operant conditioning, where, when a stimulus yields a reward, an association is made that is repeated at a cost to other behaviors (Shumway-Cook and Woollacott, 2001). However, if the stimulus yields a noxious result, the behavior is usually not repeated - in essence the "Law of Effect" (Kupfermann, 1991). An example of operant conditioning is when a button is pressed and food is provided and, due to the rewarding nature of the result, the behavior is repeated. Conversely, a button is pushed and an electronic shock is provided instead of food and, due to the harmful nature of the result, the behavior is not likely to repeat. Associative learning has undergone further classification in two types of knowledge that is acquired (Shumway-Cook and Woollacott, 2001). The first classification is procedural learning, which is performed without attention to conscious thought. This type of learning is a result of the old adage, "practice makes perfect". The second classification is declarative learning, which is derived from

knowledge that can be consciously recalled. Thus, declarative learning requires processing and cognitive awareness of the steps to perform a task. The interesting aspect of declarative learning is that with repetition declarative learning can become automatic, as in motor movements, where conscious effort is not payed to the actual movement dynamics (Shumway-Cook and Woollacott, 2001). Basically, a declarative effort can become procedural with the right level of practice. This study, henceforth, leverages this declarative/procedural interplay to take a procedural action, such as pointing and integrates a declarative action, such as moving the upper extremity within a range of frequencies. To effectively appropriate this, additional classification of associative learning has to be considered.

On the account of furthering the classification of associative learning, researchers started to develop theories of motor learning. Adams (1971) was one of the first to try and comprehensively explain motor learning. His theory was based on the concept of Closed Loop Processing in motor control, where sensory feedback is used to maintain the production of skilled movement. Adams' concept included a memory trace, which was used by the Central Nervous System (CNS), to initiate movement and a perceptual trace, which took over to finish the movement and detect errors (Adams, 1971). As fascinating as Adams' theory was, it had two major limitations. First, the memory storage system of the CNS cannot store a perceptual trace or movement template for every movement (Schmidt, 1975) and, second, humans have been observed to demonstrate movements without sensory feedback (Taub and Berman, 1968; Rothwell et al., 1982).

Schmidt, in response to the Adams' Closed Loop theory, developed a concept called Schema Theory. The critical parameter of Schema Theory is the generalized motor program, which consists of the spatial and temporal information to perform a specific movement. There are four major conditions of the schema: 1) the initial conditions (i.e., start of the movement), 2) response

specifications (i.e., parameters required to execute movement, such as velocity), 3) sensory consequence of the movement (proprioception of limbs, & environment or exteroception), and 4) the measured outcome, which is knowledge of results or terminal feedback (Schmidt, 1975). In-addition, the interplay of the motor program within the schema has two relationships. The first, is the recall schema, which organizes the motor program and initiates and controls movement while the recognition schema, or the input hypothesis, is responsible for evaluating the last executed movement attempt based on the initial conditions in preparation for the next movement (Schmidt, 1975).

Taking a slightly different perspective was Karl Newell, who in 1991, drew from Schmidt and Adams to develop a theory on motor learning based on search strategies (Newell, 1991). The learning theories proposed by Adams and Schmidt harnessed practice as a means to instill constant change in motor programs, which results in a more precise representation of movement development (the adage of "practice makes perfect"). Newell's concept of motor learning is embedded in the link between perception and movement which was contingent upon environmental constraints (Newell, 1991). What Newell is asserting is that, as a person practices a task, the CNS searches for an optimal strategy to execute the task within the constraints of the environment that support the task. Therefore, perception and movement systems are integrated into an optimal task execution and the integration vehicle is the perceptual-motor workspace (Newell, 1991). In navigating this workspace, all perceptual cues critical to executing the task need to be determined. Further, the motor workspace requires similar navigation and determination of the perceptual workspace. As a result of determining perceptual-motor cues, motor learning is characterized by optimizing task-relevant integration of perception and movement rather than a rule-based approach to movement (Newell, 1991). One salient point of

Newell's theory is that motor learning will depend on the similarities in the determined cues for the perception and motor workspace; albeit, independent of the muscles used in carrying out the task (Newell, 1991). It should be noted that, as robust as Newell's theory is, it is not without one major limitation - the lack of application to specific examples in learning motor skills in a systematic way (Shumway-Cook and Woollacott, 2001). An understanding of motor learning allowed the current study to properly leverage the declarative/procedural interplay. However, an understanding of the intrinsic feedback mechanism (proprioception) which adapts to perturbations from extrinsic environmental constraints rounds out the holistic view of the declarative/procedural interplay within the perceptual-motor workspace.

Sir Charles Sherrington defined proprioception as the awareness of movement derived from muscular, tendonous, articular, and vestibular receptors (Sherrington, 1906). The human upper extremity, which encompasses the glenohumeral joint, humerus, radius, ulna, and hand, takes into account all aspects of this definition except the vestibular receptors. Dickenson, 1976, expands upon Sherrington's definition by claiming that proprioception is the appreciation of movement and position of the body and parts of the body based on information except visual, auditory, or superficial cutaneous sources. Thus, in the context of Dickenson's definition, measuring proprioception is predominately accomplished through limb reposition sense and threshold to detection, where reposition sense is a stimulus value that marks a set point and an extremity is actively or passively repositioned to the prior set point value from a baseline position (Howard and Templeton, 1966). Here, the threshold to detection is the active awareness of the smallest change in the position of the extremity. Proprioception provides the cortex with the ability to corroborate the afferent response with the prior efference copy, similar to the motor learning theories

previously discussed. As a result, proprioception is important for providing smooth and coordinated movement, maintenance of normal body posture or center of gravity (CoG), regulation of balance and postural control, and motor learning and relearning. Furthermore, to purely learn a new motor skill, similar to retraining your brain after a traumatic event like a stroke, proprioceptive awareness of posture and movement is the corner stone (Kaya, 2014).

The important role of proprioception is shown in several studies involving the evaluation of deafferented patients, where it was stated that, without proprioception, the onset of movement is delayed and trajectory formation is impaired (Ghez et al., 1995; Ghez and Sainburg, 1995; Sainburg et al., 1995; Ribeiro and Oliveira, 2011). The brain relies on the constant interplay of efferent and afferent stimuli to correct or optimize motor control (Kaya, 2014). These corrections are a result of the interplay at three salient regions in the ascending motor and somato sensory pathways. First, the spinal cord functional joint stability and reflex motor responses are core attributes (Kaya, 2014). Second, the brain stem integrates afferent information with visual and vestibular inputs to control automatic and stereotypical movement patterns, balance, and posture (Ribeiro and Oliveira, 2011). Lastly, at the higher levels of the CNS, such as the cortex and cerebellum, the responsibility of conscious awareness of proprioception contributes to goal directed movement. Integrating proprioceptive inputs at the CNS corrects speed and timing errors during movement execution and coordinates body stability ahead of movement execution (Ribeiro and Oliveira, 2011). It would appear that the key aspect of Newell's theory is afferent proprioceptive feedback.

To take this a step further, prosthetics provide a very interesting perspective into the functional feedback of afferent proprioception. Targeted Muscle Reinnervation surgery is at the forefront of recalibrating the brain and calibrating a prosthetic arm, for example, with the natural function of the amputated limb. Targeted Muscle Reinnervation allows the individual to control the prosthetic limb with cognitive thought from the prefrontal cortex. This is accomplished through the transfer of residual arm nerves to alternate muscle sites in the amputated limb (i.e., glenohumeral joint musculature) (Kuiken et al., 2009). However, from a performance perspective, the mean motion selection and motion completion times for elbow and wrist movements were 0.06 seconds and 0.21 seconds longer than the mean times for control participants (Kuiken et al., 2009). Further, there is a lot of retraining of the fitted individual to acquire the prior results (O'Brien, 2015). The weakest link is not the prosthetic, as current prosthetic arms have similar dexterity to a natural arm, and it is not the individual (i.e., without gender consideration); rather, it is the lack of joint awareness or afferent proprioceptive feedback (Morgan, 2011).

In considering proprioception from a gender perspective, performance differences with respect to proprioception has been considered; however, definitive conclusion cannot be made primarily due to the limitation of the experimental approaches (Ribeiro and Oliveira, 2011). New technological developments have shown differences in the neuronal connections between males and females that warrant further investigation into possible gender difference, especially in goal directed movement approaches. With the use of Diffusion Tensor Imaging-based Structural Connectome technology, Ingalhalikar et al. (2013) showed that male brains are structured to facilitate connectivity between perception and coordinated action. Furthermore, they determined that males are innately structured to create coherent intra-hemispherical sub-networks that are connected to neighboring

regions. They concluded that females, however, are structured for inter-hemispherical communication, which enhances analytical and intuitive processing (Ingalhalikar et al., 2013). As a result, males are wired for more coordinated movement, while females are wired for more analytical processing. Due to the complexity of assessing the prior, the concept presented herein assess anthropometric differences in performing a goal directed pointing task or end-effector proprioception.

End-effector proprioception is defined as the appreciation of movement and position of the body and appendages of the body based on information from visual and muscle spindle fibers. Woodworth conducted one of the first experiments that examined accuracy with eyes open and closed, where subjects produced pencil strokes to the beat of a metronome (Woodworth, 1899). Results showed that accuracy is related to distance moved when time per movement was held constant and that errors increased with eyes open rather than when eyes were closed. In other experiments, Howard and Templeton incorporated vision in their definition of proprioception, especially in measuring the accuracy of fine active movements. Gibbs and Logan (1965) performed a battery of experiments to study precision and efficiency and their experiments involved proprioceptive cues, where the head and eyes were actively repositioned based on a predetermined passively set position of the participant's visually occluded hand. Smith (1969) concluded that proprioceptive information could only provide a gross representation of movement and that humans could not perceive details due to their orientation toward external cues. This suggests that exteroception from visual senses provides a supplanting correction factor to interoception from proprioceptors. Bernstein (1967) hypothesized that the nervous system possessed a central representation of movement, which is analogous to a motor image or, in

essence, a movement template, where modification could be made based on external environmental constraints. Recently, functional magnetic resonance imaging (fMRI) suggests that a much wider network of brain areas shows mirror properties in humans than previously thought. These additional areas include the somatosensory cortex and are thought to make the observer feel what it feels like to move in the observed way (Gazzola et al., 2009; Keyers et al., 2010). As previously mentioned, the somatosensory cortex is the home of proprioceptive inputs, and proprioception to Bernstein was an inherent part of arriving at the intended destination of movement. However, visual information provided the necessary criteria to formalize the intended movement. In response to visual inputs, Keele (1981) suggested that movement time increases with distance and accuracy in part because of the constraints of our visual system. Additionally, movements that are shorter than 0.25 seconds are too short to take advantage of visual feedback, where movements longer than 0.25 seconds involve visual feedback in the setup phase of the movement (Shumway-Cook and Woollacott, 2001). Whereby, the eyes are the window that reflects the light which illumines the pieces of the motor image that stimulate the final construct. Whereas, the motor and somatosensory system in concert with the cerebellum adaptively correct the body image to meet the initial motor image (Wu et al., 2015; Von Holst, 1954). The ability to adjust the motor and body images is a type of adaptive filter. If the afferent feedback portrays noise in the movement, then the efferent system will adjust the feedforward signals to absorb the noise during the motor movement (Wu et al., 2015; Von Holst, 1954). Therefore, the proprioceptive modality of the somatosensory system is vital in allowing such adaptive filtering to occur efficiently during voluntary movement (Taub and Berman, 1968; Ghez et al., 1995; Ghez and Sainburg, 1995; Gibbs and Logan, 1965; Ribeiro and Oliveira, 2011).

In scientifically assessing proprioception, several studies yielded valuable information, but in all the occurrences where upper extremity movement was performed, the studies were restricted to a seated posture and or a 2D movement pattern. The studies looked into categorizing a movement taxonomy in a seated posture with respect to standard input devices (i.e., pencil, a stylus, mouse, target pad… etc.) (Fitts, 1954; Carson et al., 1993; Roy and Elliott, 1989; Adams, 1968; Adams and Xhignesse, 1960; Ellis, 1969; Grose, 1967; Hall, 1966; Goble and Brown, 2008; Goble and Brown, 2009; Adamo et al., 2007) while other studies focused on differences in timed motor movement between dominant and non–dominant hands (Goble and Brown, 2005; Goble and Brown, 2006, Goble and Brown, 2007; Morrison et al., 2011). Ultimately, the objective of these studies was to understand how proprioception influences movement, the development of movement, and the rehabilitation of movement from either intrinsic or extrinsic trauma.

1.2 Objectives

In 2010, then-Defense Secretary Robert Gates informed congress of the decision to allow women on submarines and thereafter, in 2011, the Navy decided to begin training women for their new subsurface roles. Subsequent to the decisions, in December of 2014, the US Congress funded the new policy of the Navy Submarine Force to be inclusive of the integration of women. Naval Administration (NAVADMIN) message 19/15 detailed the integration of enlisted women aboard. Prior to this monumental action, the US Navy has allowed women to serve aboard non-hospital ships since October, 1978 (Callahan, 2003). Due to the administrative changes, submarine design modifications became necessary, especially design modifications that facilitate integration without inflating costs. Current cost levels associated with new submarine design(s) are maintained through the utilization of legacy components and systems; however, several of

these components and systems are designed to meet ergonomic standards derived using male anthropometry and performance capabilities. In addition, all design solutions involving the human factor in the submarine environment is further limited due to extreme spatial constraints. As a precursor to the events of 2014, and a consequence to the 2010 decision, the Office of Naval Research (ONR) in 2012 initiated a broad area announcement (BAA) called the Simulation Toolset for Analysis of Mission, Personnel & Systems (STAMPS). The fundamental focus of STAMPS is to understand human task execution times. Currently, many of the onboard systems are computer controlled, necessitating man-machine interfaces. As common practice, military activities that involve man-machine interfaces have always focused on the dexterity of the hands, often neglecting the role of movement in the task (Newell, 1991). When considering the use of legacy systems and components as a cost saving measure in current designs, prior military precedent only exacerbates the design challenge. Understanding upper extremity kinematics issues associated with man-machine interfaces, especially within submarines becomes an essential component in the optimal design process. While adjustable interfaces are widely recognized as an ergonomic solution (Kroemer, 2006), this approach may not be possible, or even practical within the submarine's constrained environment. To-date, there are few studies that assess human interface parameters on touch enabled devices (Hu and Ning, 2016a; 2016b; Sato and Nakajima, 2011). Therefore, studying the kinematic differences in goal-directed upper extremity movements during a man-machine interface tasks may provide insight into improving maritime equipment design, configuration, and operation, especially when factoring anthropometric gender variations into the optimization process – where males tend to be larger than their female counterparts (ADULTDATA, 1998; PeopleSize, 2008).

As a result, the STEM (Science, Technology, Engineering, and Mathematics) Innovation Laboratory at the Texas A&M University in Texarkana conducted research entitled "A Technique to Measure Visual Proprioception with Respect to Human Performance", which is a sponsored research grant from the Office of Naval Research (ONR). In this work, efforts to understand goal directed motor movement efficiency in the context of human performance is vital in modeling and predicting potential outcomes to shipboard naval damage control procedures. More importantly, understanding anthropometric gender variations in natural goal directed motor movement may provide broader insight from a biomechanical perspective, including goal directed movements with respect to kinematics that may require a higher level of acuity. This dissertation directly supports this research initiative and will provide further insight into measuring goal directed end-effector proprioceptive biomechanics.

From this study, further understanding into smooth and coordinated movement, maintenance of normal body posture, and postural control was assessed from an anthropometric perspective. The measurement technique leveraged herein uses motor control and anthropometric adaptation through learning as a means to exploit movement efficiency in performing a simple closed loop goal directed end-effector proprioceptive movement in an open and constrained space. The results will support the broader ONR STAMPS initiative, which aims to simulate the major design of naval vessels and the associated manpower and related cost variables, in order to model and optimize the trade spaces in platform design, especially as the female population in the Navy continues to increase. It will also include analysis tools, which provide Navy program managers with the information required to balance system and manning performance, as well as total life-cycle costs which are driven by manning.

1.3 Quantifying Biomechanical information in an Upper Extremity Goal Directed Movement Task

Understanding naval task execution times is vital to understanding operator performance from a damage control and maintenance capacity. Naval program managers predicate the number of operators aboard a ship based on the damage control and ships maintenance needs. A major way to improve task execution times is to optimize the ships design environment based on the operator anthropometric characteristics. Bernstein (1967) set the benchmark for experiments researching the control of reaching movements and said, " If the spatial shape of a trajectory is invariant, irrespective of the muscle scheme or joint scheme, then the motor plan must be closely related to the topology of the trajectory and considerably removed from joint and muscles". In essence, the movement pattern is never changing regardless of what is happening with muscle and joint utilization as the motor plan is based on the geometric properties that allow for such a movement trajectory to occur based on the requirement of the desired movement. Marteniuk et al. (1987) conducted a study where five right hand dominant subjects were seated at a table and where asked to point at a target of two different diameters, 2 cm and 4 cm, respectively, from a distance of 20 and 40 cm moving from right to left in a straight line and parallel to the frontal plane. The subjects were later asked to grasp a target (i.e., light bulb or tennis ball) with their first and second digit and lift it vertically in order to create a motor comparison to a pointing task. The results showed that grasping acceleration was shorter than the deceleration phase; however, for pointing with the second digit, the acceleration phase was longer than the deceleration phase, where the subjects hit the target at a greater velocity. The movement disparity between the pointing task and grabbing task is a function of the environmental

constraints that Newell described in his theory of the perceptual-motor workspace. In the grabbing task, the objective was to grab the item and then lift vertically. In order to effectively perform the task, the person needs to slow down as they grab the item, so that their next movement transitions to moving the item vertically. The pointing task is comprised of really one task, as additional motions are added (e.g., not only grab an item but lift it vertically), the time for task execution increases due to the preparation and execution of the task's first and second components. Thus, the environment or the task to be carried out in the environment dictates to the CNS what needs to be done and the CNS searches for the optimal strategy to perform the task. Therefore, developing a simple method to holistically look at human task execution as a result of the vessel's design environment would aid naval program managers in how they could optimize the design and therefore reduce the number of required operators. Measuring a goal directed pointing movement in a standing posture is a typical motion aboard a maritime vessel. The method developed in this dissertation leverages the use of anatomical planer projections from opto-electronic motion capture data, an isochronal stimulus from a metronome (to pace participants), a touchscreen procedural pattern, surface electromyography, and a force plate. The anatomical planer projections are broken down into the upper extremities movement components of flexion, extension, abduction, and adduction, where angular displacements and velocities are calculated. Surface electromyography is used to assess maximum voluntary contraction and frequency shifts in muscle recruitment from power spectral density analysis to provide a means to understand muscle recruitment and activation as well as fatigue. Lastly, the force plate is used to assess center of gravity shifts as a result of the upper extremity movement. As a result, the selected measurement modalities provide a holistic picture of upper extremity task execution in a non-sea state environment.

1.4 Validate the Technique by Assessing Upper Extremity Movement Patterns

The following objective was used to assess the validity of the measurement technique in Section 1.3 by focusing on design considerations with respect to anthropometry. This objective has three sub-topics associated with anthropometric design. First, using standard height or stature as a design specification alone is not a predictive vehicle to drive the design to optimality. Second, naval program managers may not want to have such a large sample of anthropometries with which to design; rather, a narrower sample of anthropometries will yield greater design optimization. In essence, a large population demographic makes true design optimization more difficult. To appease the smaller demographic, the design may impede the larger demographic and vice versa. Focusing less on the tails of a normal distribution, but designing to a specific range of a normal distribution, where the standard deviations are not so far apart, allows the design optimizations to have a greater impact with less implementation cost. Third, there are individual differences in how people perform a task, yet alone there are differences in how a person performs the same task on different occasions. If retraining is not part of the overall design acquisition cost, then some level of design adjustability needs to be considered, so the operator can personalize the task and therefore optimize their task execution.

2. Experimental Design and Methods

2.1 Design

Ten healthy (i.e., no known neuromuscular problems and normal to corrected vision - see Appendix A for pre and post screening questionnaire samples) self-identified right-hand dominant male and female participants between the ages of 21 and 35 provided signed

informed consent in accordance with the guidelines of the Internal Review Board (IRB) from the Texas A&M University in Texarkana. Selection of right-hand dominant participants is due to the fact that nine out of ten people are right-handed, in that they prefer their right hand over their left in reaching or manipulating a target (Annett, 1985; Gilbert and Wysocki, 1992; Oldfield, 1971). All participants either played a: sport, piano or string instrument, video games, or a combination of the three categories. Every participant was familiar with touch enabled devices, either a: smart phone, tablet, or touch enabled computer, or a combination of the three categories. Additionally, participants refrained from alcohol and nicotine for a span of 24 hours (Stroobant and Vingerhoets, 2000). Furthermore, the average prior night's sleep for all 10 participants was 6.95 hours, ±1.46 hours, with every participant self-reporting that they felt physically capable to perform the experiment as self-reported by each participant during the familiarization period and pre-survey.

Table 1. A) A summary of the anthropometric measurements of the 5 male participants, B) A summary of the anthropometric measurements of the 5 female participants, and C) The statistical power calculation using G*Power.

A)

Male-Anthropometric Categories, n=5	P3-M	P5-M	P7-M	P9-M	P10-M
Stature (in)	68.5	70.5	68.9	68.6	69.4
Eye Height (Standing) (in)	64.3	66.3	64.0	64.0	66.0
Shoulder (Acromion) Height (in)	57.3	58.0	57.0	57.0	59.0
Chest (Nipple) Height (in)	52.0	52.5	50.5	50.0	52.3
Elbow (Olecranon) Height (in)	44.5	44.8	43.8	43.5	44.5
Fingertip (Dactylion) Height (in)	28.0	27.3	26.5	27.5	28.3
Waist (Iliocristale) Height (in)	40.0	42.5	39.5	38.5	41.3
Waist (Omphalion) Height (in)	42.0	41.3	41.0	39.5	43.3
Crotch Height (in)	32.0	33.0	30.3	30.5	32.8
Knee (Mid-Patella) Height (in)	19.5	19.3	18.8	18.5	19.3
Functional Reach Extended (in)	33.0	34.3	33.0	36.0	33.5
Arm(Acromion to Lateral Epicondyle) (in)	13.8	13.8	13.2	13.4	13.9
Forearm (Lateral Epicondyle to Ulna)(in)	10.2	10.0	9.5	10.5	10.0
Breadth(Acromion to Acromion) (in)	12.4	13.6	13.5	16.9	14.0
Arm Length (Acromion to 3 Distal Phalange) (in)	31.5	31.0	30.3	31.6	31.6
Weight (Lbs)	185.2	197.0	169.0	271.5	217.0
Percentiles by Stature	35.1%	61.4%	39.8%	36.1%	47.1%
Right Hand Size (mm to in conversion)	7.5	7.1	7.6	7.6	7.8
Body Mass Index (BMI)	27.7	27.9	25.1	40.5	31.7

B)

Female-Anthropometric Categories, n=5	P1-F	P2-F	P4-F	P6-F	P8-F
Stature (in)	62.5	61.3	64.6	63.8	65.0
Eye Height (Standing) (in)	57.3	57.5	60.0	59.8	61.0
Shoulder (Acromion) Height (in)	51.5	51.0	53.5	53.0	53.5
Chest (Nipple) Height (in)	46.0	43.3	47.0	46.8	46.5
Elbow (Olecranon) Height (in)	39.8	36.8	41.0	41.5	40.3
Fingertip (Dactylion) Height (in)	23.8	23.5	24.3	26.0	24.0
Waist (Iliocristale) Height (in)	37.0	37.5	38.3	37.0	38.5
Waist (Omphalion) Height (in)	37.8	38.2	39.0	38.3	39.3
Crotch Height (in)	30.8	29.8	30.3	28.8	30.0
Knee (Mid-Patella) Height (in)	16.5	16.0	17.3	17.0	18.5
Functional Reach Extended (in)	30.8	31.0	30.5	30.8	34.3
Arm(Acromion to Lateral Epicondyle) (in)	12.1	12.2	12.7	12.2	13.6
Forearm (Lateral Epicondyle to Ulna)(in)	9.0	8.9	9.5	9.4	10.4
Breadth(Acromion to Acromion) (in)	12.0	11.7	11.8	13.9	13.5
Arm Length (Acromion to 3 Distal Phalange) (in)	28.7	28.1	29.7	28.5	32.3
Weight (Lbs)	117.2	127.5	131.0	205.0	181.0
Percentiles by Stature	26.1%	13.9%	56.8%	45.1%	62.7%
Right Hand Size (in)	7.6	7.0	7.5	6.9	8.3
Body Mass Index (BMI)	21.1	23.9	22.1	35.4	30.2

C)

t tests – Means: Difference between two independent means (two groups)

Analysis:	Post hoc: Compute achieved power		
Input:	Tail(s)	=	One
	Effect size d	=	1.6364700
	α err prob	=	0.05
	Sample size group 1	=	5
	Sample size group 2	=	5
Output:	Noncentrality parameter δ	=	2.5874863
	Critical t	=	1.8595480
	Df	=	8
	Power (1-β err prob)	=	0.7628553

A)

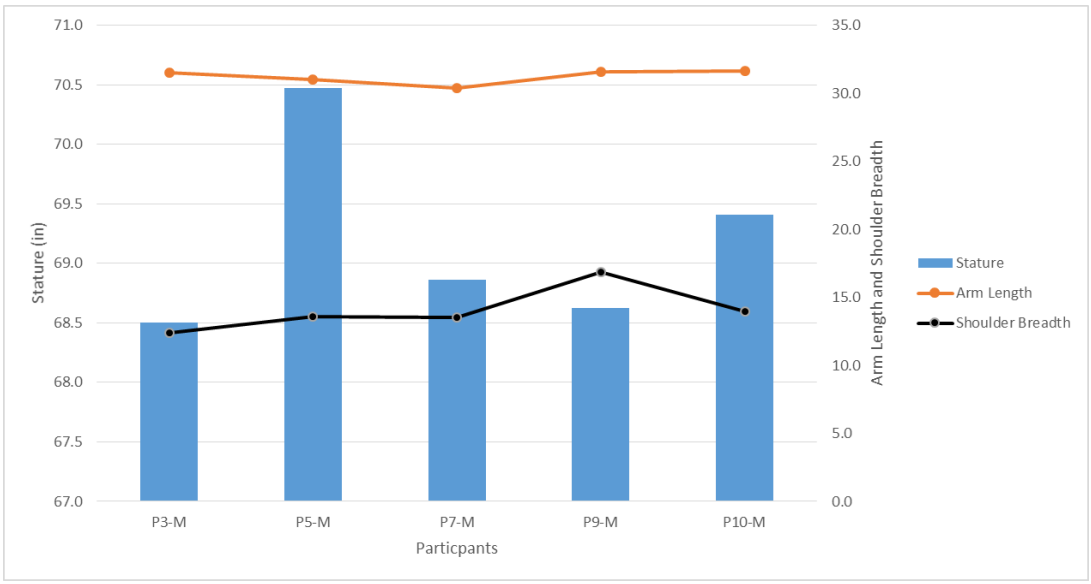
71.0
70.5
70.0
69.5
69.0
68.5
68.0
67.5
67.0
Stature (in)
35.0
30.0
25.0
20.0
15.0
10.0
5.0
0.0
Arm Length and Shoulder Breadth
P3-M
P5-M
P7-M
P9-M
P10-M
Particpants
Stature
Arm Length
Shoulder Breadth

B)

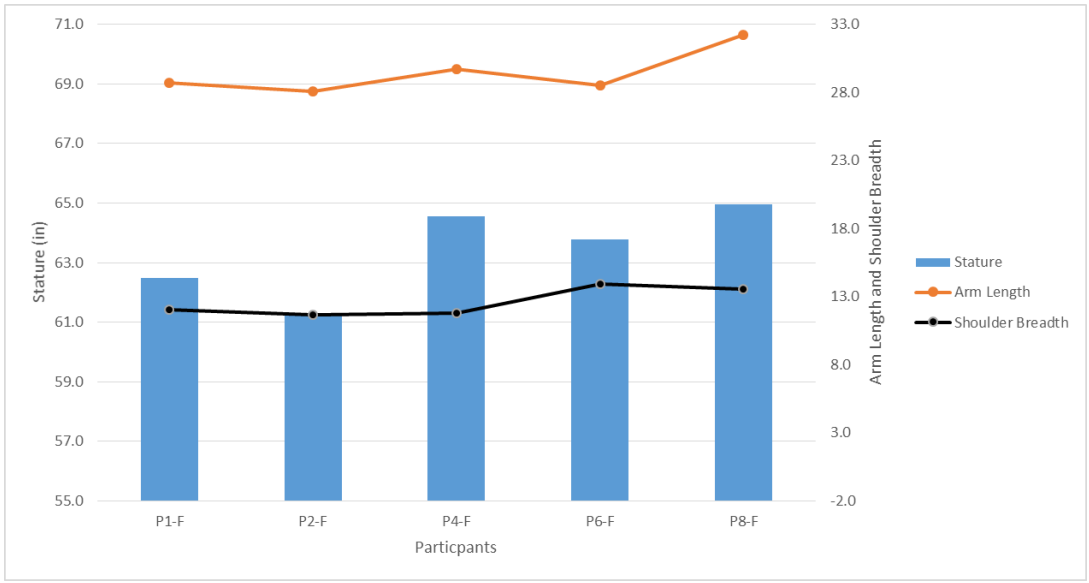
71.0
69.0
67.0
65.0
63.0
61.0
59.0
57.0
55.0
Stature (in)
33.0
28.0
23.0
18.0
13.0
8.0
3.0
-2.0
Arm Length and Shoulder Breadth
P1-F
P2-F
P4-F
P6-F
P8-F
Particpants
Stature
Arm Length
Shoulder Breadth

C)

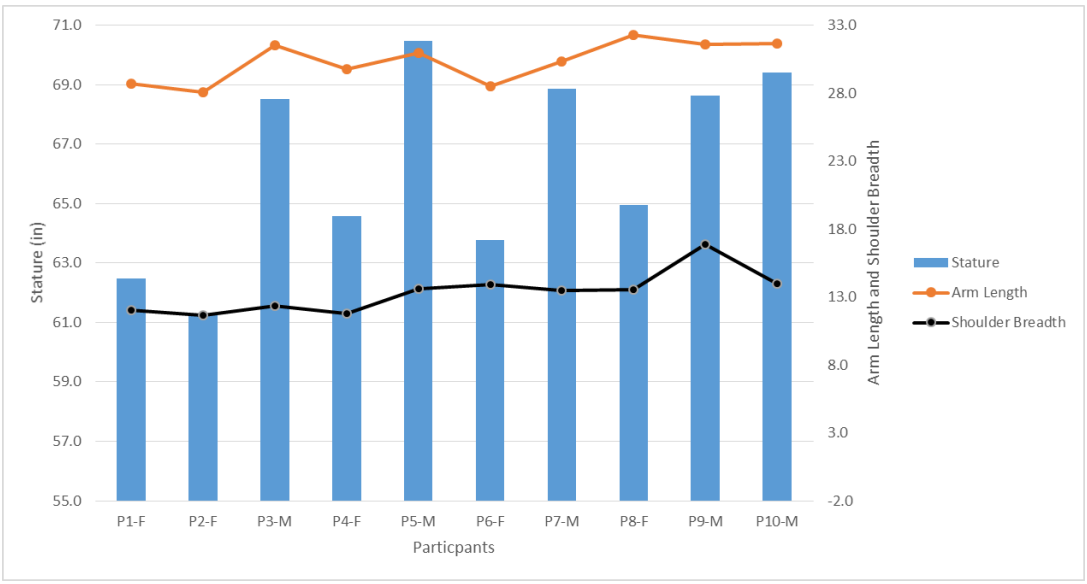

Figure 1. A) A comparison of stature to arm length and shoulder breadth for male (n=5) participants. B) A comparison of stature to arm length and shoulder breadth for female (n=5) participants C) A comparison of stature to arm length and shoulder breadth for all 10 participants.

Tables 1A and 1B provides a summary of the anthropometric measurements of the 10 participants, five male and five female. The table shows the individual measurements captured with standard anthropometric guidelines (ASTM Standard F 1166-07, 2007). From the perspective of this dissertation's experimental design consideration, stature (i.e., height), arm length, and shoulder breadth were parameters based on the environmental constraints. The coefficient of variance, for stature for the male and female participants is 1% and 2%, respectively. On the other hand, the coefficient of variance for arm length for the male and female participants is 2% and 6%, respectively. Lastly, the coefficient of variance, for shoulder breadth for the male and female participants is 12% and 8%, respectively. Figure 1A and 1B graphically shows the difference between stature, arm length, and shoulder breadth separated by male and female participants, respectively, while Figure 1C shows the comparison of all 10 participant's stature, arm length, and shoulder breadth. The conclusion is that the ratio of stature to other anthropometric measurements

is not always equivalent. There are variations from a gender breakdown and when all participants are taken as a whole. Additionally, Table 1C provides the sample size required to achieve a statistical power of 80% using the G*Power statistical power calculation tool (Faul et al., 2007; 2009). Cohen (1988) concluded that the minimum power for an ordinary study is 80%. In keeping with the Food and Drug Administration (FDA) guidelines, the sample size of the primary interest outcome is selected in situations where the sample size measurements are different for each outcome. The consistent factor and the primary focus is leveraging motor control and anthropometric adaptation through learning as a means to exploit movement efficiency in performing a simple closed loop goal directed pointing task in an open and constrained space. Therefore, human anthropometry is the one independent factor across the experiment.

The participants in Table 1A and 1B are representative of the general public and fit the anthropometric guidelines adopted for Naval design (ASTM Standard F 1166-07, 2007). The premise of the experiment was to simulate a procedural interaction with a workstation in a standing posture. The procedural interaction was governed by an isochronal stimuli using a metronome that progressively gets faster. It has been shown that isochronous auditory stimuli alters homeostatic neuromuscular cadence during gait kinematics (Housdorff et al., 1996; Delignieres and Torre, 2009; Terrier and Deriaz, 2011). The results tend toward reduced body stability in response to perturbations (Sejdic´ et al., 2012). Therefore, leveraging an isochronal stimulus with a procedural touch pattern on a touchscreen, as seen in Figure 2, harnesses themes that deal with motor learning, spatial and temporal perception, and the adaptation that must occur to thrive within those controls.

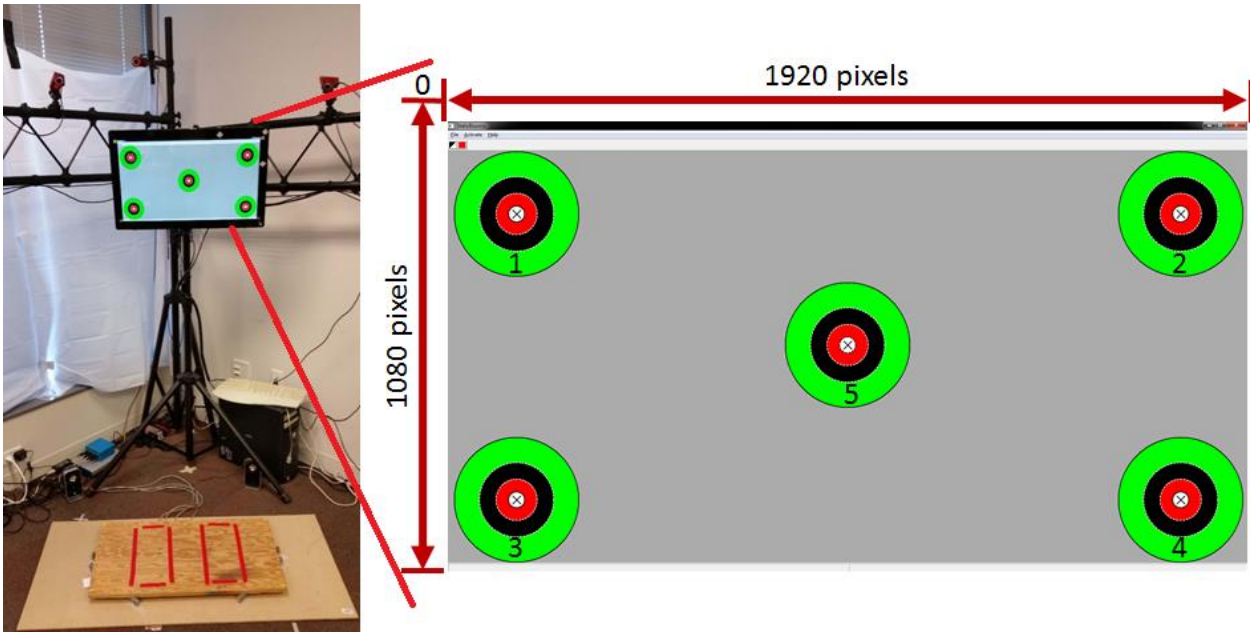

Figure 2. A close-up of the targets on the touchscreen and the order with which the touch procedure is carried out, starting at 1 and ending at 5. This is considered 1 trial.

Anthropometric dimensionality in Table 1 with respect to the touch interaction was modulated so that each participant was their own control. Each participant would participate in at least two scenarios, with three being the max. The first was an open space scenario, where the screen that the participant would interact with would be fixed at a height of 50.25 inches as measured from the force plate to the bottom of the screen (see Figure 3). This placed the center of the screen at 56.75 inches taking into account the screen's bezel and the height boost from standing on the force plate. The participant would then conduct an entire cycle at the fixed height for each stimuli: 0 Hz or no stimulus, 1 Hz or 60 beats per minute (BPM), 1.3 Hz or 80 BPM, 1.7 Hz or 100 BPM, 2 Hz or 120 BPM and 2.7 Hz or 160 BPM. This equates to a total of 6 cycles per scenario. A cycle is considered five trials, and a trial is touching all five targets, starting at target one and ending at target five, as seen in Figure 2. After the open scenario was complete, the

participant was asked if they wanted to adjust the screen based on completing the open scenario. If the participant agreed to an adjustment, then this would be the next scenario called the open-adjusted scenario. If the participant opposed the adjustment, then the constrained scenario was the next and last scenario. Only three participants requested the open-adjusted scenario. Similar to the open scenario, the open-adjusted scenario had participants perform 6 cycles which equated to the 6 stimuli. In the last scenario, or the constrained scenario, the screen was fixed at 50.25" to the bottom of the screen (similar to the open scenario) and a curtain and PVC pipe was used to simulate tight quarters similar to a maritime environment, as seen in Figure 4. Participants once again performed six cycles which equated to the six stimuli. In summary out of the 10 total participants, seven participants had an open and constrained scenario and three participants had an open, open-adjusted, and constrained scenario.

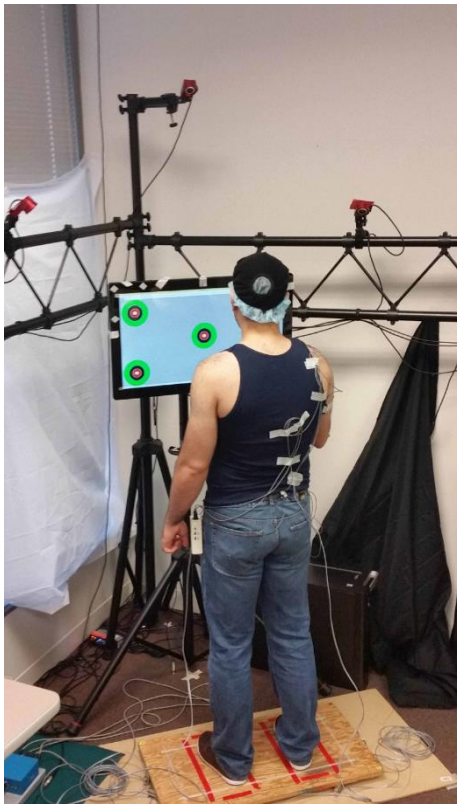

Figure 3. Measurement setup for the open screen fixed and open screen adjusted

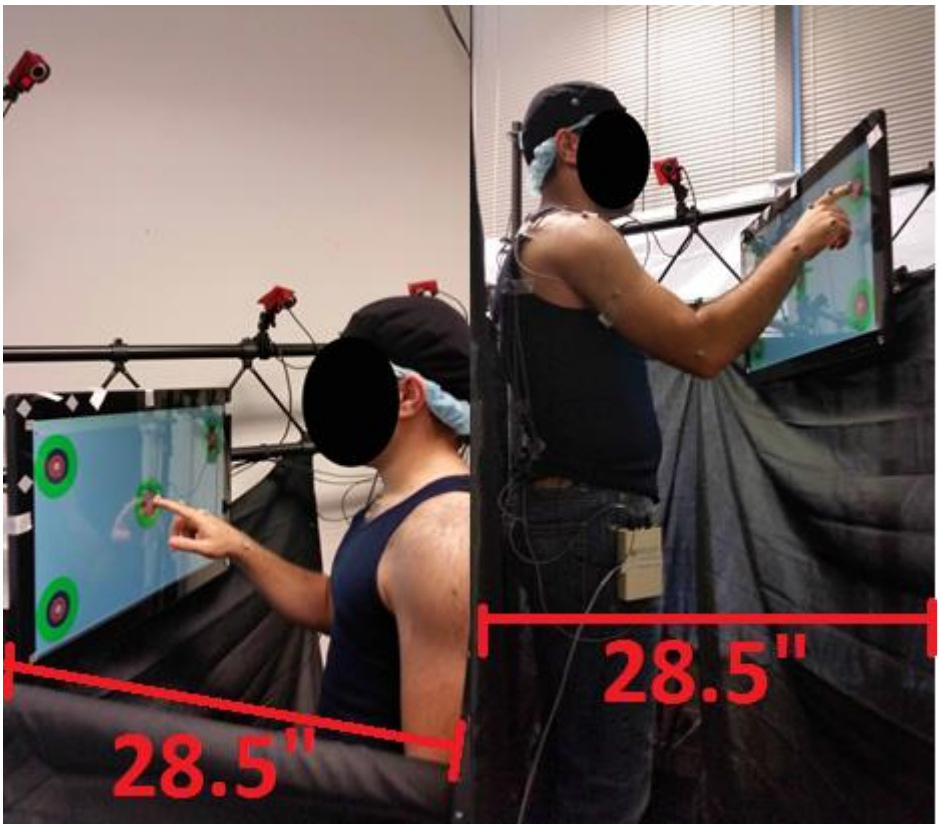

Figure 4. Measurement setup for the constrained screen fixed, Left: An image from outside the environment, and Right is an image from inside of the environment. The rectangle was 28.5 inches in depth, simulating a vessel's hallway.

Analyzing the different scenarios in a controlled environment provides a means to assess motor control and the motor learning adaptive filter that inspire the reason for the movement. The environment evokes kinematic adaptations that in some cases are beyond the person's cognizance. The participants focus in on completing the cycle accurately and within the auditory rhythm. The benefit in understanding upper extremity movement in a non-sea-state environment sets a threshold for potential future sea-state comparisons in quantifying task executions times. Task execution times are a necessity to understanding potential outcomes to shipboard naval

damage control procedures, which is of particular importance with the integration of women on maritime vessels. This is due to a significant difference in anthropometry between genders (ASTM Standard F 1166-07, 2007; ADULTDATA, 1999; PeopleSize, 2008). A critical factor to mitigating task executions times is adapting the system to the person and not the person to the system (Kroemer, 2006). An example of the prior is securing a system that has thrown a fault and the man-machine interface is out of reach of the 5th percentile male operator on watch. The operator may run to find an assist to reach the interface or they may use items (e.g., pipe, hanger, component foundation) in proximity to the faulted system as a reach assist. If the boat is in a potential rough sea-state, the chances of error or injury increases, not to mention the additional cognitive considerations that the operator experiences automatically which raises the time to execute the task. Completing the mission is the top priority and practice and training exercises do aid in reducing time execution in such scenarios but not every scenario can be accounted in the time allocated for training. From a mixed gender perspective, understanding design parameters that can facilitate task execution times, such as in man-machine interfaces, movement kinematics is a more effective way to leverage **legacy equipment** within new designs.

Legendary U.S. Naval officer Alfred Thayer Mahan surmised that those who control the oceans are militarily superior (Mahan, 1890). The last great test of ocean dominance was during World War II. Naval vessels have come a long way since that time with the birth of the nuclear powered navy and the introduction of the first nuclear powered submarine the USS Nautilus (SSN-571); however, one thing that has not changed is the lack of designing to accommodate various operators. Only recently, as the increase in demand for more platform and operator capability without additional costs, has the Navy leadership started to address the needs of operator.

2.2 Methods

In this study, the joint kinematics of 10 participants was measured using a 16-camera Opto-Electronic Motion Capture System (OEMC) (Motive Body v1.8, Natural Point, Corvallis, OR). Additionally, a force plate placed under the participant's feet measured the reaction forces in the vertical direction as a result of the participant's movement interactions with a flat-panel touchscreen (i.e., to determine changes in center of gravity (CoG)). Isochronous auditory pacing was governed using a metronome and was correlated using direct movement measurements. In a similar fashion to Morrison et al. (2011) and Ko (2000), upper extremity motor movement was randomized. The beats went from 1 Hz, or 60 beats per minute (BPM), and were increased until movements are just approaching a ballistic movement, where control of the movement, once initiated, is reduced (i.e., medium at 1.3 Hz (80 BPM), fast at 1.7 Hz (100 BPM), faster at 2 Hz (120 BPM), and fastest at 2.7 Hz (160 BPM)) (Frank et al., 2006). Additionally, the participants also performed a movement at their own pace (i.e., 0 Hz or no beat) and the order of the beat frequencies in the experiments were randomized for each participant in order to avoid learning of the familiarization period (Table 2).

Table 2. Example use of the random number function in MS Excel to generate the randomized experimental sequence

Frequency	Random #
1Hz	0.674582529
2.7Hz	0.825270481
0Hz	0.345814281
1.3Hz	0.709983703
1.7Hz	0.737459851
2Hz	0.801489192

Each participant executed each trial in a standing posture, where they were instructed to start with their hand in a neutral posture and at their side (or home position), conduct the test, and then return their hand to the home position. Participants performed movements in five quadrants of a touchscreen (Planar, Beaverton, OR) that is controlled by a computer (Dell Precision Tower 7910, Dell Inc., Round Rock, TX) and each participant performed a total of five trials per beat frequency (i.e, from 0 Hz to 2.7 Hz). The touchscreen was broken down into five sectors and each sector had static concentric circles of varying sizes and colors that were analogous to a bullseye target (see Figure 2), where the center of the bullseye represents the optimal touch point. Gur et al. (2012) conducted a sensorimotor speed-processing test called the Motor Praxis task, which requires moving a mouse and clicking on a green square that disappears after the click and reappears in a different location on the screen. This study adapted concepts from the Motor Praxis task except that the targets were kept static, which eliminated the perception and determination of the stimulus. Additionally, in keeping the targets static, a confounding factor called the 'flash lag effect' is mitigated, where the 'flash lag effect' is the delayed perception of visual information. For example, in tests where an object is moving across a subject's field of vision on a screen from left to right when the subject was asked where the object was at a specific point in time on the screen, they guessed using a past state of the object. The result is a

delay in visual perception that amounts to approximately 80ms (Eagleman and Sejnowski, 2007). As a result, this focuses more of the measurement emphasis on the upper extremity motor movements, hereby performing a proprioceptive end-effector measurement. A custom written program in C++ (Microsoft, Redmond, WA) captured all touch responses, where the bullseye center of the target was normalized to a 40-pixel diameter of the touchscreen's 1920 x 1080 resolution. Additionally, a data acquisition (DAQ) unit hardware synchronized all measurements into a custom written LabVIEW program (2012 version, National Instruments, Austin, TX). Figure 5 is an image of the measurement setup and shows the touchscreen with the five bullseye targets, the force plate, DAQ, metronome speaker, and OEMC. Lastly, what is not seen in Figure 5 is the surface electromyography (sEMG) measurement system; however, Figure 13 does show the sEMG measurement system (i.e., Bagnoli 2-Channel sEMG System from Delsys, Natick, MA) and the location of each sEMG sensor: (1) Upper Trapezius, (2) Upper Pectoralis Major, (3) Medial Head of the Triceps, (4) Short Head of the Biceps, and (5) the grounding electrode. The chosen measurement spots are indicative of the muscle groups that are required to move the arm in front of, to oppose forward movement, and to flex and extend the arm at the elbow, which is the type of movement required for the experiment. The purpose of sEMG is to quantify muscle fatigue and maximum voluntary contraction (MVC) for the experiment.

The task procedure shown in Figure 8 is similar to a shuttle run scenario performed in a physical fitness test; however, the current procedure focuses the movement at the upper extremity. The sections of the shuttle run are seen in Figure 8 and starts with D1a (19.5 inches) to D2 (21.3 inches) to D1b (19.5 inches) and ends with D3 (11.8 inches), where the total length of the movement pattern for each participant is held constant at 72.1 inches. As the auditory pacing

increases, the difficulty increases and the potential for fatigue increases as well. Thus, anthropometry with respect to biacromial breadth, stature, and arm length factor into adequate performance across cycles for the open and constrained scenarios.

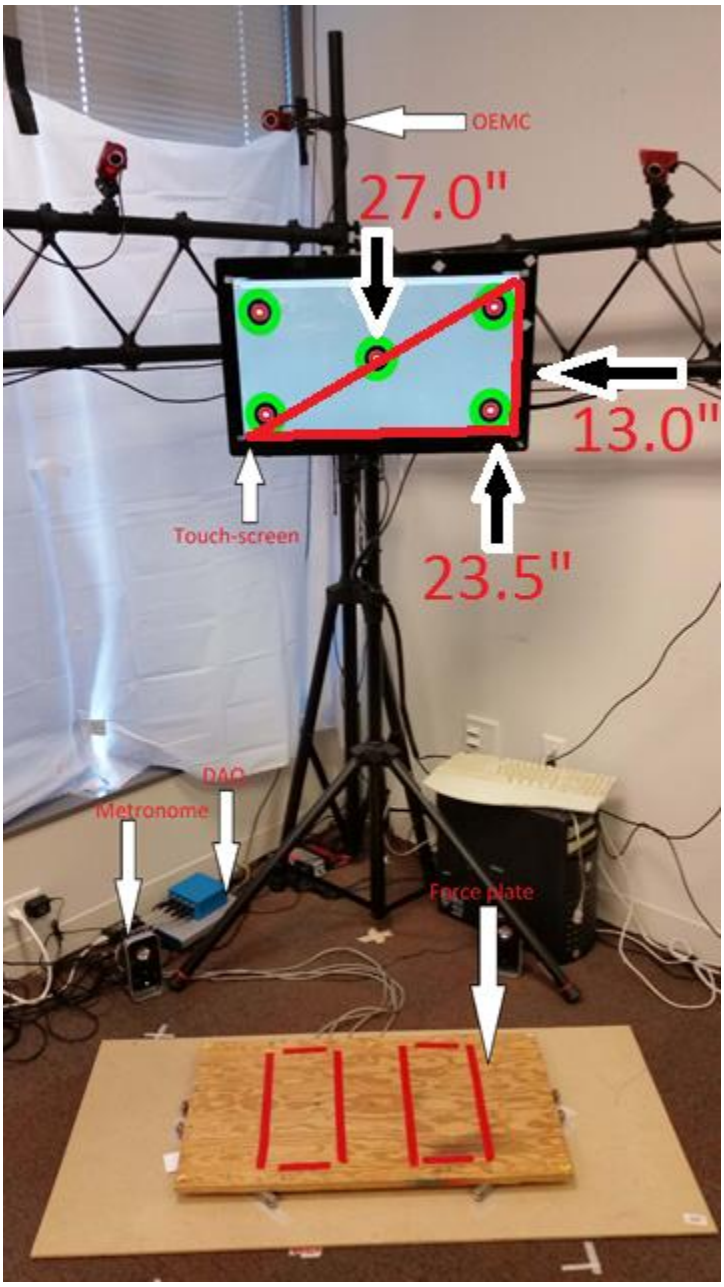

Figure 5. Provides a label of all the measurement modalities except sEMG

2.2.1 C++ Target Software Pixel Size

In order to settle on a center target with a diameter of 40 pixels, a pilot was performed to test the accuracy of several mixed-gender participants (i.e., four males and four females). The pilot results are shown in Figure 7, where the majority of the participants were within the 20-pixel center target with a few outliers; none of which exceeded 30 pixels. Each participant conducted six trials, where one trial was touching all five targets in five different sectors of the touchscreen following the movement pattern shown in Figure 8. The average for the eight participants was 7.8 pixels with a sample standard deviation of ±4.7. With a pretty high coefficient of variance of 60.8%, the design of the target considered three standard deviations in order to provide adequate coverage for a broad range of a sample population, where three standard deviations was determined at 28.4 pixels. Correlating anthropometric data for the width of the second digit yields a value of ~0.5in (13mm) for the 5th percentile female and ~0.8in (20mm) for the 95th percentile male (PeopleSize, 2008). It can be determined that 28.4 pixels is equal to ~0.3in (8.8mm); however, it should be noted that the plano-convex nature of the distal aspect of human phalanges is much less than the value of 0.5in, as seen in Figure 6. This would be considered the touching or interfacing aspect of the digit with a very sensitive capacitive touchscreen with a single pixel size of 311.25 x 311.25 µm per triad square, where a triad is the red, green, and blue (RBG) color combinations that make up the screens color palette. As a result of the participant tests, the experimental design established a 40-pixel diameter center target, which is ~0.5in (12.5mm) or greater than three standard deviations of the studies sample population.

Figure 6. The second phalange of the right upper extremity displaying the plano-convex nature of the fingertip (black lines).

For the actual measurement capture of touching the touchscreen, the Planar touchscreen has a 12ms response time. The stimulus from the metronome requires a movement for 0 Hz, 1 Hz, 1.3 Hz, 1.7 Hz, 2 Hz, and 2.7 Hz, there is a total of six stimuli with one cycle per stimuli. The movement for the metronome stimulus is 1s, 0.75s, 0.6s, 0.5s, and 0.375s, respectively. With a 12ms touchscreen response time, the conversion to seconds yields 0.012s, which demonstrates that the touch response speed is robust enough to handle the stimulus conditions proposed for this experiment.

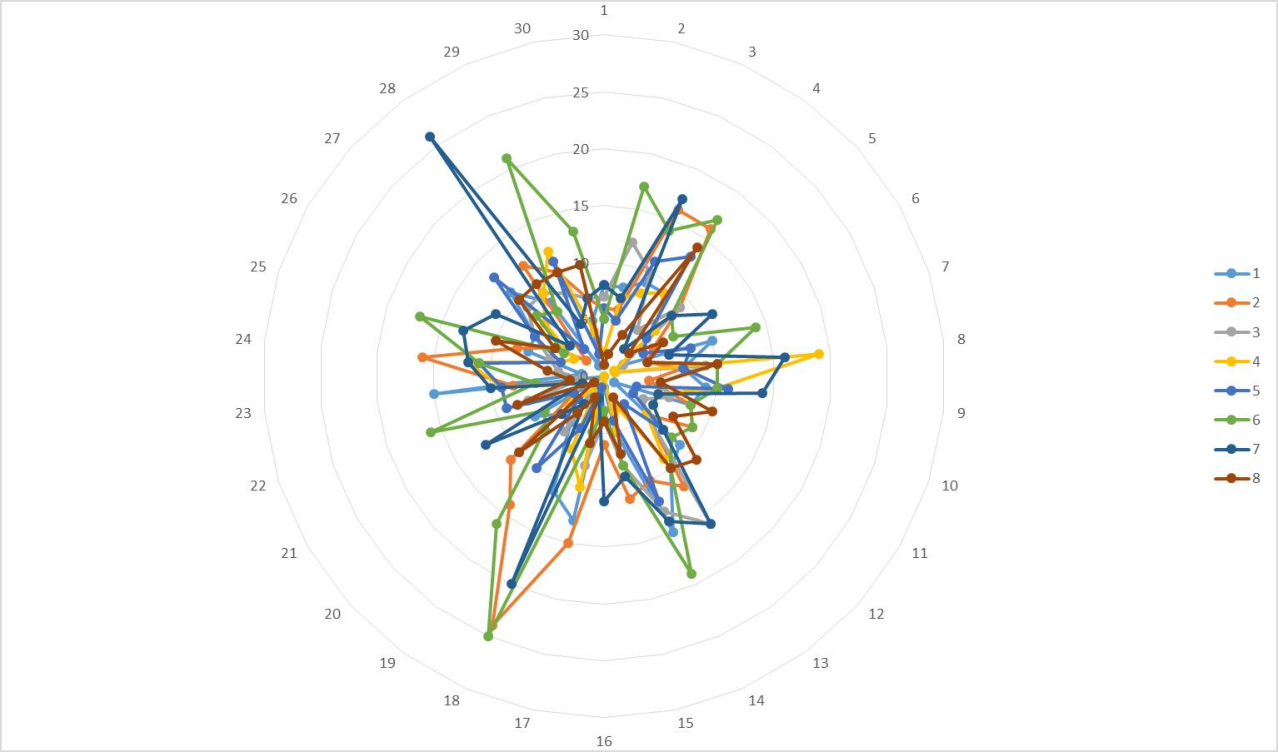

Figure 7. Radial plot of accuracy of touching the center of the target of eight pilot subjects (with distance measured, in pixels, from absolute center of the target)

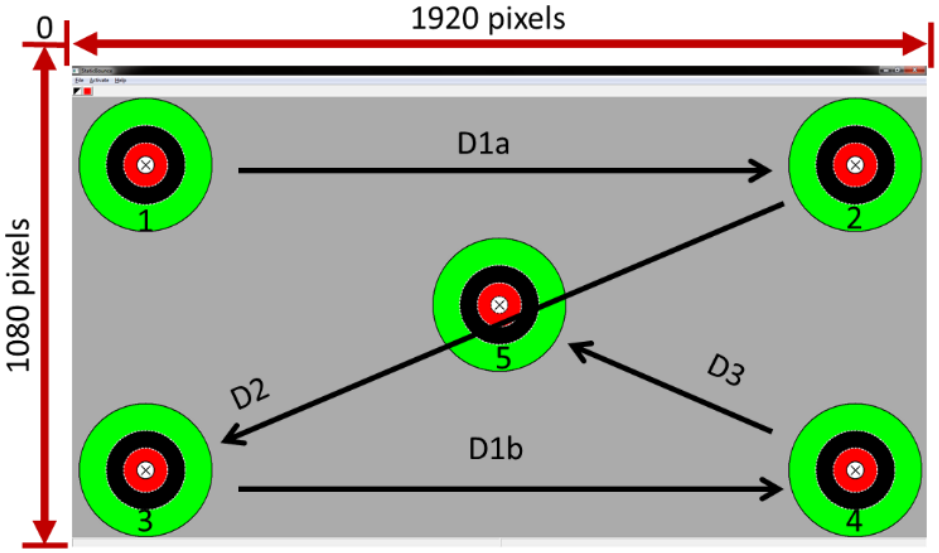

Figure 8. Pre-determined movement procedure throughout five touchscreen quadrants (total movement displacement 5,890 pixels (px) or 72.1in, where D1a & b = 1595px or 19.5in; D2 = 1736px or 21.3in; D3 = 964px or 11.8in) where the subject repeated the path five times (i.e., one experimental cycle)

In certain circumstances, participant touches were not registered. This is either due to double touching with the knuckles of the same hand, not touching the target with the appropriate pressure, long finger nails, or oils on the participants second digit or touchscreen (even though the second digit/touchscreen was wiped with an alcohol prep-pad at the experiment start to mitigate oils). When touches were not registered, the participant received a green location touch in all instances, where the touch location was the same for all participant as a means of consistency and control. As a result, the distance from center for the one target is 113px, the second target is 133px, the third target is 119px, the fourth target is 119px, and the fifth target is 117px, as seen in Figure 8.

2.2.2 Angular Joint Displacement Measurement

The technique developed by Peterson (1999) using Opto-Electronic Motion Capture (OEMC) to measure and track an infrared marker in three-dimensional space on the fingers of a keyboard typist was novel. At that time, OEMC units were widely used; however, they tracked large structures, such as the legs and the hips in the case of gait analyses using a rigid body approach (Peterson, 1999). This was impart due to the size and shape of the markers and the optical and digital limitations of the system. The size ratio of the marker to the measured object is critical in assessing skeletal kinematics of the body. The smaller the marker is in diameter and height the more accurate a representation of the palpated bony landmarks (Peterson, 1999).

Figure 9. The retro-reflective marker used for the current assessment was a half centroid with a diameter of 12.08mm and a height of 7mm.

OEMC systems are able to calculate the orientation of a rigid body by specifying a unit orthogonal axis from three markers whose positions are defined by palpating anatomical landmarks (Peterson and Bronzino, 2015). Several methods exist to define a rigid body: Euler/Cardan angles, attitude vector, screw/twist axis method, and planar projections (Peterson, 1999; Tupling and Pierrynowski, 1987; Woltring, 1994; Chao, 1980).

Euler or Cardan (or Tait-Bryan) angles are very similar but Cardan angles represent rotations about three distinct axes (e.g., x-y-z), while Euler angles could use the same axis for both the first and the third elemental rotations (e.g., z-x-z). Euler rotations are an accepted method for assessing lower extremity orientations, but not for upper extremity orientations. This is due to a major issue called Gimbal Lock, which occurs when two axes fall on the same axis line and is not typically a factor in the dynamics of large rotations in gait analyses. It has been determined that there is a greater error threshold for posture calculations of the upper extremity when using the Euler method (Tupling and Pierrynowski, 1987; Chao, 1980; Coates and Peterson, 2007). In addition to Gimbal Lock, Euler angles are influenced by cross talk, where rotations from one

plane influence rotations on the other two planes (Coates and Peterson, 2007). This effect can be exacerbated as rotations get larger.

A method using attitude vectors takes advantage of quaternion calculations to interchange the rotation matrix for anatomical rotations. This, in essence, defines a single rotation about an axis and coverts the rotation into three Euler angles (Tantawy, 2012). The benefit of attitude vectors is avoiding Gimbal Lock and cross talk, but their major limitation is the complex calculations and the lack of direct anatomical correlation (Woltring, 1994).

The screw/twist axis method uses an axis that is simultaneously the axis of rotation and the line along which translation of an item or body occurs. In Euclidean movements, the screw axis can be isolated into a rotation about, and a slide along, the same axis. Due to the complex dexterity of human upper extremity movement, defining such movement using the screw/twist axis method is not readily feasible. This method best describes robotic movements, protein molecular manipulation, and single anatomical joint moments such as the knee.

The planar projection method involves projecting the unit coordinate axes of the body segments onto anatomical planes to calculate their orientation with respect to a referenced anatomical body segments. The planar projection method has been successfully used by several researchers to calculate intricately complex movement of the upper extremity (Peterson and Cherniack, 2001a; 2001b; Coates and Peterson, 2007; Chowaniec and Peterson, 2007; Peterson et al., 2012; Tantawy, 2012). With the planar projection method, errors occur when the reference vector on the projection plane rotates about an axis of the two-dimensional planar projection. The error

that occurs when this happens can be quantified and calculated along with the angle values (Peterson, 1999). The planar method circumvents the Gimbal Lock issue and it directly associates to anatomical conventions for flexion/extension, abduction/adduction, and medial/lateral rotations, thereby making it very easy for clinicians to interpret.

Due to the ease of interpreting planar projections and the ability to quantify the maximum projected angle error for an entire test sequence, simple anatomical marker locations were used to expound upon the planar projection method defined by Peterson (Peterson, 1999). Figure 10, provides an image of the marker locations on the upper extremity as defined in the Experimental Protocol provided in Appendix B. Table 3, provides a list of the palpated bony land marks with which the retro-reflective makers seen in Figure 10 was applied with double sided tape.

In calculating upper extremity angles, an understanding of the rotational degrees of freedom (DoF) of the individual components of the upper extremity is necessary. The shoulder or glenohumeral joint has 3 DoF: flexion and extension, adduction and abduction, and internal and external rotation. The elbow on the other-hand has 1 DoF: flexion and extension. Similar to the shoulder, the wrist has 3 DoF: flexion and extension, adduction and abduction, and pronation and supination. When the DoF for a goal directed movement such as a pointing task is assessed, the DoF can decrease dramatically. This is a result of a phenomenon called self-organization, which is the ability of the motor control system to conduct itself in a manner that does not require supervisory control (Frank et al., 2006). As a result of self-organization, the DoF available at the motor control system is reduced once motion is carried out at the end-effector. If the architectural makeup of a PC hard drive configuration is considered, there can be two or

more hard drives connected with only one wire, where a master and slave relationship is established. The concept of self-organization is very similar in that, as the attached arm components move away from the motor control unit sequentially, they become slaves to the prior component. Therefore in a goal directed pointing task, the shoulder is the master and the elbow is slave to the shoulder, the wrist is slave to the elbow, and the second digit is slave to the wrist (Haken, 1977). A type of synergy is accomplished in-order to optimally perform a goal directed movement. Thus, there are 3 DoF for the upper extremity considered in this experiment: the shoulder has 2 DoF (i.e., flexion and extension and adduction and abduction), the elbow has 1 DoF (i.e., flexion and extension), and the wrist has 0 DoF. This result identifies the necessary parameters when performing angular kinematic analyses of the upper extremity that is specific to this goal-directed pointing movement.

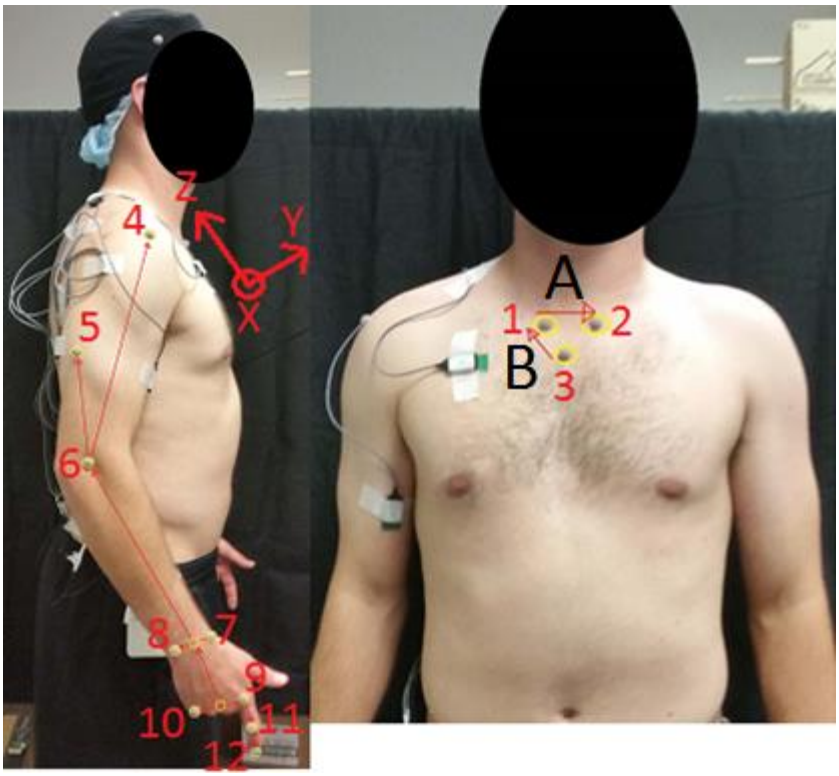

Figure 10. Palpated bony landmarks for upper extremity (4-12) and torso (1-3) marker placement

Table 3. The palpated bony landmarks shown in Figure 10

# of Markers	Matlab Abbreviation	Anatomical Name
1	TorsoSCR	Sternoclavicular Joint Right
2	TorsoSCL	Sternoclavicular Joint Left
3	TorsoMS	Manubrium Sterni
4	ArmGT	Greater Tubercle
5	ArmTri	Tricep (muscle belly of the lateral head of tricep)
6	ArmLE	Lateral Epicondyle
7	ArmRS	Radial Styloid
8	ArmUS	Ulna Styloid
9	Arm2MCP	Second Metacarpophalangeal Joint
10	Arm5MCP	Fifth Metacarpophalangeal Joint
11	ArmHPP	Hand Head of Proximal Phalange
12	ArmTDP	Hand Tuberosity Distal Phalange

A 16-camera OEMC system sampled data at 25 frames per second, where data was cleaned and the marker coordinate information was exported into comma separated value (CSV) format using a proprietary program of the OEMC system (Motive Body 1.8.0, Natural Point, Corvallis, OR). Custom MATLAB (Mathworks, Natick, MA) programs were written to import the CSV, rearrange the order of the file, and save the data in Microsoft Excel format for manipulation and calculation of the projection angles.

Prior to performing angle calculations, it is necessary to standardize the local orthogonal axis with the global orthogonal axis. To standardize the orientation convention of the orthogonal axes, each body segment was assumed to be a rigid body. In calculating the local orthogonal axes, a similar convention was used by Tantawy (2012) with opposite directions for the X and Y axis. The axis orientation on the torso (markers: 1-3) in Figure 10 represents the orthogonal axes for the arm (markers: 4-6), forearm (markers: 6-8), and the wrist (markers: 7-10). Vectors were calculated using the markers that defined the torso (markers: 1-3), arm (markers: 4-6), forearm (markers: 6-8), and wrist (markers: 7-10) (see Figure 10). Equation 1a and 1b, generically represents how vectors are calculated using the (X,Y,Z) components from the OEMC data. Once the vectors are calculated, normal vectors are calculated using Equations 2a and 2b, where $\vec{A}$ and $\vec{B}$ in this instance represents 'A'and 'B' in Figure 10 respectively; and $|A|$ and $|B|$ is their magnitude. The orthogonal axis starts to take shape with the cross product in Equation 3. The cross product results in a vector normal to the crossed vectors (Figure 11).

$$\vec{A} = (X_2 - X_1)\hat{\imath} + (Y_2 - Y_1)\hat{\jmath} + (Z_2 - Z_1)\hat{k} \quad (1a)$$

$$\vec{B} = (Y_4 - Y_3)\hat{\imath} + (Y_4 - Y_3)\hat{\jmath} + (Z_4 - Z_3)\hat{k} \quad (1b)$$

$$\overrightarrow{eA_x} = \frac{\vec{A}}{|A|} = \frac{A\hat{\imath}+A\hat{\jmath}+A\hat{k}}{\sqrt{A\hat{\imath}^2+A\hat{\jmath}^2+A\hat{k}^2}} \quad (2a)$$

$$\overrightarrow{eB_t} = \frac{\vec{B}}{|B|} = \frac{B\hat{\imath}+B\hat{\jmath}+B\hat{k}}{\sqrt{B\hat{\imath}^2+B\hat{\jmath}^2+B\hat{k}^2}} \quad (2b)$$

$$\vec{C}_y = \overrightarrow{eA_x} \times \overrightarrow{eB_t} \quad (3)$$

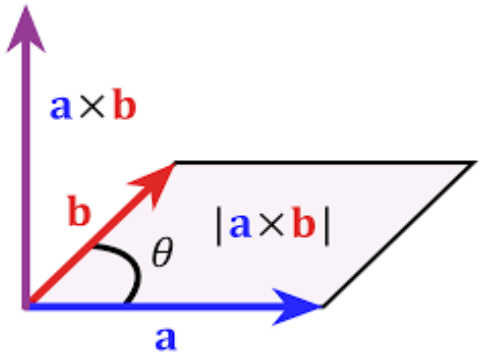

Figure 11. An example of the cross product (Sobolev, 2015)

Once the axes met a standard orientation, the global reference plane needed to be rotated to reflect the angle of the chest, in-order to accurately calculate shoulder abduction and adduction angles. Thereafter, neutral posture files were captured for each participant individually, where the participant stood still for 2 seconds. With a sampling rate of 25 Hz, that was 50 data points that were averaged and an angle was calculated using Equation 4, where A and B are 3D vectors and $|A||B|$ are their magnitude vectors (Tantawy, 2012; Peterson, 1999).

$$\theta = \cos^{-1}\left(\frac{\vec{A}\cdot\vec{B}}{|A||B|}\right) \tag{4}$$

As previously mentioned, the rotation for the purposes of this dissertation was about the X – axis, using a rotation matrix in Equation 5. Equation 6, reflects the newly rotated coordinate system, where $\hat{\imath}, \hat{\jmath}, \ and\ \hat{k}$ are the original coordinates and $\hat{\imath}'$, $\hat{\jmath}'$, and $\hat{k}'$ are the rotated coordinates.

$$R_x(\theta) = \begin{bmatrix} 1 & 0 & 0 \\ 0 & \cos\theta & -\sin\theta \\ 0 & \sin\theta & \cos\theta \end{bmatrix} \tag{5}$$

$$\begin{bmatrix} \hat{\imath}' \\ \hat{\jmath}' \\ \hat{k}' \end{bmatrix} = \begin{bmatrix} 1 & 0 & 0 \\ 0 & \cos\theta & -\sin\theta \\ 0 & \sin\theta & \cos\theta \end{bmatrix} \begin{bmatrix} \hat{\imath} \\ \hat{\jmath} \\ \hat{k} \end{bmatrix} \tag{6}$$

After rotating all the 3D vectors, 2D projection calculations were performed using Equations 7a, 7b, and 7c, and angular displacements between the projections were calculated using Equation 8.

$$\vec{A}_{XY} = (X_2 - X_1)\hat{\imath} + (Y_2 - Y_1)\hat{\jmath} \quad \text{and} \quad \vec{B}_{XY} = (X_4 - X_3)\hat{\imath} + (Y_4 - Y_3)\hat{\jmath} \tag{7a}$$

$$\vec{A}_{YZ} = (Y_2 - Y_1)\hat{\jmath} + (Z_2 - Z_1)\hat{k} \quad \text{and} \quad \vec{B}_{YZ} = (Y_4 - Y_3)\hat{\jmath} + (Z_4 - Z_3)\hat{k} \tag{7b}$$

$$\vec{A}_{XZ} = (X_2 - X_1)\hat{\imath} + (Z_2 - Z_1)\hat{k} \quad \text{and} \quad \vec{B}_{XZ} = (X_4 - X_3)\hat{\imath} + (Z_4 - Z_3)\hat{k} \tag{7c}$$

$$\theta_D = \cos^{-1}\left(\frac{\overrightarrow{A_{YZ}}\cdot\overrightarrow{B_{YZ}}}{|A_{YZ}||B_{YZ}|}\right) \tag{8}$$

As part of the planar projection assessment, understanding the limits of the method was vital to accurately portraying joint motions of the upper extremity. Y-Z planar projections measured the flexion and extension for three components of arm movement. First was the angle at the shoulder, where the reference vector was the torso vector, $\hat{\boldsymbol{k}}$, and the moving vector was the shoulder or commonly called the arm. Second, for the angle at the elbow, the reference vector, in this case, was the arm and the moving vector was the forearm. Lastly, for the angle at the wrist, the reference vector was the forearm and the moving vector was the wrist. Error angles in the Y-Z plane were taken with the arm vector rotating in 5 degree increments about a line penetrating the Greater Tubercle marker and parallel to the global Y-axis. The X-Y projection captured ulnar and radial deviations of the wrist. This time, the reference vector was the forearm and the moving vector was the wrist. Similarly, error angles were calculated for the Y-X projection with the forearm rotating about a line penetrating the lateral epicondyle marker and parallel to the global Y-axis in 5 degree increments. X-Z projections measured the abduction/adduction of the arm and forearm. In the case for abduction/adduction, the torso vector, $\hat{\boldsymbol{k}}$, was the reference vector and the arm was the moving vector. Error angles in the X-Z plane were taken with the vector, $\hat{\boldsymbol{\imath}}$, as the reference vector while the torso vector, $\hat{\boldsymbol{k}}$, rotates about a line parallel to the global Z-axis in 5 degree increments. In both the Y-X and X-Z angle errors at each rotation increment of 5 degrees, the flexion/extension, abduction/adduction, and radial/ulnar deviations were performed with their respective planes through the full range of motion of a goal directed movement for the largest anticipated angle of the entire testing sequence. Due to the nature of the goal directed pointing movement and the analysis method, it is was not necessary to calculate pronation/supination due to the fact that the forearm remained pronated throughout the movement of the entire testing sequence.

The error angle measurement was conducted as part of the validation procedure. A Computer Aided Design (CAD) program (Solidworks, Dassault Systems, Waltham, MA) was used to perform error angle measurements as previously described by Peterson (1999). Tables 4, 5, and 6 encompass the error angles for Y-Z projections, X-Z projections, and X-Y projections, respectively, where the error angle is the difference between the actual angle and the projected angle based on 5 degree rotations.

Table 4. Y-Z projection reference vector angle error rotations

Rotation Angle About a Vector Parallel to the Y-axis at the Shoulder			Angle Projected Between the Reference Vector (Arm) and Moving Vector (Forearm)															
start at 90	Angle between arm		5	10	15	20	25	30	35	40	45	50	55	60	65	70	75	80	85
	85	5	0	0	0	0	0	0	0	0	0	0	0	0	0	0	0	0	0
	80	10	0	0	0	0	0	0	0	0	0	0	0	0	0	0	0	0	0
	75	15	0	0	1	1	1	1	1	1	1	1	1	1	1	1	0	0	0
	70	20	0	1	1	1	1	2	2	2	2	2	2	2	1	1	1	1	0
	65	25	1	1	1	2	2	3	3	3	3	3	3	2	2	2	1	1	0
	60	30	1	2	2	3	3	4	4	4	4	4	4	3	3	3	2	1	1
	55	35	1	2	3	4	5	5	6	6	6	6	5	5	4	3	3	2	1
	50	40	2	3	4	5	6	7	7	8	8	7	7	6	5	4	3	2	1
	45	45	2	4	6	7	8	9	10	10	10	9	9	8	7	6	4	3	1
	40	50	3	5	8	10	11	12	12	13	12	12	11	10	8	7	5	4	2
	35	55	4	7	10	12	14	15	16	16	15	14	13	12	10	8	6	4	2
	30	60	5	9	13	16	18	19	19	19	18	17	16	14	12	10	7	5	3
	25	65	7	13	17	21	23	24	24	23	22	20	19	16	14	11	9	6	3
	20	70	9	17	23	27	29	29	29	28	26	24	22	19	16	13	10	7	3
	15	75	14	24	31	35	36	36	35	33	30	28	25	22	18	15	11	7	4
	10	80	22	35	42	44	45	43	41	38	35	32	28	24	20	16	12	8	4
	5	85	40	54	57	57	54	51	48	44	40	36	32	27	23	18	14	9	5

Table 5. X-Z projection reference vector angle error rotations

Rotation Angle About a Vector Parallel to the Z-axis at the Torso			Angle Projected Between the Reference Vector (Torso) and Moving Vector (Arm)															
start at 85	Angle between arm		5	10	15	20	25	30	35	40	45	50	55	60	65	70	75	80	85
	85	5	0	0	0	0	0	0	0	0	0	0	0	0	0	0	0	0	0
	80	10	0	0	0	0	0	0	0	0	0	0	0	0	0	0	0	0	0
	75	15	0	0	0	1	1	1	1	1	1	1	1	1	1	1	1	0	0
	70	20	0	1	1	1	1	2	2	2	2	2	2	2	1	1	1	1	0
	65	25	0	1	1	2	2	2	3	3	3	3	3	3	2	2	1	1	1
	60	30	1	1	2	3	3	3	4	4	4	4	4	4	3	3	2	2	1
	55	35	1	2	3	3	4	5	5	6	6	6	6	5	5	4	3	2	1
	50	40	1	2	3	4	5	6	7	7	8	8	7	7	6	5	4	3	2
	45	45	1	3	4	6	7	8	9	9	10	10	10	9	8	7	6	4	2
	40	50	2	4	5	7	8	10	11	12	12	13	12	12	11	10	8	5	3
	35	55	2	4	6	8	10	12	13	14	15	16	16	15	14	12	10	7	4
	30	60	3	5	7	10	12	14	16	17	18	19	19	19	18	16	13	9	5
	25	65	3	6	9	11	14	16	19	20	22	23	24	24	23	21	17	13	7
	20	70	3	7	10	13	16	19	22	24	26	28	29	29	29	27	23	17	9
	15	75	4	7	11	15	18	22	25	28	30	33	35	36	36	35	31	24	14
	10	80	4	8	12	16	20	24	28	32	35	38	41	43	45	44	42	35	22
	5	85	5	9	14	18	23	27	32	36	40	44	48	51	54	57	57	54	40

Table 6. X-Y projection reference vector angle error rotations, where (A) is a flexion at the elbow and (B) is an abduction at the shoulder where the elbow is held at 90^{o} flexion

A)

Rotation Angle About a Vector Parallel to the Y-axis at the Elbow			Angle Projected Between the Reference Vector (Forearm) and Moving Vector (Wrist)					
start at 85	Angle between arm and forea		5	10	15	20	25	30
	85	5	0	0	0	0	0	0
	80	10	0	0	0	0	0	0
	75	15	0	0	1	1	1	1
	70	20	0	1	1	1	1	2
	65	25	1	1	1	2	2	3
	60	30	1	2	2	3	3	4
	55	35	1	2	3	4	5	5
	50	40	2	3	4	5	6	7
	45	45	2	4	6	7	8	9
	40	50	3	5	8	10	11	12
	35	55	4	7	10	12	14	15
	30	60	5	9	13	16	18	19
	25	65	7	13	17	21	23	24
	20	70	9	17	23	27	29	29
	15	75	14	24	31	35	36	36
	10	80	22	35	42	44	45	43
	5	85	40	54	57	57	54	51

B)

Rotation Angle About a Vector Parallel to the Y-axis at the Shoulder, Elbow Constant at 90 Flexion			Angle Projected Between the Reference Vector (Forearm) and Moving Vector (Wrist)					
start at 5	Angle between arm and f		5	10	15	20	25	30
		5	0	0	0	0	0	0
		10	0	0	0	0	0	0
		15	0	0	0	1	1	1
		20	0	1	1	1	1	2
		25	0	1	1	2	2	2
		30	1	1	2	3	3	3
		35	1	2	3	3	4	5
		40	1	2	3	4	5	6
		45	1	3	4	6	7	8
		50	2	4	5	7	8	10
		55	2	4	6	8	10	12
		60	3	5	7	10	12	14
		65	3	6	9	11	14	16
		70	3	7	10	13	16	19
		75	4	7	11	15	18	22
		80	4	8	12	16	20	24
		85	5	9	14	18	23	27

In addition to calculating the rotation error angles, random frames where chosen and angles with regard to flexion/extension, abduction/adduction, and radial/ulnal deviations were performed in Solidworks. The results were corroborated with the calculated angle results of the MATLAB program and Tables 4 through 6 affords a threshold level that is well within the movement pattern for the test sequence of the proposed research.

Lastly, in representing angular displacements with respect to joint motions the slope of a reference and moving vector was calculated to define a positive joint motion (extension and abduction), and a negative joint motion (flexion and adduction). Figure 12 shows an example of the marker configuration used to signify the reference and moving vectors that were analyzed using MATLAB (Mathworks, Natick, MA). In Figure 12, AB is the reference vector and BC is the moving vector.

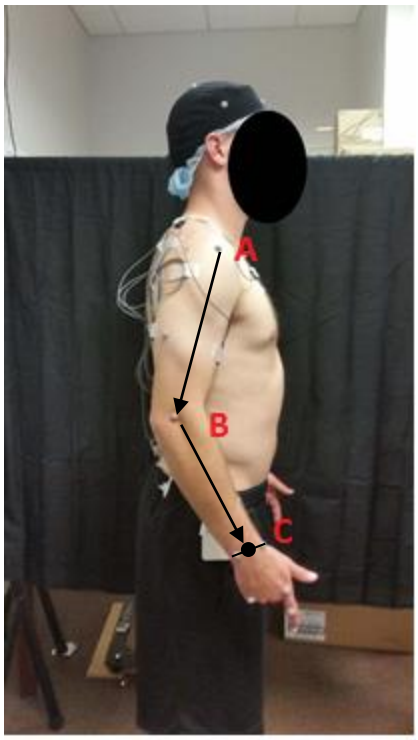

Figure 12. Reference and moving vectors to be projected on anatomical planes (Reference (AB) & Moving (BC) to capture elbow angle)

Lastly, angular velocities were also calculated using Equation 9, where the derivative of θ_D is taken with respect to time.

$$\omega = \frac{d\theta_D}{dt} \tag{9}$$

After data smoothing with a 7 point moving average to remove marker noise as a result of motion artifact, all kinematic data is assessed with respect to trials 2, 3, and 4 of the 5 trial cycle per stimulus in the open and constrained scenarios.

2.2.3 Surface Electromyography Measurement

Figure 13 shows the anatomical positions with which muscle voltage potentials were captured. Prior to placing the electrodes, the skin was prepared as per the guidelines in the protocol, as described in Appendix B. The electrodes were positioned in parallel with the muscle belly using an oscilloscope to capture the best signal to noise ratio of muscle activity. Figure 13, labels each of the sensors with respect to the superficial muscle voltage read. The locations are as follows: (1) Upper Trapezius, (2) Upper Pectoralis Major, (3) Medial Head of the Triceps, and (4) Short Head of the Biceps. Location (5) Grounding Electrode accounts for the ground electrode to read the voltage difference from the sensors. Additionally, item (6) is the Bagnoli 2 Channel EMG System (Delsys, Natick, MA). As can be seen in Figure 13, the Bagnoli system, although wired, is very portable and unencumbering to the participant. Double sided tape, as well as medical grade tape, was used to hold the sensor to the participant and to secure the sensor's wires.

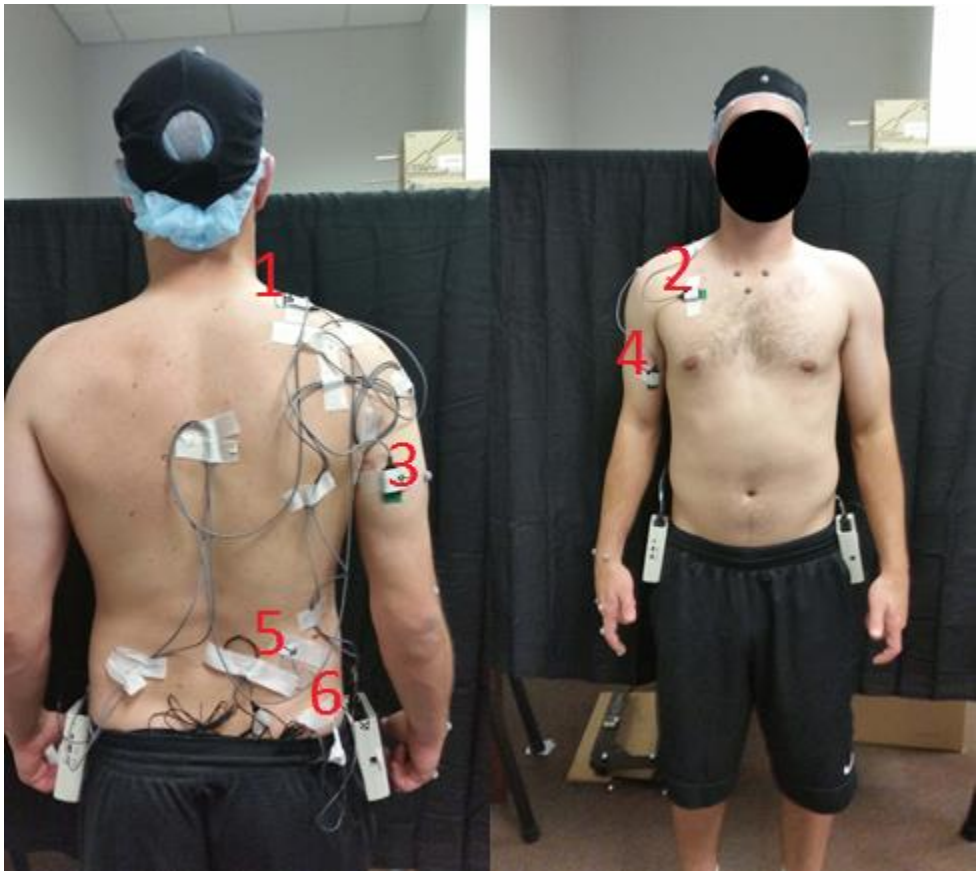

Figure 13. Portrays the sEMG measurement locations: (1) Upper Trapezius, (2) Upper Pectoralis Major, (3) Medial Head of the Triceps, (4) Short Head of the Biceps, (5) Grounding Electrode, and (6) Bagnoli 2 Channel EMG System.

The Bagnoli 2-Channel EMG System is bandpass filtered from 20 Hz (±5 Hz) to 450 Hz (±50). The system was set to a 1K gain and connected to the DAQ and raw data sampled at 4 kilo-samples per second (Ks/s). Participant comparisons were carried out via percent maximum voluntary contraction (MVC) and Muscle Fatigue analysis via Fourier transform.

For the MVC comparisons, the Bagnoli system settings were similar to the experiment setup except that the sampling rate was 2 kilo-samples per second. Five trial runs each, for 5 seconds each, were captured for each muscle group, shown in Figure 13, for every participant. Participants were asked to contract the muscle of interest as hard as they could and to hold that

contraction for a count of 5 seconds. The MVC data was full wave rectified using a 55ms root mean square window with no overlap or zero-pad on the last window (i.e., 110 samples given a sampling frequency of 2Ks/s). The maximum values for each of the 5 trials was averaged to denote the MVC voltage for each of the muscle groups in Figure 13 (Seils, 2012).

To compare and integrate the experiment data with the MVC, the experiment data was full wave rectified using a 110ms root mean square sampling window with no overlap or zero-pad on the last window (i.e., 410 sample given a sampling frequency of 4Ks/s) (Seils, 2012). Prior to performing this, the experimental data was split into the data which associated with trials 2, 3, and 4. Since the OEMC provided the discrimination of each trial within each stimuli cycle, there was a scaling factor that was necessary. The OEMC was captured at 25 Hz, and the sEMG was captured at 4K Hz. Therefore, a scaling factor of 160 was required. Trials 2, 3, and 4 were averaged for each of the specified muscle groups. Finally, Equation 10 was used to convert the V_{rms} to a percentage of MVC, where m_i is the experiment muscle value, and v_{mvc} is the participant's MVC for that particular muscle.

$$\%_{MVC} = \frac{\sum_{i=1}^{n} m_i}{v_{mvc}} \times 100 \quad (10)$$

The power of using MVC is that it allows the researcher to compare results across participants. This is due in part to each person's muscle contraction being an extremely subjective measure. Thus, to remove the subjectivity of the measure, the conversion to MVC is required.

2.2.4 Power Spectral Density Measurement

The muscle fatigue analysis leveraged the Fourier Transform, which is a mathematical formula that related a signal in time to the same signal sampled in frequency. In signal processing the Fourier transform can reveal important frequency component characteristics. In MATLAB, a built in function called the Fast Fourier Transform (FFT) is utilized. The FFT is a computationally efficient implementation of the Discrete Fourier Transform (DFT). Typically, a one-dimensional DFT uses n^2 floating-point operations for a vector of n data points. However, the FFT operation uses $n \log n$ operations, which drastically reduces the computational processing.

$$y_{k+1} = \sum_{j=0}^{n-1} \omega^{jk} \; x_{j+1} \tag{11}$$

Equation 11 is used to calculate the DFT, where i is the imaginary unit, $\omega = e^{-2\pi i/n}$ is one of n complex roots of unity, and j and k are indices that run from 0 to $n-1$. The x and y indicies are shifted by one to reflect MATLAB's starting vector indices. FFT was used within a custom written MATLAB code to perform the time to frequency domain conversion.

The firing rate of the motor units, or the number of cycles the motor unit depolarizes/repolarizes per unit time, is specific to the type of muscle fibers. The two predominate skeletal muscle fibers are Slow Twitch motor units, or Type I fibers, and Fast Twitch motor units, or Type II fibers. The predominate difference between Type I and Type II fibers are Type I are aerobic and thus have a higher number of mitochondria present than their Type II counterparts. As a result,

Type II fibers are anaerobic and thus fatigue at a faster rate than their Type I counterparts. Due to Type I carrying out oxidative phosphorylation, their contraction speed and conduction velocity are slow, versus fast for Type II fibers. Conduction velocity is the key factor in leveraging the FFT to move from the time to frequency domain. The muscle frequency range for Type I and Type II is from 10 Hz to 250 Hz depending on muscle function, and the distribution of Type I and II fibers within the muscle (Bellemare et al., 1983). Within this range, Type II have a frequency range from 126 to 250 Hz, and it is this salient range which signifies muscle fatigue or a decrease in conduction velocity. Fatigue signifies a decrease in amplitude and an increase in duration and, thus, a decrease in force (Enoka, 1994). To asses a frequency shift within the FFT, the median and mean frequencies are assessed pre-fatigue and post-fatigue to ascertain a shift from higher to lower frequencies. Figure 14, portrays the concept of a spectral shift of higher frequencies to lower frequencies.

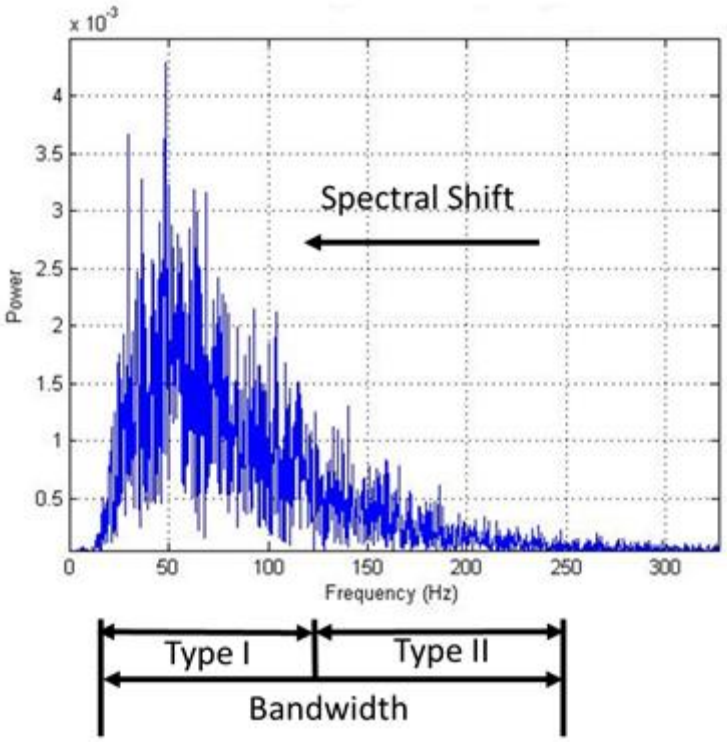

Figure 14. The concept of a shift within the frequency spectrum from Type II to Type I

In this study, since participants were allowed to rest between stimuli, pre-fatigue is the comparison of the 0 Hz to 2.7 Hz stimuli, with respect to the open and constrained scenarios. The power spectral density results were studied for all trials (trials 1, 2, 3, 4, and 5). This was done to look at the entire captured cycle as a means to develop a trend of spectral information so a more valid comparison to trials 2, 3, and 4 could be made. As a result, the median and mean was calculated at 1-second intervals for the entire cycle, thus 4,000 samples were analyzed for their medians and means. If a fatiguing shift was seen, then it would have lasted from the point of occurrence in the cycle until the end of the cycle. The median frequency is calculated using a built in MATLAB function called *interp1*. The function is given specific query points for a 1D data set and returns the results using linear interpolation.

$$MNF = \frac{\sum_{i=1}^{n} f_i P_i}{\sum_{i=1}^{n} P_i} \tag{12}$$

Equation 12 (Alty, 2011) was used to calculate the mean frequency of the FFT, where P_i is the *i*th line of the power spectrum, f_i is frequency, and n is the highest harmonic below the Nyquist Frequency. Taken holistically, the median and mean shifts, in-addition to the MVC, provide insight into muscular recruitment tendency and performance.

2.2.5 Center of Gravity (CoG) Measurement

The biomechanics of postural adjustments often involves upper extremity movement as well as shifts in the Center of Gravity (CoG). Measurement of such shifts in this dissertation are accomplished using a four-loadcell force plate (i.e., custom-built rectangular force plate having a

loadcell at each corner), where calibration and measurement error are of utmost importance in understanding how precise the quantities are and exactly what can be determined (Haung, 2009).

The approach to validate the measurement error for the force plate was performed using the Least Significant Bit (LSB) method. LSB is the smallest level that an analog-to-digital convertor (ADC) can convert or the smallest increment a digital-to-analog converter (DAC) can output. Either converter operates at the boundaries between the analog and digital realms, thus affording the ability for the analog circuit to communicate with the digital circuits and vice versa.

The DAQ used to capture voltage readings from four loadcells, after signal conditioning, was an NI USB 6363 (National Instruments, Austin TX), which is a 16-bit ADC. The setting for data capture through LabVIEW (National Instruments, Austin TX) was 4,000 Hz, with a 100 samples per second or 40 samples per second, where, for every 1 second of data, the LabVIEW program captured 40 data points. The general voltage reading was ±5V and, after calibrating the force plate by way of isolating each individual loadcell on a test block and placing a weight on the loadcell from 0 to 75 lbs, voltage readings were captured and a linear relationship was developed for each loadcell, as seen in Table 7. Additionally, Figure 15 is a graph of the data in Table 7, with the addition of a trend line with R^2 values. Loadcell 1 was observed to be the only load cell with an R^2 below one. The slope for the linear relationships was calculated for each loadcell and used in the next step in the measurement error validation.

Table 7. Calibration information for each loadcell of the force plate

Lbs	Volts Ch 1 #4498	Volts Ch 2 #4488	Volts Ch 3 #4497	Volts Ch 4 #4499
0	0.6420	0.6882	0.4794	0.6078
2.5	0.6659	0.7096	0.5052	0.6319
5	0.6929	0.7339	0.5265	0.6552
7.5	0.7139	0.7544	0.5512	0.6794
10	0.7400	0.7765	0.5754	0.7046
12.5	0.7625	0.7969	0.5994	0.7287
15	0.7908	0.8221	0.6245	0.7533
17.5	0.8150	0.8444	0.6483	0.7777
20	0.8371	0.8644	0.6722	0.7977
22.5	0.8606	0.8864	0.6961	0.8220
25	0.8874	0.9080	0.7211	0.8472
27.5	0.9095	0.9301	0.7450	0.8715
30	0.9349	0.9506	0.7706	0.8946
35	0.9856	0.9944	0.8175	0.9405
40	1.0260	1.0370	0.8663	0.9862
45	1.0775	1.0815	0.9167	1.0341
50	1.1238	1.1240	0.9675	1.0800
55	1.1695	1.1698	1.0159	1.1275
60	1.2168	1.2139	1.0630	1.1776
65	1.2670	1.2580	1.1123	1.2210
70	1.3599	1.3012	1.1614	1.2692
75	1.4140	1.3450	1.2100	1.3185

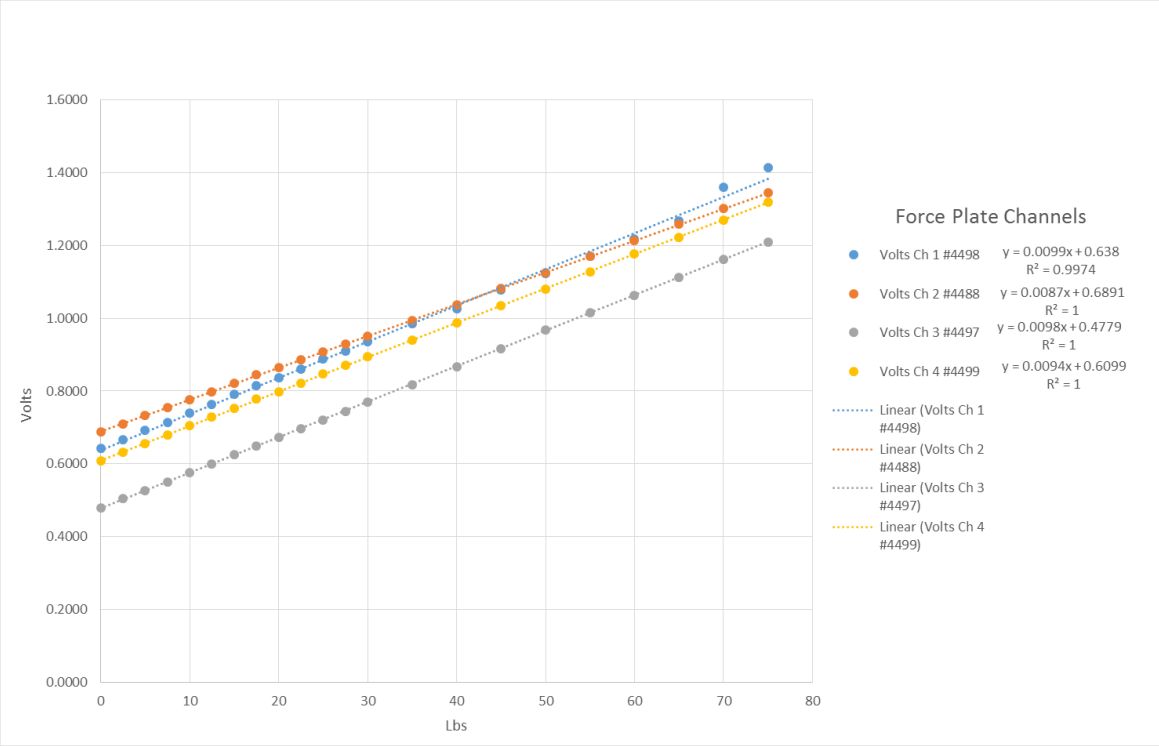

Figure 15. A graph of the four loadcell voltages with respect to weight in pounds. The linear fit for each loadcell's trend line's R^2 value is 0.99 for loadcell 1, and 1 for the other 3 loadcells.

The LSB formula is calculated with Equation 13, where $V_{ref}(+)$ is the +5 voltage reading, $V_{ref}(-)$ is the -5 voltage reading, and N is the ADC's number of bits,

$$LSB = \Delta V = \frac{|V_{ref}(+)|+|V_{ref}(-)|}{2^N} \tag{13}$$

Calculating CoG uses an X and Y relationship on the force plate, where, if you took a Cartesian coordinate system and overlaid it onto the force plate, the top and bottom would be positive Y and negative Y, respectively, the left and right side of the plate would be negative X and positive X, respectively, and the center would be the origin or the (0,0) point, as seen in Figure 16.

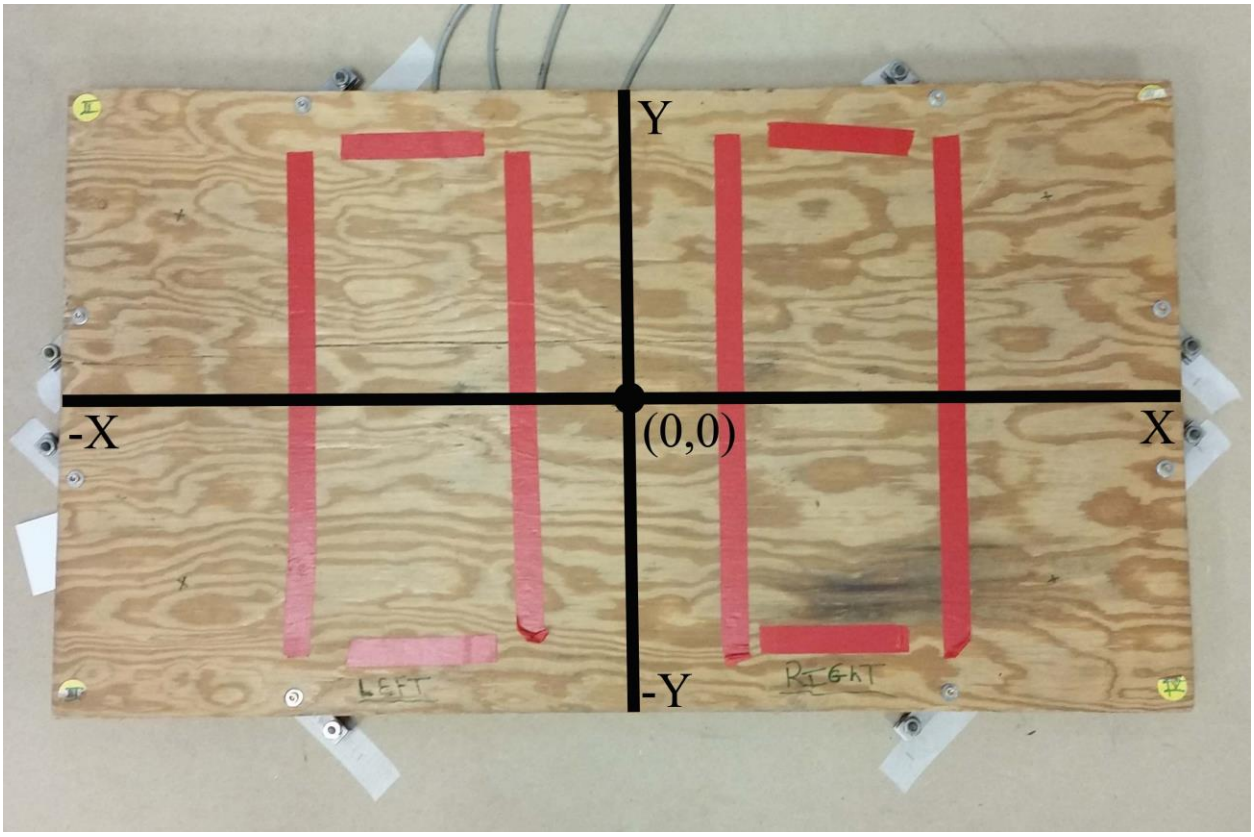

Figure 16. The force plate and the 4 quadrants of a Cartesian coordinate system

Now, utilizing the calibration information, particularly the slope of the lines, the ΔX and ΔY can be calculated by way of ΔVolts (or ΔV).

Table 8. Calculations to determine the LSB reading in pounds

	Slope	Slope * ΔV	Force Reading (lbs)
Loadcell 1 =F_1	100.3788	100.3788*0.000152588V	0.015316599
Loadcell 2 = F_2	114.4227	114.4227*0.000152588V	0.017459533
Loadcell 3 = F_3	102.5047	102.5047*0.000152588V	0.015640988
Loadcell 4 = F_4	105.9959	105.9959*0.000152588V	0.016173697

Table 8 provides the calculation that converted the voltage readings into force for each loadcell. Equations 14 and 15, respectively, calculated ΔX and ΔY readings, in inches, as the CoG shifts

on the force plate. In Equations 14 and 15, x_1 and y_1 are the physical measurement of the sensing areas of the force plate and these values are divided by 2 in order to designate the center starting location of (0, 0),

$$X = \frac{x_1}{2} \times (F_1 - F_2 - F_3 + F_4) \tag{14}$$

$$Y = \frac{y_1}{2} \times (F_1 + F_2 - F_3 - F_4) \tag{15}$$

Table 9 shows the various readings from the 16 different combinations of the four loadcell readings and X[in] and Y[in] are the result of Equations 14 and 15, respectively. Since the positions are calculated by the combinations of the four loadcell readings, the increment of X and Y displacement was determined to be 0.003 in the X directions and 0.001 in the Y direction. It should be noted that this is not the true meaning of the noise floor; rather, for this example, this is a result of the loadcells not being engaged or loaded. Lack of engagement of the loadcells produces random noise, which is then amplified by the signal conditioning box. Therefore, the minimum and maximum values for X and Y provide a ±0.4 in the X and a ±0.2 in the Y. To test this, weights were added to the force plate to assess the output. As the loadcells became loaded in increments of 10 pounds to a maximum of 30 pounds, the significant digits for the X and Y reading were valid to the second decimal place. To check that these measurements actually showed a reduction in the noise of the loadcells, the LabVIEW code was amended to produce a histogram of the X and Y position information of the force plate. The histogram information was then segregated into X-axis values and Y-axis values. Finally, the difference of a "Max" and "Min" function was used on the segregated data to show six standard deviations or ±3 sigma. One can, thus, conclude that the force plate reading is valid to 1/10 of an inch.

Table 9. Calculation of the various combinations of the 4 loadcells utilizing Equations 14 and 15 (values highlighted in green portend the possible resolution in the X and Y directions with absolute values taken)

Load Cell 1	Load Cell 2	Load Cell 3	Load Cell 4	X [in]
0	0	0	0	0.000
0	0	0	0.015849262	0.184
0	0	0.015830978	0	-0.184
0	0	0.015830978	0.015849262	0.000
0	0.016214483	0	0	-0.188
0	0.016214483	0	0.015849262	-0.004
0	0.016214483	0.015830978	0	-0.372
0	0.016214483	0.015830978	0.015849262	-0.188
0.015555467	0	0	0	0.180
0.015555467	0	0	0.015849262	0.364
0.015555467	0	0.015830978	0	-0.003
0.015555467	0	0.015830978	0.015849262	0.181
0.015555467	0.016214483	0	0	-0.008
0.015555467	0.016214483	0	0.015849262	0.176
0.015555467	0.016214483	0.015830978	0	-0.191
0.015555467	0.016214483	0.015830978	0.015849262	-0.007
			Max	**0.364**
			Min	**-0.372**

Load Cell 1	Load Cell 2	Load Cell 3	Load Cell 4	Y [in]
0	0	0	0	0.000
0	0	0	0.015849262	-0.081
0	0	0.015830978	0	-0.081
0	0	0.015830978	0.015849262	-0.162
0	0.016214483	0	0	0.083
0	0.016214483	0	0.015849262	0.002
0	0.016214483	0.015830978	0	0.002
0	0.016214483	0.015830978	0.015849262	-0.079
0.015555467	0	0	0	0.079
0.015555467	0	0	0.015849262	-0.001
0.015555467	0	0.015830978	0	-0.001
0.015555467	0	0.015830978	0.015849262	-0.082
0.015555467	0.016214483	0	0	0.162
0.015555467	0.016214483	0	0.015849262	0.081
0.015555467	0.016214483	0.015830978	0	0.081
0.015555467	0.016214483	0.015830978	0.015849262	0.000
			Max	**0.162**
			Min	**-0.162**

2.2.5.1 Center of Gravity (CoG) Analysis

Raw data samples were captured as tab delimited text files with a sampling rate at 4 Kilo-samples per second. These files were read into a custom written MATLAB code for processing. Prior to running the code, the start and stop of trials 2, 3, and 4 of each cycle were captured based on the OEMC kinematic data. Since the OEMC data was captured at 25 Hz, a scaling factor was necessary to processes the data. The scaling factor was 1.6, which was due to processing the data at 100 samples per second for a capture rate of 40 Hz.

$$D_x = \sum_{i=1}^{n} x_{i+1} - x_i \quad (16)$$

$$D_y = \sum_{i=1}^{n} y_{i+1} - y_i \quad (17)$$

$$x = \sqrt{{D_x}^2 + {D_y}^2} \quad (18)$$

$$t = 1/f \quad (19)$$

$$v = \frac{dx}{dt} \quad (20)$$

$$a = \frac{dv}{dt} \quad (21)$$

CoG displacement was calculated using Equations 16 and 17, where x_i and x_{i+1} represent the initial and consecutive movement in the X-axis of the force plate, respectively. Similarly, y_i and y_{i+1} represent the initial and consecutive movement in the Y-axis of the force plate, respectively. Equation 18 is the magnitude of the X and Y vectors, while Equation 19 defines how the time is calculated. Recall that the frequency is 40 Hz, which defines f. Lastly, Equations 20 and 21 are the first and second derivative, respectively, of Equation 18 with respect to time. As a result,

displacement, velocity, and acceleration are calculated for the force CoG postural adjustment with respect to upper extremity goal directed movement.

2.2.6 Equipment Integration

The equipment connection and time synchronization are diagramed in Figure 17.

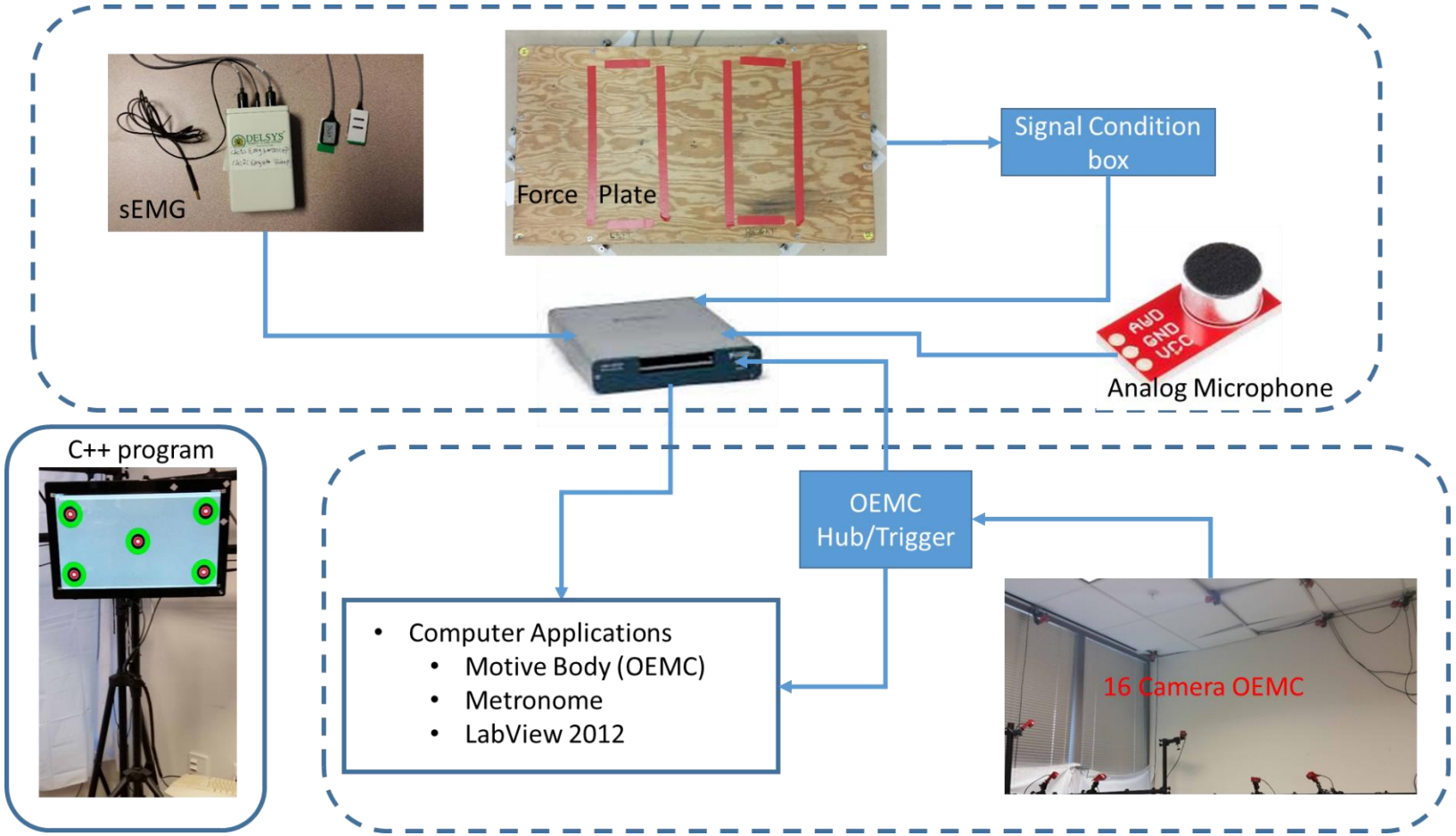

Figure 17. Equipment connection and hardware synchronization

Figure 17 shows all the measurement equipment connections and hardware trigger, while the touchscreen and C++ program are stand alone. This is due to the fact that, in the sequence of motor execution, the touchscreen is the end parameter and therefore is not dependent on any other item. The C++ code is programed to capture the X and Y pixel coordinate of the touched point on the touchscreen. Additionally, the program keeps a time stamp for each target touched and the time stamp does not initiate until the first target is touched. The DAQ and OEMC are both connected to the same computer to alleviate inconsistencies in central processing unit clock cycles. Running on the computer is the Motive Body 1.8 software for the OEMC, the metronome software (TempoPerfect 4.08), and LabVIEW 2012. All the connection protocols for the DAQ and OEMC hubs were universal serial bus (USB) version 2.0 as the OEMC hubs connect to the computer and send a hardware trigger in the form of a +5 volt spike to the DAQ. As a result, the LabVIEW software, once engaged, enters a dormant mode until the start execution occurs on the Motive Body software. Prior to starting the Motive Body, the participant is readied and then the metronome software is engaged, which is sequentially followed by the start of the Motive Body OEMC software. DAQ connections consist of the sEMG system, the signal conditioning box for the force plate, and the analog microphone. The microphone captures the sounds emitted from the metronome software to allow for the investigation of timed correlations between a screen touch and the actual stimulus.

3. Statistical Analysis

Following the experimental design and methodology, descriptive statistics of the kinematic, terminal touch point, sEMG, and Force data are presented in various tables in the results section.

The premise of the study was to understand goal directed movement with respect to anthropometry. The three prominent anthropometric characteristics that contribute to a goal directed movement in a standing posture are: stature, arm length (acromion to 3 distal phalange), and shoulder breadth (biacromial). As a result, an analysis of variance (ANOVA) was conducted on the main effects of, and interaction between, shoulder breadth (biacromial), and arm length (acromion to 3 distal phalange) in comparison to the respective anthropometric lengths of the 50^{th} percentile male for the open and constrained scenarios (see Figures 18 and 19). Additionally, an ANOVA was also conducted on the main effect of and interaction between the six stimuli (0 Hz or no stimulus, 1 Hz or 60 beats per minute (BPM), 1.3 Hz or 80 BPM, 1.7 Hz or 100 BPM, 2 Hz or 120 BPM and 2.7 Hz or 160 BPM). ANOVA is a technique which tests for the difference in group means. This is done by bifurcating the total variation into two components: the variation of group means from the overall mean and the variation of observations in each group from their group mean results. In essence, ANOVA separates the total sum of squares into the sum of squares due to the effect occurring between groups and the sum of squared errors. As a result, ANOVA compares the between group variation to the variation within groups. A ratio of within-group variation to between-group variation being high warrants the group means being significantly different from each other. This is measured using an F-distribution where significance is an F-value greater than the F-critical value and a $p < 0.05$. Rejection of the null hypothesis leads to the conclusion that not all of the group means are the same; however, ANOVA's limitation is that it does not provide information as to which group means are actually different. Therefore, when significant interactions were found, post hoc Tukey-Kramer, and Bonferroni-Holm tests were performed to determine which variable produced the effect. The Tukey's honestly significant difference procedure or Tukey-Kramer is

ideal for a one-way ANOVA with equal sample sizes. However, Tukey-Kramer has also been proven conservative for a one-way ANOVA with different sample sizes. The Bonferroni method is an eloquent way to compare various statements, while still maintaining an overall confidence coefficient. Bonferroni utilizes an ANOVA approach, where a set of pairwise comparisons are picked in advance. The Bonferroni is fairly robust in that its pairwise comparisons are not infinite, but they do exceed the pairwise comparisons specified in the Tukey-Kramer procedure. Additionally, the Bonferroni method is valid for equal and unequal sample sizes.

The null hypothesis in this dissertation is to accept that there is not a significant difference between the means of a dataset versus rejecting the null for the alternative hypothesis, where there is a significant difference between a means of a dataset. Unfortunately, all participants in this study were under 69.6" (PeopleSize, 2008), which is the stature of the 50^{th} percentile male, so stature comparisons were not considered except from a gender perspective. Thus, participants were initially separated by gender, since traditionally male anthropometries tend to be larger than female anthropometries. A t-test assuming unequal variances showed a significant difference of $p = 0.0003$ between the mean statures of females (63.4") and males (69.2"). Additionally, the stature coefficient of variance in this dissertation was 4.9%, which was equal to the arm length (acromion to 3 distal phalange). In order to understand additional anthropometric dimensions contributing to design performance, arm length and shoulder breadth were considered. Four participants had lengths greater than the 50^{th} percentile male, as seen in Figure 19. The rational for basing the comparison with the 50^{th} percentile males lies in design strategy, where, with respect to a normal distribution, the 50^{th} percentile is the majority of the population. Even more so, the 50^{th} percentile male encompasses the $5 - 95^{th}$ percentile female demographic of the Navy's anthropometric design range (ASTM Standard F 1166-07, 2007). Normal design

practice is to design for the 50th percentile male demographic, since it accounts for a large portion of the female population. The selection of the fixed screen height of 50.25 inches reflects this design principle as this number falls within the median design range specified in ASTM Standard F 1166-07 (2007), where this standard is the anthropometric reference document leveraged by the Navy for the design of maritime vessels. Further, comparisons of the open and constrained scenarios were performed based on the ANOVA results with statistical significances at $p < 0.05$.

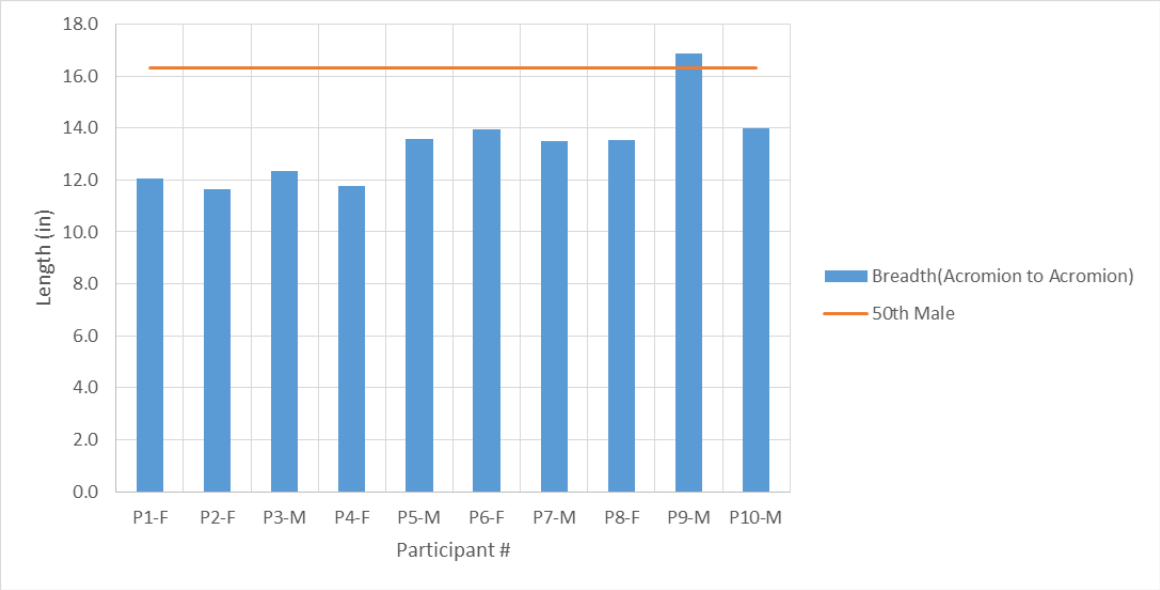

Figure 18. Shoulder breadth (acromion to acromion) comparison with the 50th percentile male

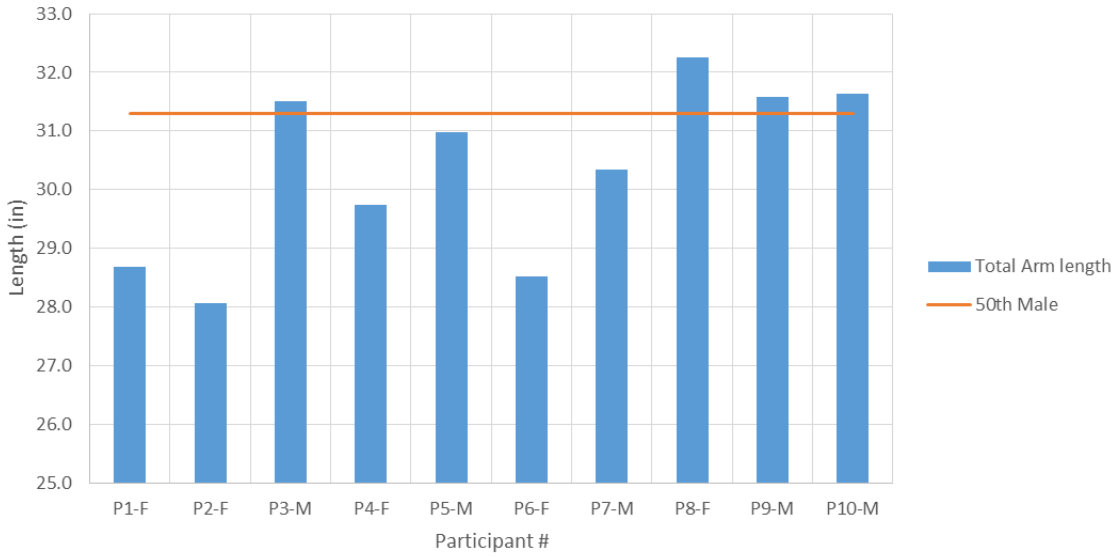

Figure 19. Arm length (acromion to 3 distal phalange) comparison with the 50th percentile male

4. Results

4.1 Touchscreen Targeting

4.1.1 Targeting

The results of the touchscreen component provides the end-effector position of the second digit upon performing a goal directed upper extremity pointing movement. Sample results for Participant 4's 1 Hz cycle is shown in Figure 20. The results fell within the white 40 pixel diameter circle, which reflects the normalized parameter for an accurate end-effector touch.

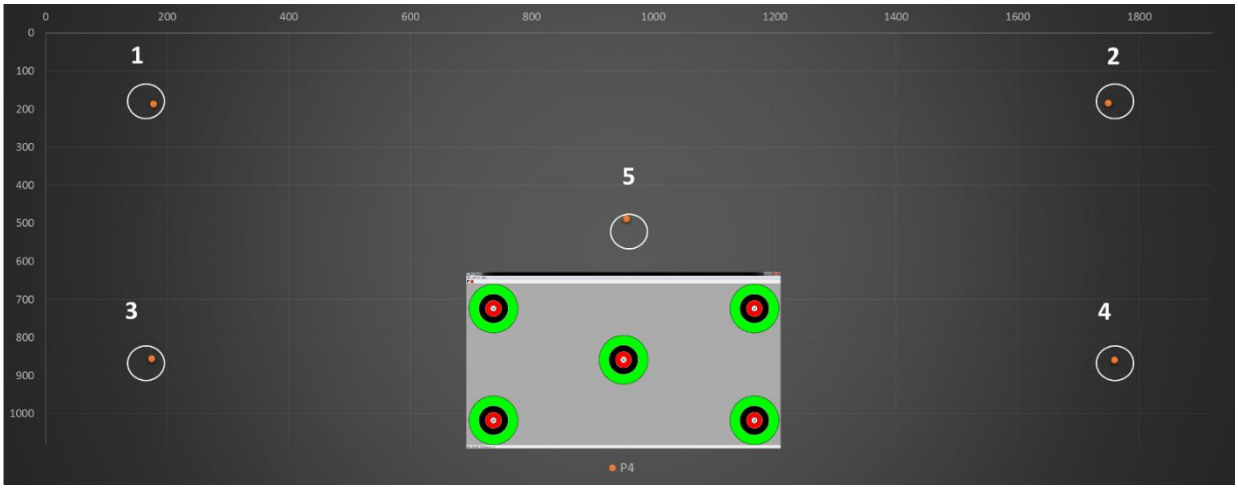

Figure 20. End-effector results for Participant 4's 1 Hz open-cycle

Table 10. End-effector averaged results for all cycles with respect to the open, constrained, and open-adjusted scenarios. A two-way ANOVA without replication is provided in the second table.

	0Hz	Radial Std -0Hz	1Hz	Radial Std -1Hz	1.3Hz	Radial Std -1.3Hz	1.7Hz	Radial Std -1.7Hz	2Hz	Radial Std -2Hz	2.7Hz	Radial Std -2.7Hz
Open	12	17	40	20	6	12	11	3	17	16	5	13
	20	19	49	23	9	15	8	3	19	19	9	16
	43	21	39	22	9	13	13	3	22	18	9	14
	41	22	43	21	13	13	21	4	19	18	5	21
	46	20	43	20	8	12	5	3	23	16	12	13
Constrained	14	17	38	21	14	3	13	17	66	54	23	20
	21	19	45	24	15	4	24	18	43	23	36	22
	22	17	41	21	17	17	30	20	36	22	26	21
	20	17	24	22	17	18	35	19	31	22	26	23
	21	16	44	20	19	16	21	16	43	19	31	19
Open-Adjusted	12	5	75	21	15	2	11	3	10	3	24	25
	12	5	85	26	12	1	11	1	16	4	42	20
	22	1	77	23	16	4	14	5	20	7	40	22
	24	5	71	26	18	3	15	3	22	9	31	26
	7	4	75	23	10	2	12	3	10	2	44	2

ANOVA-End-effector						
Source of Variation	*SS*	*df*	*MS*	*F*	*P-value*	*F crit*
Scenarios	1847.191	14	131.9422	0.776022101	0.690786	1.835683166
Stimuli Cycles	14879.05	5	2975.81	17.50231279	<0.001	2.345586327
Error	11901.67	70	170.0238			
Total	28627.91	89				

Table 10 provides a summary of end-effector results for all cycles with respect to the open, constrained, and open-adjusted scenarios. As a result from Table 10, there are no significant

differences between the scenarios; however, there is a significant difference between the stimuli cycles. This is expected as previously mentioned under the methods section for touch, where, if the end effector result did not register, then the participant received a default distance from target center for all 5 targets. Therefore, not a lot of emphasis can be placed on the accuracy of touch with respect to stimuli cycles as the 1 Hz and 2 Hz stimuli reflected a greater amount of unregistered touches. Additionally, for the open-adjusted scenario, the numbers with respect to participants is not equivalent to the open and constrained scenarios. Only 3 participants requested a screen adjustment (i.e., Participant 3, 6, and 10), thus in this case, the null hypothesis is not rejected as a result of sampling and participant error.

4.1.2 Reaction Time

Figure 21 shows sample results for participant 4's 1 Hz open-cycle. The results for all participants were similar across all participants with respect to when touch information was captured based on the isochronal stimulus. There was a slight delay between when the stimulus is heard and when the touch is initiated. This delay varied with each participant but, for the data showed in Figure 21, the average delay for all three trials was 0.11s. In considering the characteristic roundtrip neural peak latency, the delay was 0.10s for cortical areas to register ascending proprioceptive feedback from the hand (Frank et al., 2006). Since these movements were continuous once the cycle was initiated with the first target (Figure 8), the response correlated in preempting the next stimulus beat as the frequency increased to the fasted stimulus of 2.7 Hz. After the first trial of any particular pattern, the participant's internal clock takes over to keep time in a feedback loop with the physical stimulus. This interchange results in an

anticipatory phase shift with the actual touch coming prior to the stimulus (Frank et al., 2006). The prior is self-evident when comparing Figure 21 and Figure 22. In Figure 21, there are four peaks and four x's after the x at the zero mark, which initiates the touch capture. In Figure 22, however, there are five peaks for trials 2 and 4 of the plots, and six on trial 3's plot. The actual touch points 'x' still reflect only four touches. Therefore, the touches have shifted so they come prior to the isochronous stimulus, which in itself is a kind of compensatory mechanism to deal with the increased speed of the stimulus and the neural delay.

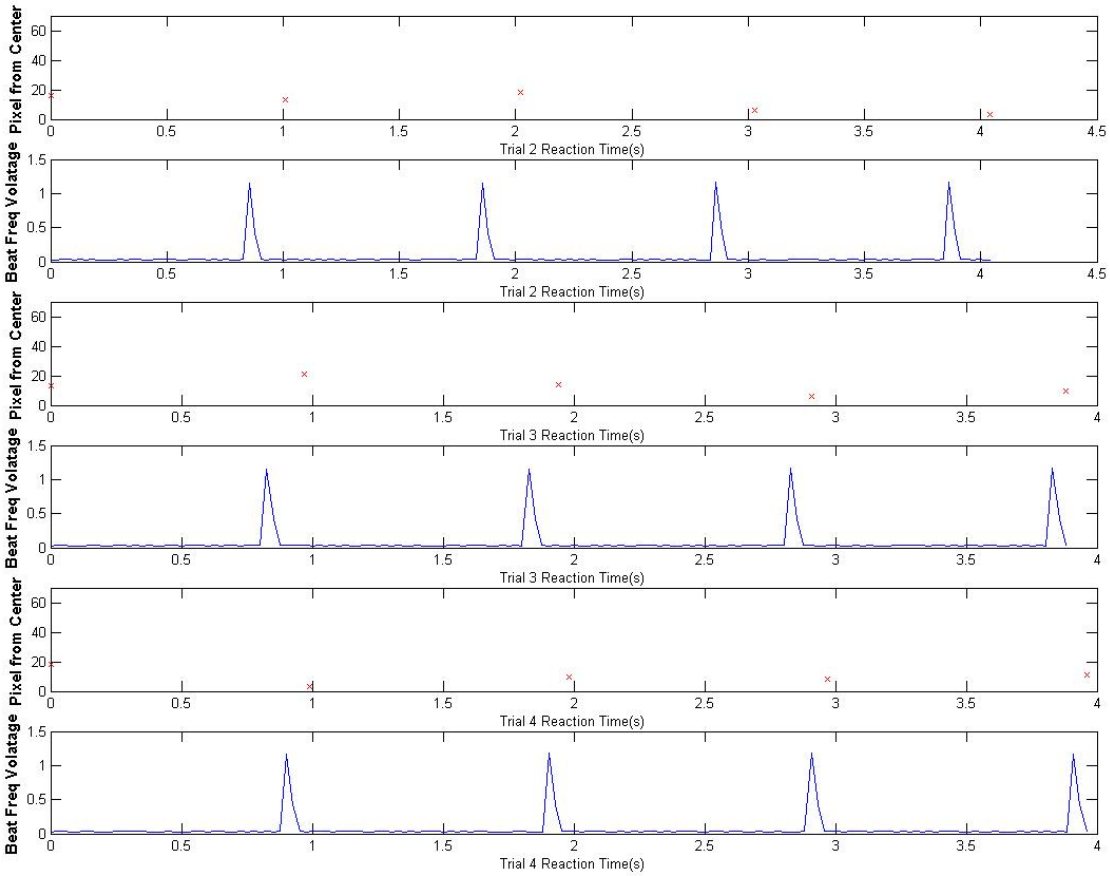

Figure 21. Touch reaction time with respect to isochronous stimulus and touch distance from center for participant 4's 1 Hz open-cycle.

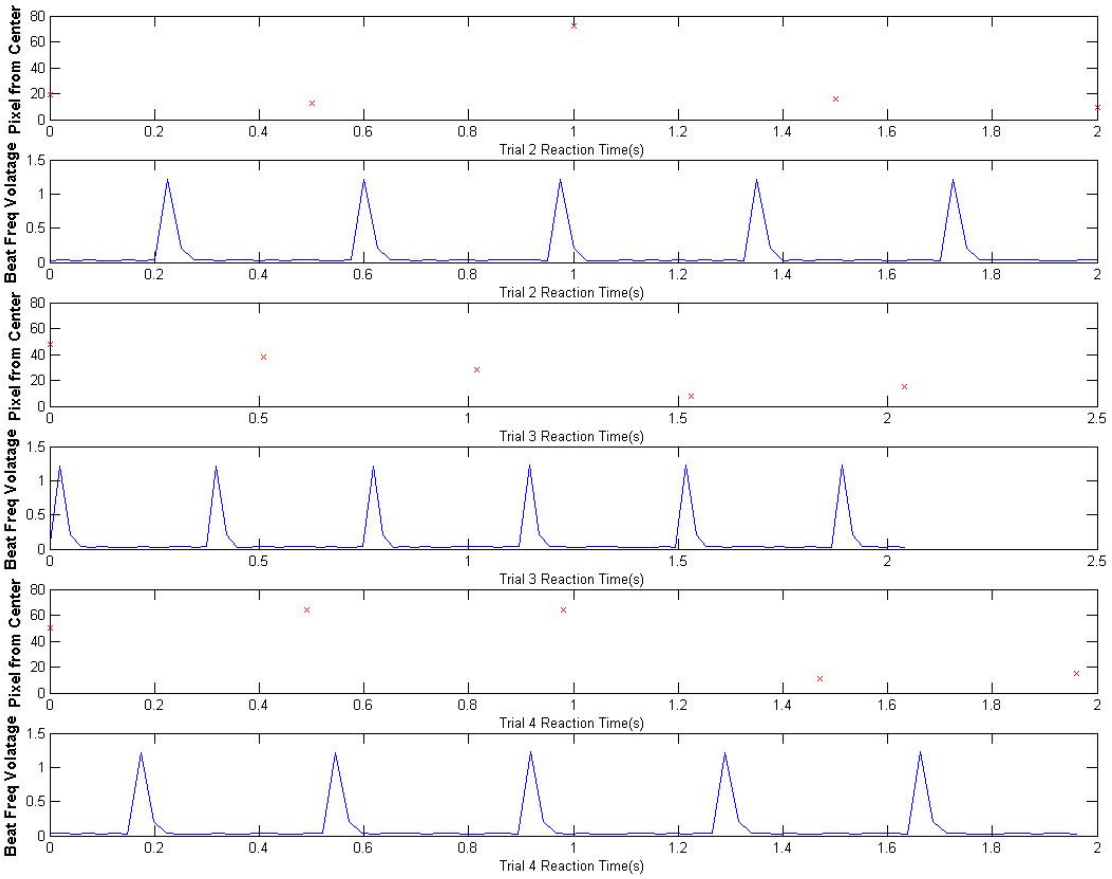

Figure 22. Touch reaction time with respect to isochronous stimulus and touch distance from center for participant 4's 2.7 Hz open-cycle.

4.2 Angular Joint Displacements

Figures 23 and 24 show sample kinematic plots for participant 4's 1 Hz cycle. The green line in Figure 23 reflects shoulder flexion/extension, while the blue line reflects shoulder abduction/adduction. In considering this study's focus on anthropometry and how anthropometry facilitates design considerations, comparisons of arm length, shoulder breadth were analyzed with respect to the 3 DoF in an upper extremity pointing movement.

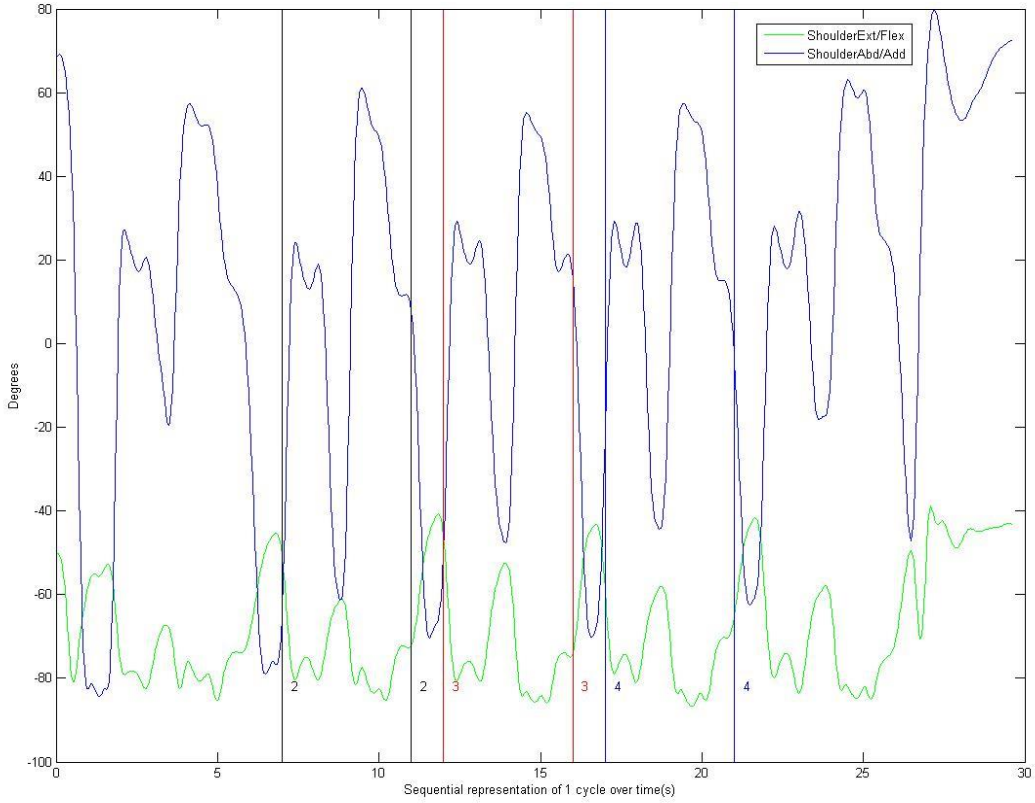

Figure 23. Shoulder kinematic response for participant 4's 1 Hz arm movements. The green line represents shoulder extension and flexion, while the blue represents shoulder abduction and adduction. The black, red, and blue vertical lines are the start and stop points for trials 2, 3, and 4.

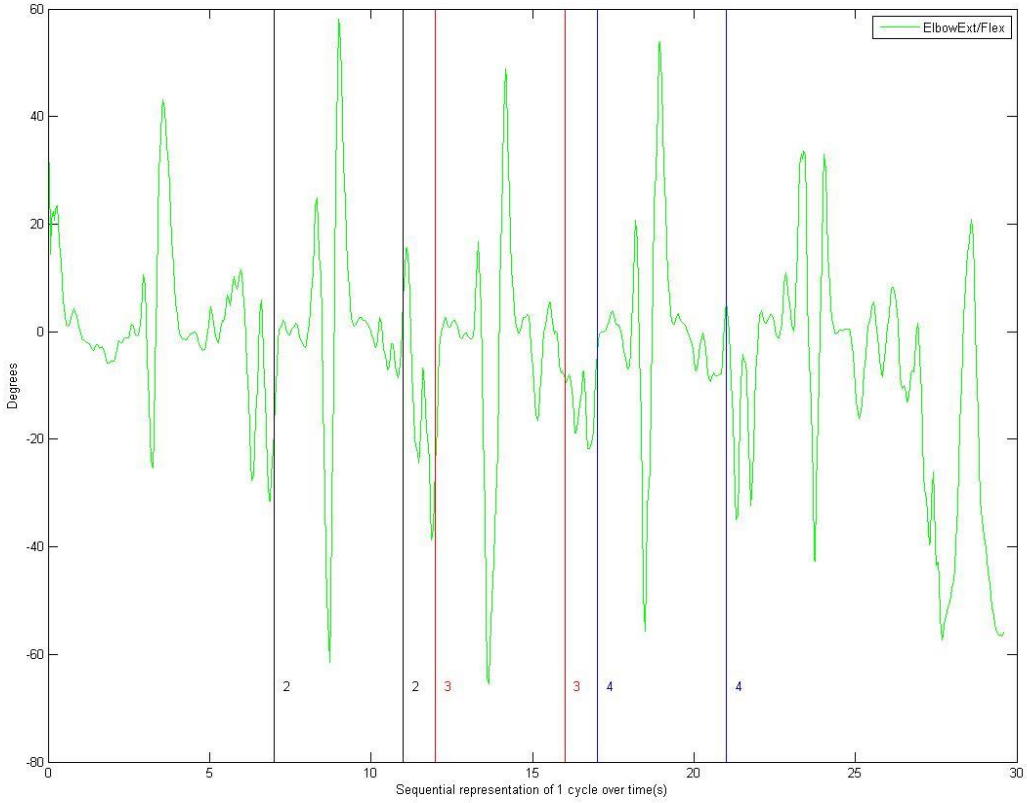

Figure 24. Elbow flexion and extension kinematic response for participant 4's 1 Hz arm movements. The black, red, and blue vertical lines are the start and stop point for trials 2, 3, and 4.

Tables 11 through 16 provide summative kinematic parameters for all of the 10 participants. The tables are broken down by 'everyone' or all 10 participants, 'Male', 'Female', '<50th Male' or less than 50th percentile male, '>50th Male' or greater than 50th percentile male. This is done for each scenario: open (white highlight), open-adjusted (green highlight), and constrained (blue highlight). The components are broken down by shoulder flexion and extension, shoulder abduction and adduction, and elbow flexion and extension. Tables C1 through C69 (Appendix C) are descriptive statistics for trials 2, 3, and 4 of both angular displacement in degrees and angular velocity in degrees per second for each of the 10 participants. The descriptive statistics

provides the: mean, median, mode, standard deviation, kurtosis (how flat or thin compared to a normal distribution), skewness (a measure of the asymmetry of the distribution about its mean), minimum value, maximum value, sum total of degrees, a count of data values, and the standard error of the mean (an estimate used to determine how precisely the mean of a sample estimates the population mean). The data in Tables 11 through 16 summarize Tables C1 through C69 in Appendix C with the mean and standard deviations among the participant breakdown specified. Additionally, for the angular displacements, there are maximum and minimum values separated into male and female participants (Tables 11B, 11C, 13B, 13C, 15B, and 15C), respectively. The summative tables vary for each participant, but across stimulus cycles the data is pretty consistent. Even across scenarios, including participants that requested an adjustment to the open scenario, there are not gross variations in the values. However, from a male and female perspective, there are certainly differences between the means and standard deviations for each of the anatomical components. Additionally, in assessing the data, the shoulder abduction and adduction angular velocities are higher for females as opposed to males. This reflects back to the self-organization of the motor control system and the environment variable of screen size, which potentially forces such a result. Additionally, it should be noted that, in the constrained scenario, the distance the participant was from the screen did not change. Visually, the environment changed to be closed off or constrained rather than open. This in effect was to see if the motor control approach would be altered based on the visual appearance of the environment. From the kinematic results, the environment appeared to not have an apparent effect, as seen in Tables 11 through 16). As part of Participant 10's self-report, the constrained cycle did not make him feel restricted but his kinematic approach shifted, where he was striking the screen with more force. Participant 10 decided to slow his approach, which caused accuracy drift based on visual

feedback of the screen. Participant 10 ended up having to twist his body side to side because his peripheral vision was not working well. What is interesting is that Table C76 does not show a marked difference in total CoG displacement between the open, open-adjusted, and constrained scenarios. In fact, a two-way ANOVA showed no significant difference between the scenarios as $p = 0.611$. However, using the motion capture video to compare the center of gravity shift for the 1 Hz open and constrained cycles, there is a pronounced forward and back movement in the constrained cycle compared to the open cycle. Thus, the environment caused a cognitive reaction to the experiment, to change the participants approach carrying out the constrained cycle but the bodies adaptive filter was able to compensate based on the participant's total CoG displacement, as seen in Table C76.

To assess the statistical significance of Tables C1 through C69, an average of trials 2, 3, and 4 was taken and ANOVAs were performed on: stimulus, gender, arm length, and shoulder breath for the open and constrained scenarios. Figures 25, 26, and 27 show the results of the ANOVA with respect to the main effect of and interaction between the six stimuli, for the open, constrained, and open-adjusted scenarios. Recall that only three participants requested the adjustment (i.e., Participants 3, 6, and 10). Additionally, an ANOVA was conducted on the main influence of, and interaction between, gender, arm length, and shoulder breadth for only the open and constrained scenarios. This was due to the fact that the comparison was slated towards understanding whether having an arm length or shoulder breadth greater than the 50th percentile male showed greater significance than not with respect to human machine design considerations.

Table 11. A) Summative tables for shoulder flexion and extension angular displacement (deg) for all the participants in the experiment. B) Summative male maximum and minimum tables for shoulder flexion and extension angular displacement. C) Summative female maximum and minimum tables for shoulder flexion and extension angular displacement. The white highlight is the open scenario, the green is the open-adjusted scenario, and the blue is the constrained scenario.

A)

Shoulder Flex/Ext. (deg)	Angular Displacement-0Hz Mean (SD)	Angular Displacement-1Hz Mean (SD)	Angular Displacement-1.3Hz Mean (SD)	Angular Displacement-1.7Hz Mean (SD)	Angular Displacement-2Hz Mean (SD)	Angular Displacement-2.7Hz Mean (SD)
Everyone	-73.07 (11.11)	-73.44 (10.48)	-73.05 (11.42)	-72.42 (12.46)	-73.01 (11.07)	-72.17 (72.86)
Male	-76.34 (9.11)	-76.19 (8.83)	-76.18 (9.25)	-74.62 (12.83)	-75.88 (9.43)	-76.05 (10.17)
Female	-58.16 (12.80)	-58.92 (11.91)	-58.27 (13.24)	-58.52 (12.09)	-58.45 (12.49)	-56.91 (13.92)
< 50th Male	-70.46 (11.69)	-71.91 (10.80)	-70.47 (11.90)	-70.76 (11.08)	-70.86 (11.45)	-70.14 (12.12)
> 50th Male	-76.98 (8.32)	-75.75 (8.40)	-76.91 (8.85)	-74.91 (13.17)	-76.22 (8.77)	-75.21 (10.71)
P3, P6, & P10	-75.00 (9.47)	-74.84 (8.72)	-75.38 (8.75)	-74.16 (11.34)	-76.02 (8.58)	-76.08 (8.09)
Everyone	-72.49 (12.96)	-73.68 (10.68)	-71.77 (13.86)	-73.39 (10.62)	-65.32 (12.21)	-73.41 (11.28)
Male	-77.02 (8.52)	-76.21 (9.62)	-73.86 (14.71)	-76.56 (8.72)	-60.24 (11.83)	-76.26 (10.15)
Female	-67.96 (16.22)	-71.15 (11.64)	-69.69 (12.95)	-70.22 (12.22)	-70.40 (12.58)	-70.56 (12.31)
< 50th Male	-69.31 (15.35)	-72.05 (11.40)	-68.47 (16.01)	-71.07 (11.85)	-58.70 (11.45)	-71.70 (11.80)
> 50th Male	-77.26 (8.14)	-76.12 (9.50)	-76.73 (9.78)	-76.87 (8.44)	-75.26 (13.27)	-75.99 (10.47)

B)

Shoulder Flex/Ext. (deg)	Angular Displacement-0Hz Mean (SD)	Angular Displacement-1Hz Mean (SD)	Angular Displacement-1.3Hz Mean (SD)	Angular Displacement-1.7Hz Mean (SD)	Angular Displacement-2Hz Mean (SD)	Angular Displacement-2.7Hz Mean (SD)
Min	-88.28 (0.52)	-88.51 (0.57)	-88.55 (0.22)	-88.30 (0.80)	-88.08 (0.84)	-88.04 (1.09)
Max	-54.38 (6.70)	-55.06 (4.37)	-52.22 (7.03)	-37.53 (35.09)	-50.79 (3.42)	-48.36 (21.75)
Min	-88.47 (1.90)	-89.19 (0.62)	88.58 (0.77)	-88.40 (0.75)	-70.89 (39.63)	-87.62 (2.46)
Max	-56.41 (6.09)	-51.31 (12.45)	-31.23 (35.01)	-56.06 (4.21)	-29.83 (25.24)	-50.97 (18.53)
P3 & P10-Min	-80.05 (9.62)	-81.79 (8.71)	-80.96 (10.02)	-81.50 (8.51)	-81.22 (9.15)	-80.53 (8.77)
P3 & P10-Max	-62.97 (16.49)	-65.76 (15.50)	-65.90 (13.30)	-46.15 (41.57)	-66.19 (13.69)	-66.13 (12.77)

C)

Shoulder Flex/Ext. (deg)	Angular Displacement-0Hz Mean (SD)	Angular Displacement-1Hz Mean (SD)	Angular Displacement-1.3Hz Mean (SD)	Angular Displacement-1.7Hz Mean (SD)	Angular Displacement-2Hz Mean (SD)	Angular Displacement-2.7Hz Mean (SD)
Min	-72.72 (35.64)	-73.05 (35.80)	-72.79 (35.72)	-72.96 (35.79)	-72.55 (35.57)	-72.91 (35.73)
Max	-33.21 (22.00)	-35.93 (20.62)	-32.36 (24.15)	-37.88 (21.75)	-36.16 (22.59)	-30.65 (21.72)
Min	-86.16 (2.46)	-86.62 (1.06)	-86.43 (2.11)	-87.26 (2.02)	87.14 (2.18)	-86.29 (0.41)
Max	-33.00 (33.07)	41.55 (16.59)	-41.75 (16.73)	42.09 (13.31)	-37.27 (19.83)	-38.71 (11.84)
P6-Min	-87.20	-86.84	-86.87	-88.04	-89.16	-87.53
P6-Max	-50.79	-50.95	-53.66	-56.19	-55.00	-54.30

Table 12. Summative tables for shoulder flexion and extension angular velocity (deg/sec) for all the participants in the experiment. The white highlight is the open scenario, the green is the open-adjusted scenario, and the blue is the constrained scenario.

Shoulder Flex/Ext. (deg/sec)	Angular Velocity-0Hz Mean (SD)	Angular Velocity-1Hz Mean (SD)	Angular Velocity-1.3Hz Mean (SD)	Angular Velocity-1.7Hz Mean (SD)	Angular Velocity-2Hz Mean (SD)	Angular Velocity-2.7Hz Mean (SD)
Everyone	-2.45 (58.75)	-1.72 (38.04)	-2.02 (65.17)	-3.68 (70.54)	-3.68 (71.99)	-4.01 (86.56)
Male	-2.60 (45.94)	-1.69 (33.98)	-2.30 (45.57)	-4.05 (85.72)	-3.94 (59.28)	-5.68 (81.32)
Female	-2.31 (69.22)	-1.74 (41.71)	-1.74 (80.11)	-3.32 (51.02)	-3.42 (82.78)	-2.34 (91.50)
< 50th Male	-2.41 (67.85)	-2.12 (43.75)	-2.09 (75.37)	-3.61 (51.91)	-3.94 (81.82)	-3.11 (86.53)
> 50th Male	-2.52 (41.50)	-1.11 (27.32)	-1.92 (45.80)	-3.80 (91.63)	-3.28 (54.01)	-5.36 (86.60)
P3, P6, & P10	-2.44 (58.47)	-1.79 (34.21)	-2.06 (46.14)	-2.59 (58.18)	-3.51 (52.41)	-4.81 (61.75)
Everyone	-2.81 (89.00)	-1.85 (56.34)	-3.05 (105.99)	-2.91 (59.63)	-3.40 (69.17)	-3.76 (83.78)
Male	-1.85 (51.94)	-1.89 (50.19)	-3.71 (115.76)	-2.88 (50.16)	-3.04 (65.41)	-3.60 (71.19)
Female	-3.78 (114.65)	-1.81 (61.88)	-2.39 (95.23)	-2.93 (67.78)	-3.75 (72.74)	-3.92 (94.71)
< 50th Male	-3.61 (105.82)	-2.02 (58.99)	-3.57 (125.34)	-3.22 (125.34)	-3.39 (66.36)	-4.68 (92.95)
> 50th Male	-1.63 (54.84)	-1.60 (52.11)	-2.27 (67.26)	-2.43 (49.06)	-3.41 (73.18)	-2.38 (67.74)

Table 13. A) Summative tables for shoulder abduction and adduction angular displacement (deg) for all the participants in the experiment. B) Summative male maximum and minimum tables for shoulder abduction and adduction angular displacement. C) Summative female maximum and minimum tables for shoulder abduction and adduction angular displacement. The white highlight is the open scenario, the green is the open-adjusted scenario, and the blue is the constrained scenario.

A)

Shoulder Abd/Add (deg)	Angular Displacement-0Hz Mean (SD)	Angular Displacement-1Hz Mean (SD)	Angular Displacement-1.3Hz Mean (SD)	Angular Displacement-1.7Hz Mean (SD)	Angular Displacement-2Hz Mean (SD)	Angular Displacement-2.7Hz Mean (SD)
Everyone	49.95 (38.44)	49.56 (39.61)	50.64 (38.01)	43.45 (37.71)	44.08 (43.68)	45.13 (57.82)
Male	58.62 (35.85)	57.01 (35.47)	60.68 (35.10)	58.84 (35.57)	58.60 (34.60)	58.33 (32.50)
Female	41.27 (40.86)	42.12 (43.36)	41.19 (40.71)	28.07 (39.73)	29.56 (51.18)	31.92 (75.03)
< 50th Male	49.50 (40.52)	49.18 (41.66)	48.53 (39.29)	38.50 (40.65)	40.10 (48.88)	39.84 (69.18)
> 50th Male	50.61 (35.07)	50.13 (36.32)	53.79 (36.00)	50.88 (32.80)	50.06 (34.45)	53.05 (34.34)
P3, P6, & P10	53.32 (42.42)	53.38 (42.64)	55.86 (45.65)	54.19 (41.60)	51.06 (38.67)	48.91 (36.47)
Everyone	49.16 (36.69)	50.86 (38.88)	49.96 (37.92)	47.71 (36.46)	45.28 (33.56)	47.64 (34.21)
Male	57.77 (34.56)	57.95 (35.22)	58.24 (35.86)	58.68 (35.94)	51.24 (30.78)	58.85 (33.62)
Female	40.54 (38.71)	43.78 (42.23)	41.68 (39.87)	36.74 (36.97)	39.33 (36.13)	36.43 (34.80)
< 50th Male	49.05 (39.48)	50.11 (41.02)	50.49 (40.39)	46.17 (37.72)	40.71 (33.37)	46.33 (36.24)
> 50th Male	49.21 (32.07)	51.98 (35.44)	49.17 (33.86)	50.02 (34.49)	52.14 (33.85)	49.60 (30.93)

B)

Shoulder Abb/Add. (deg)	Angular Displacement-0Hz Mean (SD)	Angular Displacement-1Hz Mean (SD)	Angular Displacement-1.3Hz Mean (SD)	Angular Displacement-1.7Hz Mean (SD)	Angular Displacement-2Hz Mean (SD)	Angular Displacement-2.7Hz Mean (SD)
Min	-9.13 (65.00)	-22.18 (60.48)	-16.48 (67.68)	-12.72 (60.96)	-16.23 (71.30)	0.46 (65.61)
Max	68.84 (24.90)	79.12 (7.57)	80.28 (9.66)	60.71 (39.67)	68.32 (25.59)	61.05 (38.67)
Min	-1.18 (72.41)	-14.97 (60.90)	12.52 (67.26)	-11.87 (65.68)	-2.87 (57.79)	-8.14 (68.23)
Max	65.65 (28.94)	72.77 (16.23)	66.66 (26.60)	62.45 (35.44)	50.99 (44.81)	59.91 (39.52)
P3 & P10-Min	-25.43 (85.82)	-20.66 (79.93)	-26.71 (85.52)	-21.43 (90.81)	-24.93 (86.13)	-18.24 (86.64)
P3 & P10-Max	65.47 (30.92)	68.22 (30.00)	62.05 (36.53)	79.58 (12.09)	48.51 (52.35)	42.92 (57.22)

C)

Shoulder Abb/Add. (deg)	Angular Displacement-0Hz Mean (SD)	Angular Displacement-1Hz Mean (SD)	Angular Displacement-1.3Hz Mean (SD)	Angular Displacement-1.7Hz Mean (SD)	Angular Displacement-2Hz Mean (SD)	Angular Displacement-2.7Hz Mean (SD)
Min	-62.29 (31.91)	-68.31 (34.10)	-65.76 (33.46)	-62.88 (32.47)	-59.06 (30.08)	-62.16 (30.99)
Max	51.09 (28.72)	59.35 (30.84)	50.73 (28.40)	44.06 (24.95)	46.95 (27.24)	52.67 (25.87)
Min	-66.39 (12.43)	-76.05 (14.29)	-73.19 (14.99)	-70.35 (12.34)	-64.84 (14.98)	-63.29 (17.28)
Max	63.22 (22.23)	67.92 (14.09)	65.28 (21.50)	64.60 (10.27)	62.49 (10.38)	58.09 (14.97)
P6-Min	-78.48	-68.63	-86.55	-80.14	-63.44	-61.94
P6-Max	81.41	87.68	88.34	82.46	63.81	51.07

Table 14. Summative tables for shoulder abduction and adduction angular velocity (deg/sec) for all the participants in the experiment. The white highlight is the open scenario, the green is the open-adjusted scenario, and the blue is the constrained scenario.

Shoulder Abd/Add (deg/sec)	Angular Velocity-0Hz Mean (SD)	Angular Velocity-1Hz Mean (SD)	Angular Velocity-1.3Hz Mean (SD)	Angular Velocity-1.7Hz Mean (SD)	Angular Velocity-2Hz Mean (SD)	Angular Velocity-2.7Hz Mean (SD)
Everyone	133.79 (199.07)	128.72 (218.37)	132.62 (207.50)	135.67 (183.17)	148.52 (207.69)	149.19 (197.89)
Male	93.71 (141.24)	94.67 (183.31)	105.10 (200.03)	99.67 (151.82)	131.44 (214.67)	96.11 (131.35)
Female	173.87 (243.53)	162.77 (248.54)	160.14 (214.72)	171.66 (209.89)	165.59 (200.47)	202.28 (247.12)
< 50th Male	152.52 (231.49)	133.82 (225.94)	133.05 (191.86)	155.74 (201.38)	162.68 (225.54)	166.18 (209.68)
> 50th Male	104.19 (136.70)	121.07 (206.51)	131.96 (228.97)	105.56 (151.81)	127.27 (177.57)	123.72 (178.76)
P3, P6, & P10	172.68 (236.51)	147.09 (243.83)	172.44 (262.49)	187.42 (264.46)	180.82 (231.63)	184.57 (229.15)
Everyone	121.19 (168.65)	104.82 (163.52)	122.34 (184.01)	127.40 (169.80)	114.75 (162.93)	147.51 (209.71)
Male	83.60 (168.65)	76.54 (163.52)	92.66 (184.01)	99.09 (169.80)	68.50 (162.93)	109.48 (209.71)
Female	158.79 (185.74)	133.10 (170.52)	152.03 (186.72)	155.70 (177.25)	161.00 (182.14)	185.53 (212.62)
< 50th Male	139.37 (192.47)	115.26 (175.84)	146.14 (213.34)	145.67 (188.99)	115.74 (169.51)	183.25 (250.57)
> 50th Male	93.94 (124.68)	89.14 (143.07)	86.65 (127.98)	99.99 (136.05)	113.27 (152.54)	93.89 (125.57)

Table 15. A) Summative tables for elbow flexion and extension angular displacement (deg) for all the participants in the experiment. B) Summative male maximum and minimum tables for elbow flexion and extension angular displacement. C) Summative female maximum and minimum tables for elbow flexion and extension angular displacement. The white highlight is the open scenario, the green is the open-adjusted scenario, and the blue is the constrained scenario.

A)

Elbow Flex/Ext. (deg)	Angular Displacement-0Hz Mean (SD)	Angular Displacement-1Hz Mean (SD)	Angular Displacement-1.3Hz Mean (SD)	Angular Displacement-1.7Hz Mean (SD)	Angular Displacement-2Hz Mean (SD)	Angular Displacement-2.7Hz Mean (SD)
Everyone	-3.90 (13.12)	-3.76 (13.45)	-3.92 (13.44)	-4.01 (13.64)	-4.24 (12.02)	-5.31 (11.71)
Male	-4.24 (15.07)	-3.48 (15.11)	-5.02 (16.34)	-4.96 (14.65)	-3.99 (13.77)	-5.36 (12.52)
Female	-3.56 (10.82)	-4.04 (11.55)	-2.82 (9.72)	-3.05 (12.56)	-4.48 (9.97)	-5.25 (10.85)
< 50th Male	-5.45 (13.92)	-4.96 (13.60)	-4.88 (12.44)	-4.76 (14.50)	-6.07 (12.78)	-7.22 (12.54)
> 50th Male	-1.57 (11.80)	-1.95 (13.22)	-2.47 (14.82)	-2.87 (12.25)	-1.49 (10.78)	-2.45 (10.35)
P3, P6, & P10	-2.57 (11.16)	-4.14 (14.01)	-5.09 (14.09)	-5.46 (10.63)	-2.18 (10.17)	-4.39 (8.14)
Everyone	-5.25 (12.55)	-5.05 (14.33)	-5.71 (14.66)	-5.44 (14.03)	-4.69 (9.88)	-5.33 (11.11)
Male	-5.89 (13.72)	-6.41 (17.19)	-6.77 (17.83)	-6.65 (16.82)	-4.29 (9.83)	-6.13 (11.91)
Female	-4.62 (12.55)	-3.69 (14.33)	-4.65 (14.66)	-4.22 (14.03)	-5.10 (9.88)	-4.53 (11.11)
< 50th Male	-6.76 (13.45)	-5.23 (12.61)	-7.34 (13.83)	-6.77 (14.66)	-5.68 (9.52)	-6.29 (11.63)
> 50th Male	-2.99 (11.06)	-4.77 (16.57)	-3.26 (15.82)	-3.44 (13.02)	-3.21 (10.39)	-3.88 (10.27)

B)

Elbow Flex/Ext. (deg)	Angular Displacement-0Hz Mean (SD)	Angular Displacement-1Hz Mean (SD)	Angular Displacement-1.3Hz Mean (SD)	Angular Displacement-1.7Hz Mean (SD)	Angular Displacement-2Hz Mean (SD)	Angular Displacement-2.7Hz Mean (SD)
Min	-47.51 (30.23)	-47.02 (29.09)	-48.93 (30.14)	-49.23 (32.54)	-41.24 (23.94)	-35.21 (23.83)
Max	33.05 (12.00)	34.07 (18.59)	32.51 (15.72)	27.22 (13.85)	27.12 (14.31)	23.24 (14.94)
Min	-39.34 (27.36)	-51.86 (27.77)	-53.04 (31.33)	-50.40 (27.35)	-23.85 (14.85)	-36.02 (20.50)
Max	30.51 (15.72)	35.51 (14.82)	33.86 (26.64)	30.79 (19.64)	18.70 (19.80)	20.60 (14.95)
P3 & P10-Min	-40.98 (20.70)	-43.05 (33.54)	-42.02 (26.40)	-41.77 (23.59)	-27.58 (9.71)	-23.73 (7.44)
P3 & P10-Max	29.03 (13.40)	34.01 (20.86)	29.72 (14.49)	21.61 (8.87)	31.98 (21.08)	18.25 (13.79)

C)

Elbow Flex/Ext. (deg)	Angular Displacement-0Hz Mean (SD)	Angular Displacement-1Hz Mean (SD)	Angular Displacement-1.3Hz Mean (SD)	Angular Displacement-1.7Hz Mean (SD)	Angular Displacement-2Hz Mean (SD)	Angular Displacement-2.7Hz Mean (SD)
Min	-31.46 (20.82)	-33.09 (24.41)	-30.73 (20.17)	-34.26 (24.45)	28.85 (20.96)	-30.73 (24.64)
Max	26.37 (22.91)	22.92 (21.29)	23.74 (14.60)	23.80 (28.04)	16.38 (13.90)	15.59 (9.11)
Min	-35.05 (23.43)	-33.59 (11.72)	-33.83 (15.35)	-35.07 (19.23)	-33.85 (11.94)	-28.22 (10.33)
Max	27.44 (14.34)	26.65 (12.36)	21.71 (12.27)	18.80 (10.62)	25.18 (18.54)	20.50 (5.49)
P6-Min	-51.82	-42.25	-47.96	-30.99	-36.12	-30.90
P6-Max	26.24	22.43	34.47	13.60	14.61	17.02

Table 16. Summative tables for elbow flexion and extension angular velocity (deg/sec) for all the participants in the experiment. The white highlight is the open scenario, the green is the open-adjusted scenario, and the blue is the constrained scenario.

Elbow Flex/Ext. (deg/sec)	Angular Velocity-0Hz Mean (SD)	Angular Velocity-1Hz Mean (SD)	Angular Velocity-1.3Hz Mean (SD)	Angular Velocity-1.7Hz Mean (SD)	Angular Velocity-2Hz Mean (SD)	Angular Velocity-2.7Hz Mean (SD)
Everyone	0.52 (155.24)	0.54 (128.48)	0.06 (144.34)	-0.15 (143.92)	0.25 (136.57)	0.55 (129.90)
Male	-0.31 (164.78)	-0.43 (139.41)	-0.77 (163.35)	0.40 (141.95)	0.21 (159.18)	0.47 (134.68)
Female	-0.74 (145.09)	0.65 (116.52)	0.89 (122.41)	-0.70 (145.85)	0.30 (109.39)	0.62 (124.93)
< 50th Male	-0.96 (162.25)	0.72 (124.97)	-0.21 (129.08)	-0.12 (151.08)	0.67 (134.72)	1.40 (146.38)
> 50th Male	0.14 (144.09)	0.26 (133.57)	0.46 (164.59)	-0.20 (132.45)	-0.37 (139.31)	-0.74 (100.20)
P3, P6, & P10	0.20 (136.28)	0.26 (135.81)	0.19 (155.36)	0.69 (114.15)	1.62 (108.68)	1.50 (94.30)
Everyone	-0.24 (119.97)	0.13 (133.15)	0.63 (143.56)	0.96 (144.78)	-0.75 (116.59)	0.12 (134.65)
Male	-0.15 (124.32)	-0.06 (152.42)	0.56 (178.46)	1.59 (175.75)	-1.48 (119.50)	0.53 (151.09)
Female	-0.32 (119.97)	0.31 (133.15)	0.69 (143.56)	0.33 (144.78)	-0.01 (116.59)	-0.29 (134.65)
< 50th Male	0.02 (125.31)	0.19 (120.01)	0.48 (128.68)	0.95 (140.45)	-0.52 (110.43)	0.48 (144.84)
> 50th Male	-0.62 (111.49)	0.03 (150.73)	0.85 (163.34)	0.98 (151.03)	-1.09 (125.25)	-0.42 (117.73)

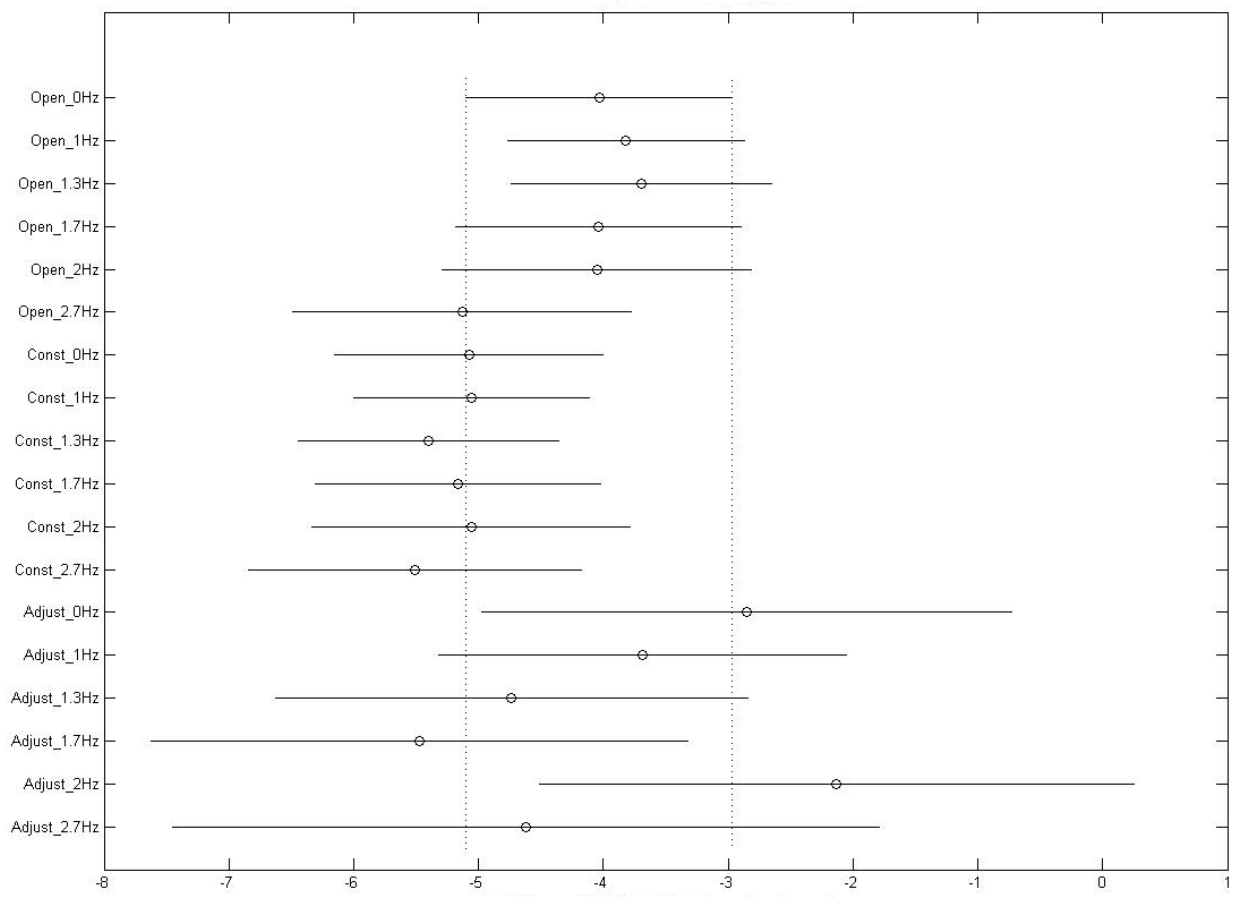

ANOVA Table

Source	SS	df	MS	F	Prob>F
Groups	5494.04	17	323.179	2.4	0.001
Error	1282638.89	9545	134.378		
Total	1288132.93	9562			

Figure 25. ANOVA and post hoc results for main effect and interaction between the six stimuli within the open, constrained, and open-adjusted scenarios for elbow flexion/extension. The X-axis is the anatomical mean angular displacements.

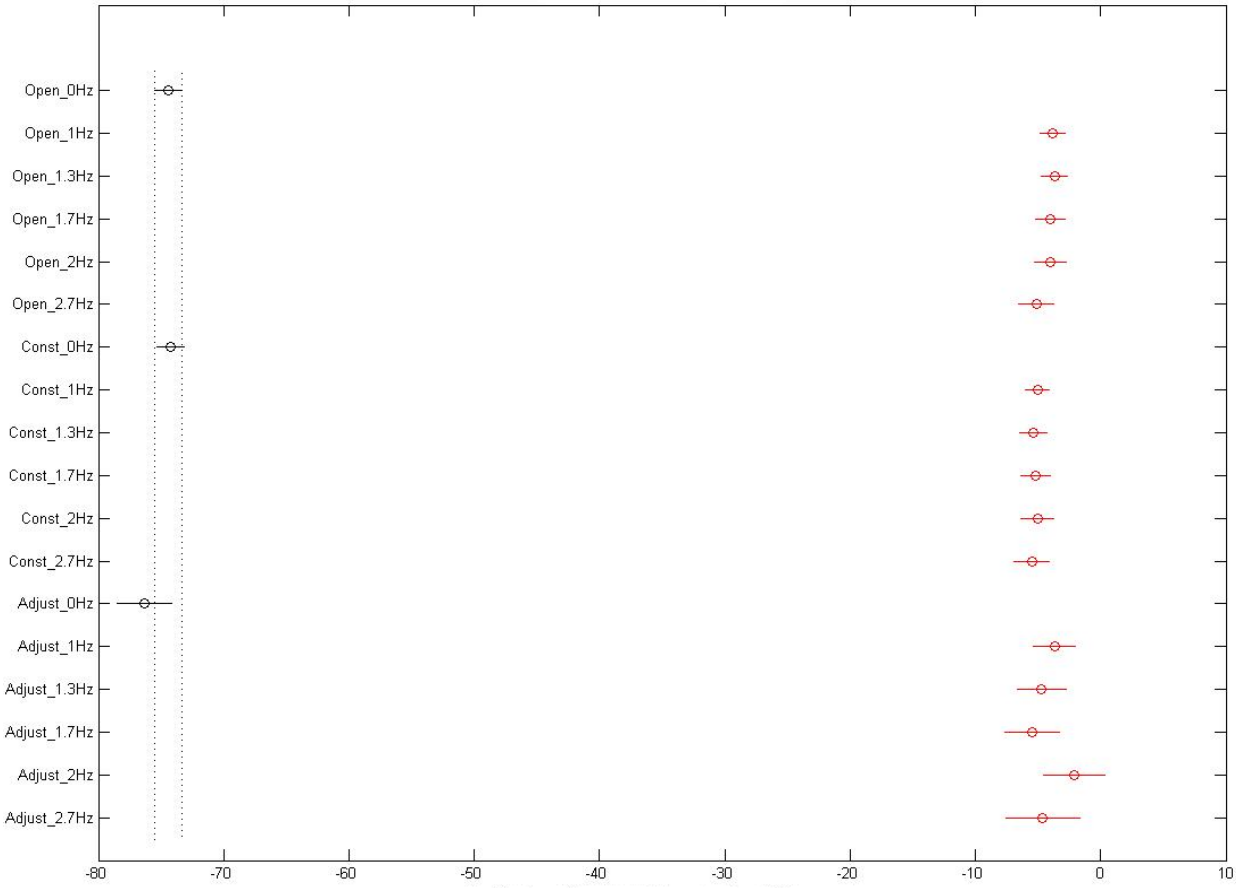

ANOVA Table

Source	SS	df	MS	F	Prob>F
Groups	6330.19	17	372.364	3.28	5.39391e-006
Error	1083510.49	9545	113.516		
Total	1089840.67	9562			

Figure 26. ANOVA and post hoc results for main effect and interaction between the six stimuli within the open, constrained, and open-adjusted scenarios for shoulder flexion/extension. The X-axis is the anatomical mean angular displacements.

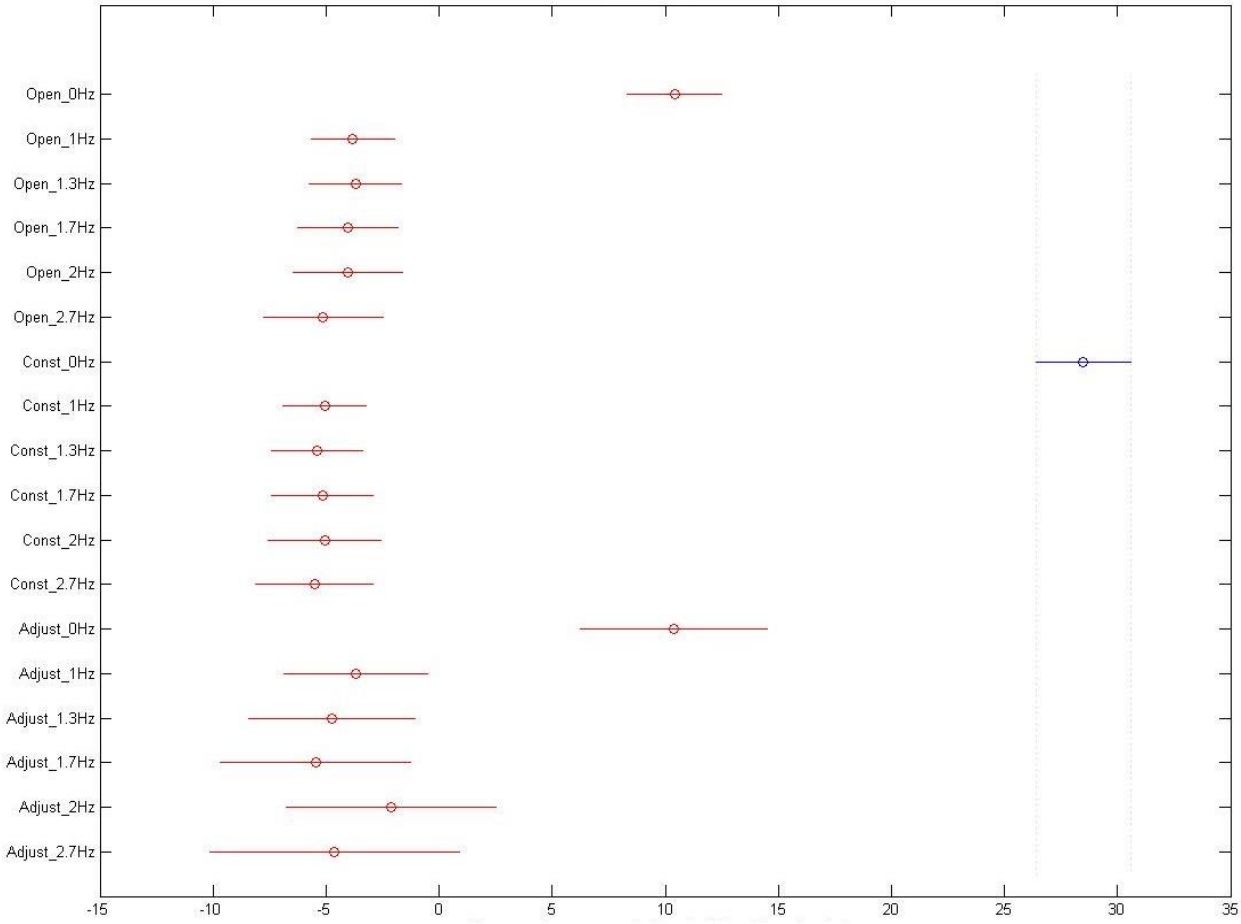

ANOVA Table

Source	SS	df	MS	F	Prob>F
Groups	512309.3	17	30135.8	13.3	0
Error	21628085.8	9545	2265.9		
Total	22140395.1	9562			

Figure 27. ANOVA and post hoc results for main effect and interaction between the six stimuli within the open, constrained, and open-adjusted scenarios for shoulder abduction/adduction. The X-axis is the anatomical mean angular displacements.

Figure 25 shows no statistically significant difference for the elbow flexion/extension results; however, the ANOVA chart showed a $p = 0.001$. As a result, the null hypothesis would be rejected but, after Tukey – Kramer and Bonferroni post hoc analysis, the conclusion is very clear

to accept the null hypothesis. Figure 26 on the other hand, showed that there was only a statistical difference (i.e., $p < 0.001$ in the ANOVA table) between the 0 Hz for the open-cycle, constrained-cycle, and open-adjusted-cycle. Actually, the open and open-adjusted cycles were not statistically different but they were with respect to the constrained-cycle, while the 0 Hz constrained-cycle was different from all cycles. Additionally, the stimuli-cycles were all similar with no statistical difference. The results are interesting with respect to shoulder abduction/adduction in that the angular displacement at the shoulder was similar when following a stimulus pattern but different when not following a stimulus pattern. In essence, the concept of self-organization has more of an effect in stimulus lead cycles rather than non-stimulus cycles. Similar to Figure 26, Figure 27 captures much of the same sentiment but for shoulder abduction/adduction. The only difference is that the 0 Hz for the open-cycle, constrained-cycle, and open-adjusted-cycle are statistically different from the stimulus-cycles but only the open and open-adjusted are distinct from constrained cycle. It is hard to make a clear distinction between stimulus led cycles and non-stimulus led cycles without the post hoc analysis.

Figures 28 through 30 show statistical differences in male and female genders for the open and constrained scenarios. The female open and constrained scenarios are statistically different; however, the male open and constrained are not for shoulder abduction/adduction, and flexion/extension. Figure 30 on the other hand, the roles reverse, where the female open and constrained scenarios are not statistically significant and the male open and constrained scenarios for elbow flexion/extension are significantly different. Figure 31 brings this more to light where participants are separated by arm length and elbow flexion/extension is significantly different for all participants greater than the 50^{th} percentile male and those less than the 50^{th} percentile male. Figure 1C shows the breakdown of participants by arm length, where the males had longer right

upper extremities than the females. In trying to cover the shuttle run total distance of 72.1 inches (seen in Figure 8) and at a standard distance from the screen for all participants, the participants with the longer upper extremity would have a different kinematic approach at the elbow based on what they do at the shoulder.

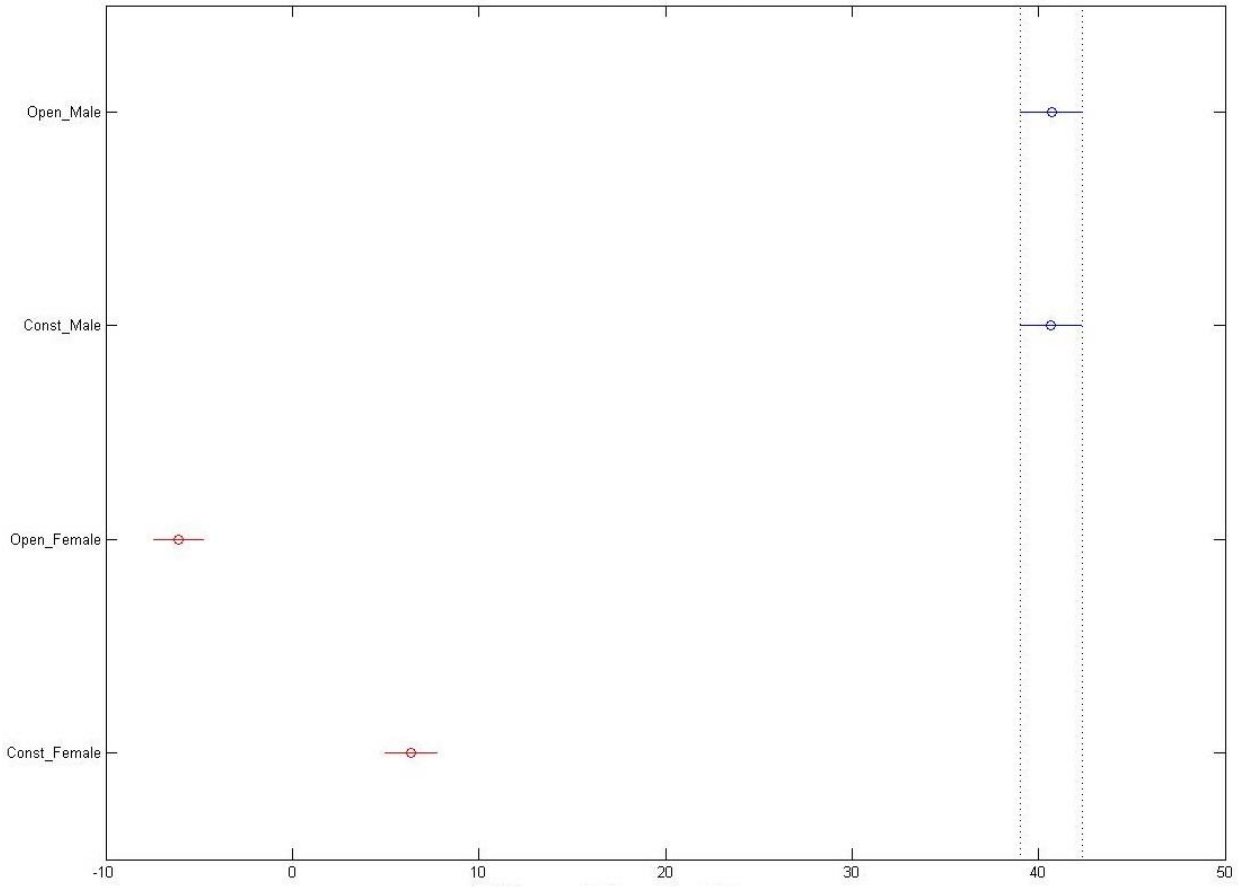

ANOVA Table

Source	SS	df	MS	F	Prob>F
Groups	4.08832e+006	3	1362772.8	897.86	0
Error	1.46725e+007	9667	1517.79		
Total	1.87608e+007	9670			

Figure 28. ANOVA and post hoc results for main effect and interaction between genders within the open, constrained, and open-adjusted scenarios for shoulder abduction/adduction. The X-axis is the anatomical mean angular displacements.

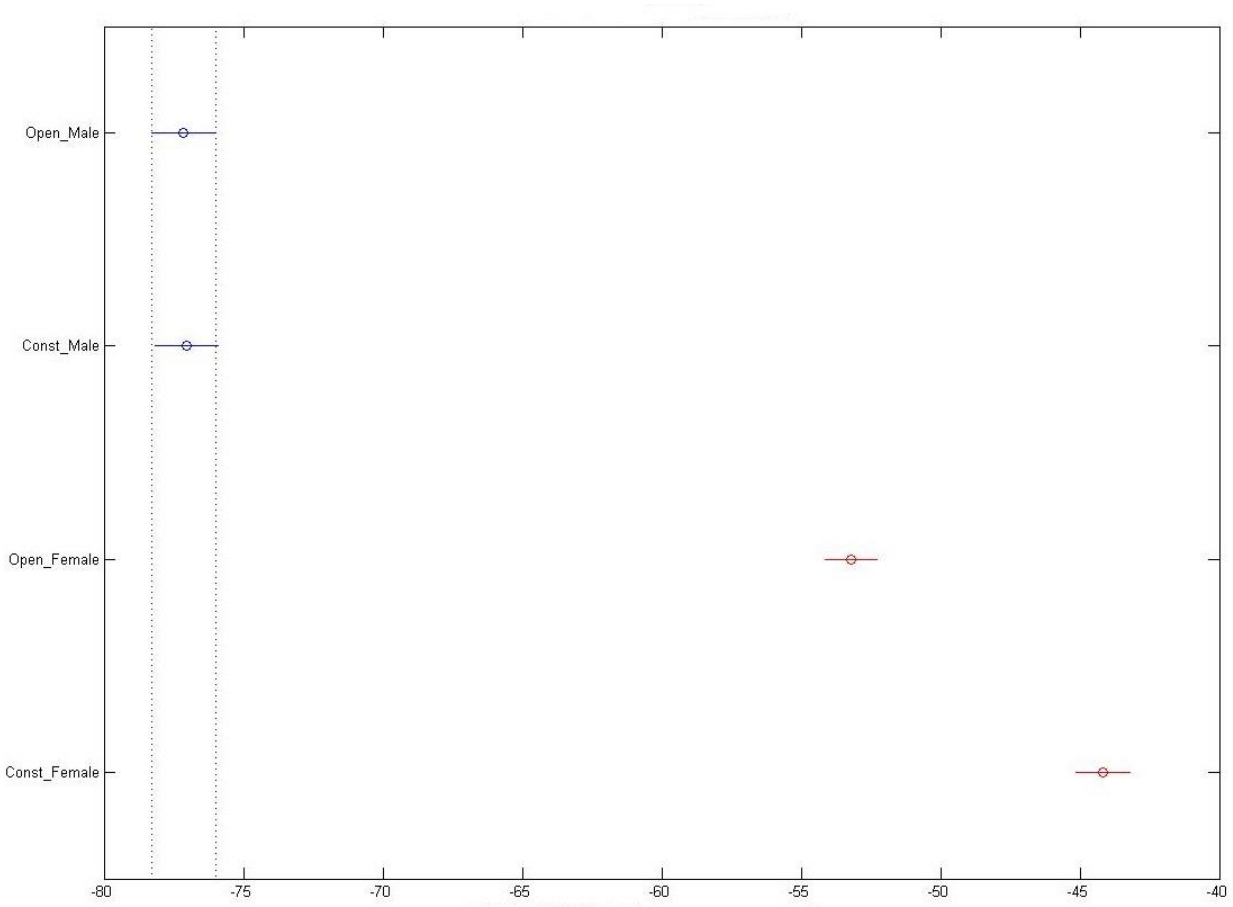

ANOVA Table

Source	SS	df	MS	F	Prob>F
Groups	1.98877e+006	3	662922.7	864.1	0
Error	7.41639e+006	9667	767.2		
Total	9.40516e+006	9670			

Figure 29. ANOVA and post hoc results for main effect and interaction between genders within the open, constrained, and open-adjusted scenarios for shoulder flexion/extension. The X-axis is the anatomical mean angular displacements.

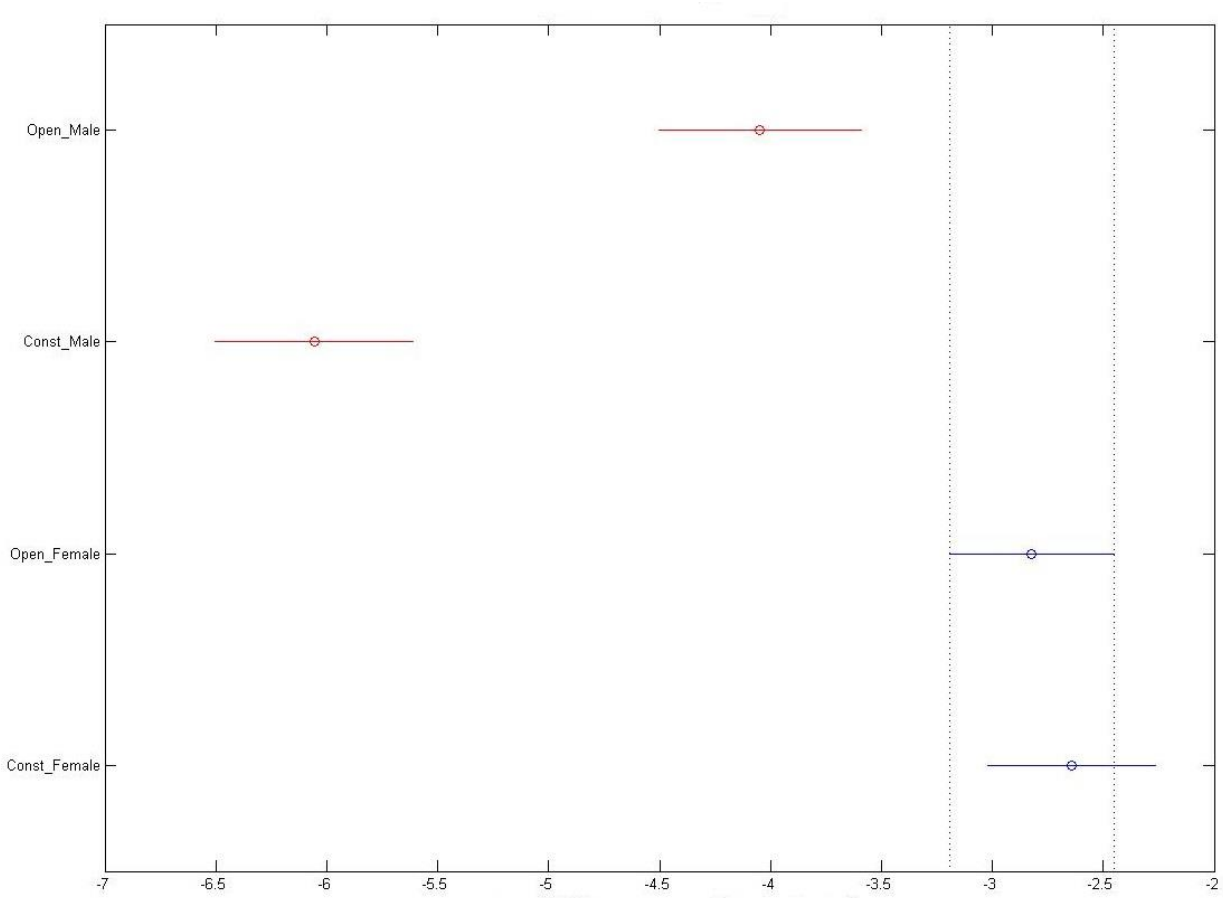

ANOVA Table

Source	SS	df	MS	F	Prob>F
Groups	16767.01	3	5589.002	48.97	0
Error	1103294.52	9667	114.13		
Total	1120061.52	9670			

Figure 30. ANOVA and post hoc results for main effect and interaction between genders within the open, constrained, and open-adjusted scenarios for elbow flexion/extension. The X-axis is the anatomical mean angular displacements.

Figures 31 through 36 show the statistical results for the arm length (i.e., elbow flexion/extension, shoulder abduction/adduction, and shoulder flexion/extension) and shoulder breadth (elbow flexion/extension, shoulder abduction/adduction, and shoulder flexion/extension) kinematics.

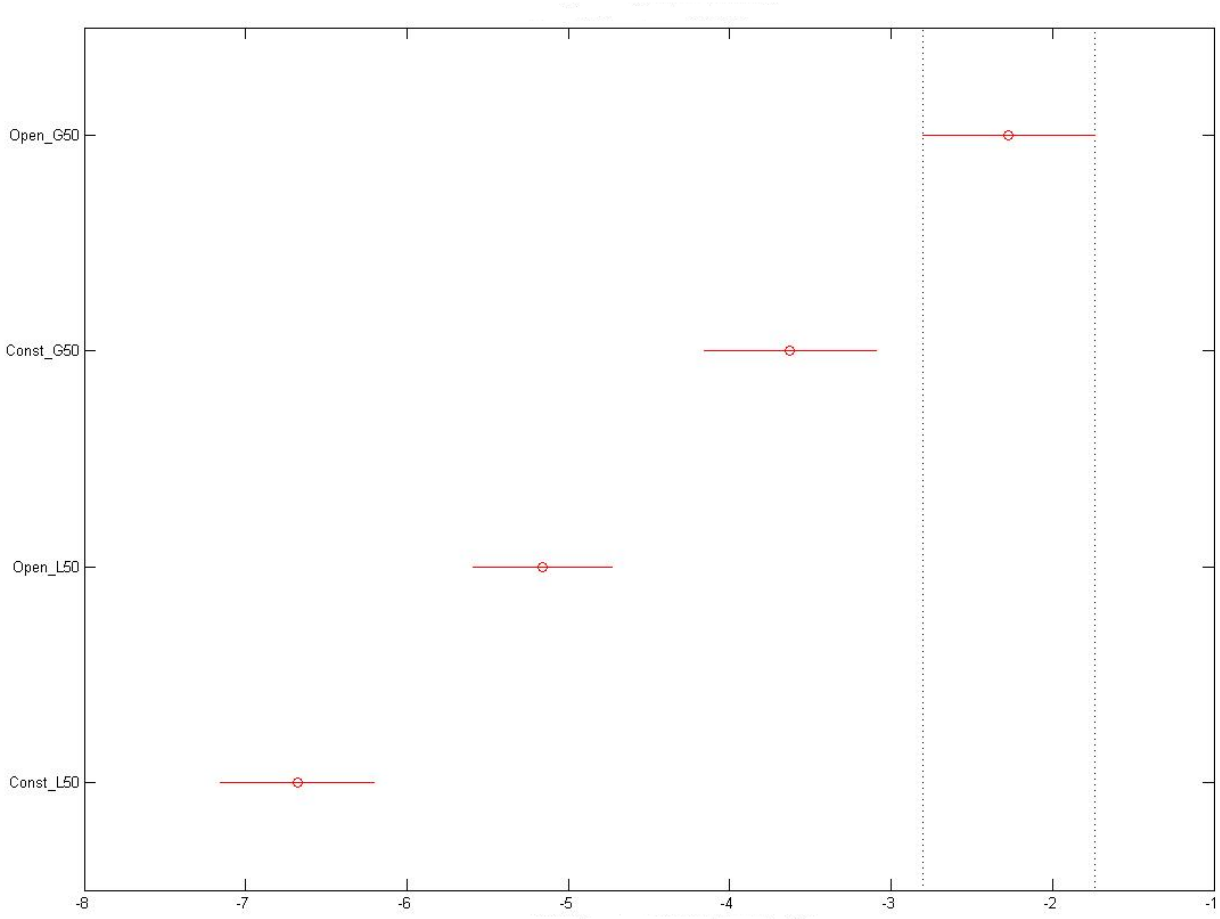

ANOVA Table

Source	SS	df	MS	F	Prob>F
Groups	20000.7	3	6666.92	47.27	0
Error	1110871.1	7877	141.03		
Total	1130871.8	7880			

Figure 31. ANOVA and post hoc results for main effect and interaction between the arm length within the open, and constrained scenarios for elbow flexion/extension. The X-axis is the anatomical mean angular displacements.

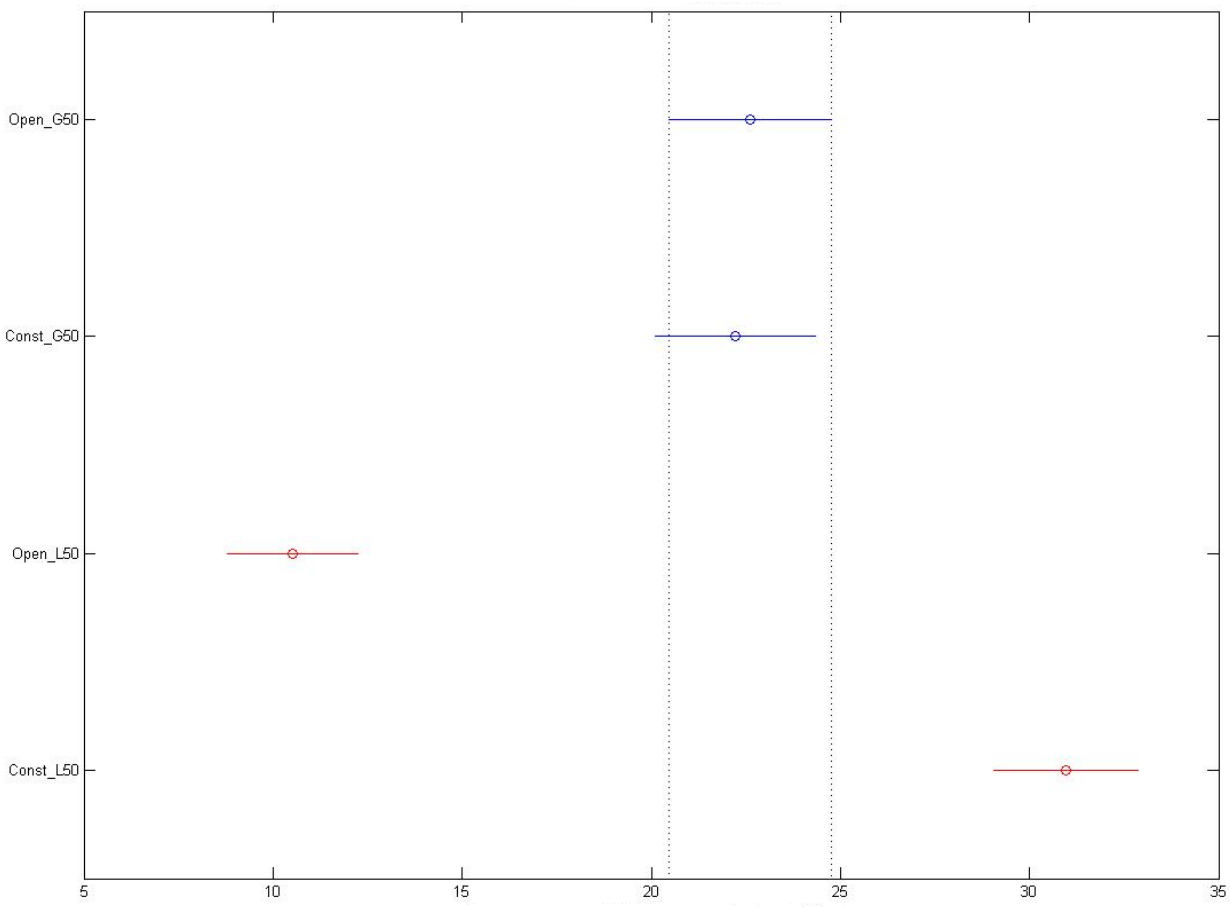

ANOVA Table

Source	SS	df	MS	F	Prob>F
Groups	490504.7	3	163501.6	72.72	0
Error	17709387.7	7877	2248.2		
Total	18199892.4	7880			

Figure 32. ANOVA and post hoc results for main effect and interaction between the arm length within the open, and constrained scenarios for shoulder abduction/adduction. The X-axis is the anatomical mean angular displacements.

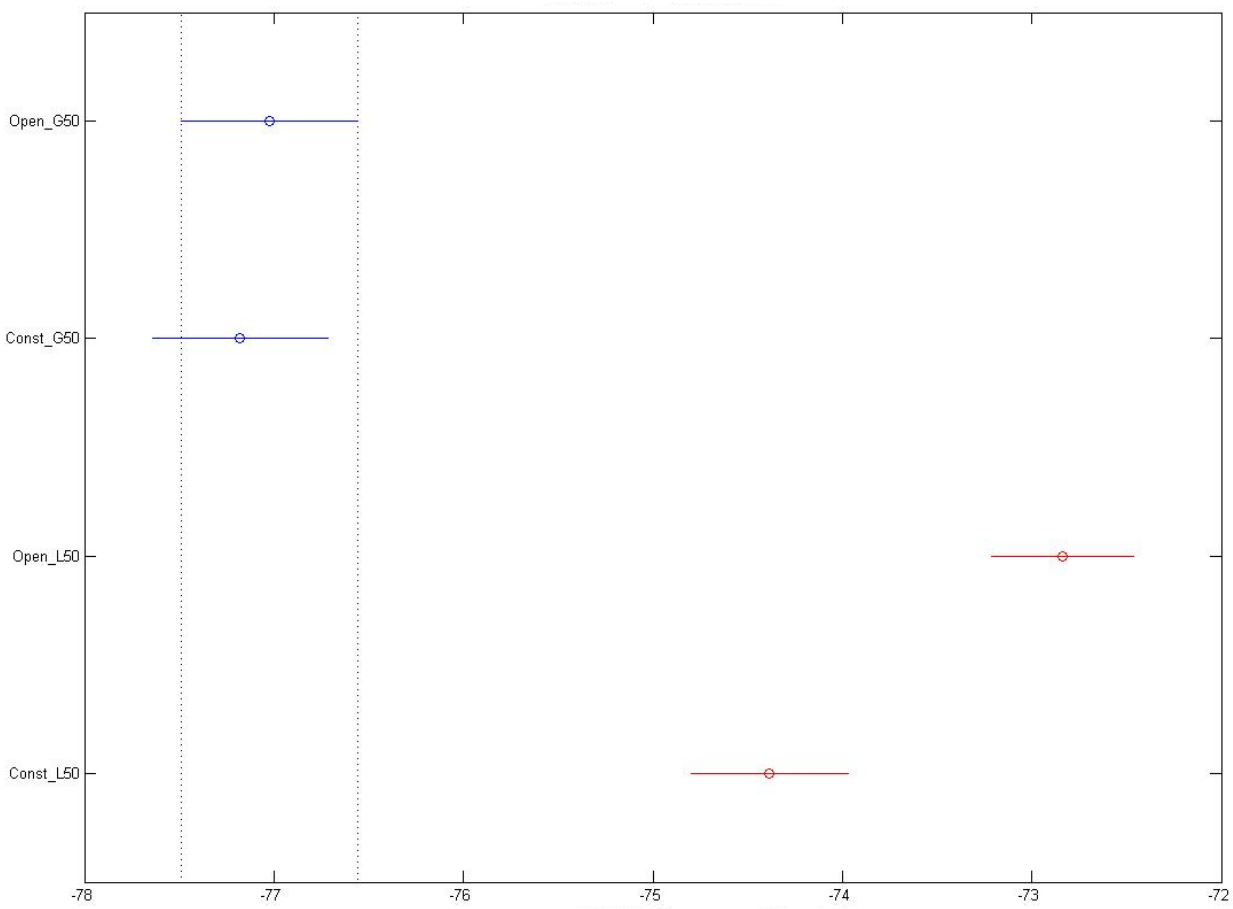

ANOVA Table

Source	SS	df	MS	F	Prob>F
Groups	27246	3	9082.01	85.51	0
Error	836637.7	7877	106.21		
Total	863883.7	7880			

Figure 33. ANOVA and post hoc results for main effect and interaction between the arm length within the open, and constrained scenarios for shoulder flexion/extension. The X-axis is the anatomical mean angular displacements.

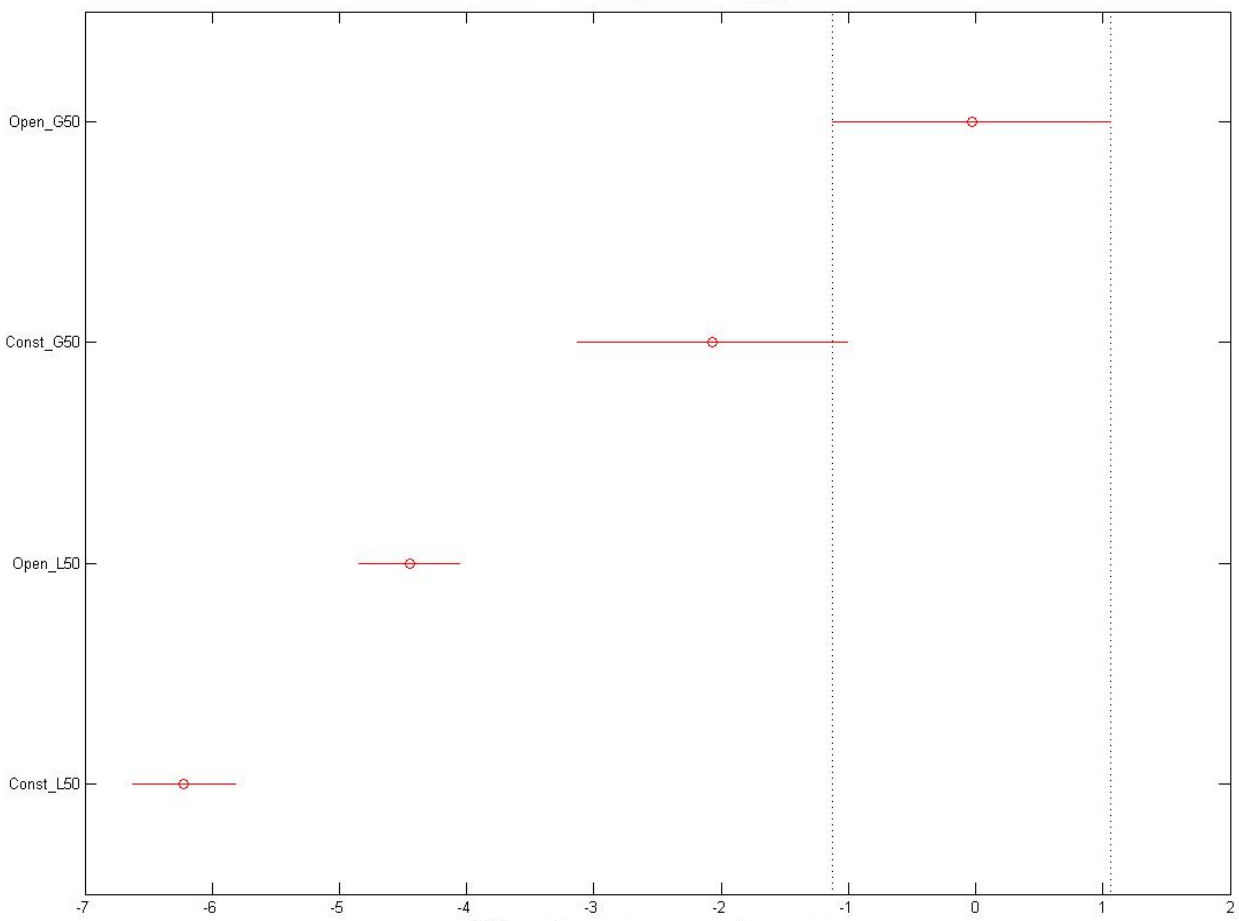

ANOVA Table

Source	SS	df	MS	F	Prob>F
Groups	18955.6	3	6318.54	49.61	0
Error	998481.8	7840	127.36		
Total	1017437.4	7843			

Figure 34. ANOVA and post hoc results for main effect and interaction between the shoulder breadth within the open, and constrained scenarios for elbow flexion/extension. The X-axis is the anatomical mean angular displacements.

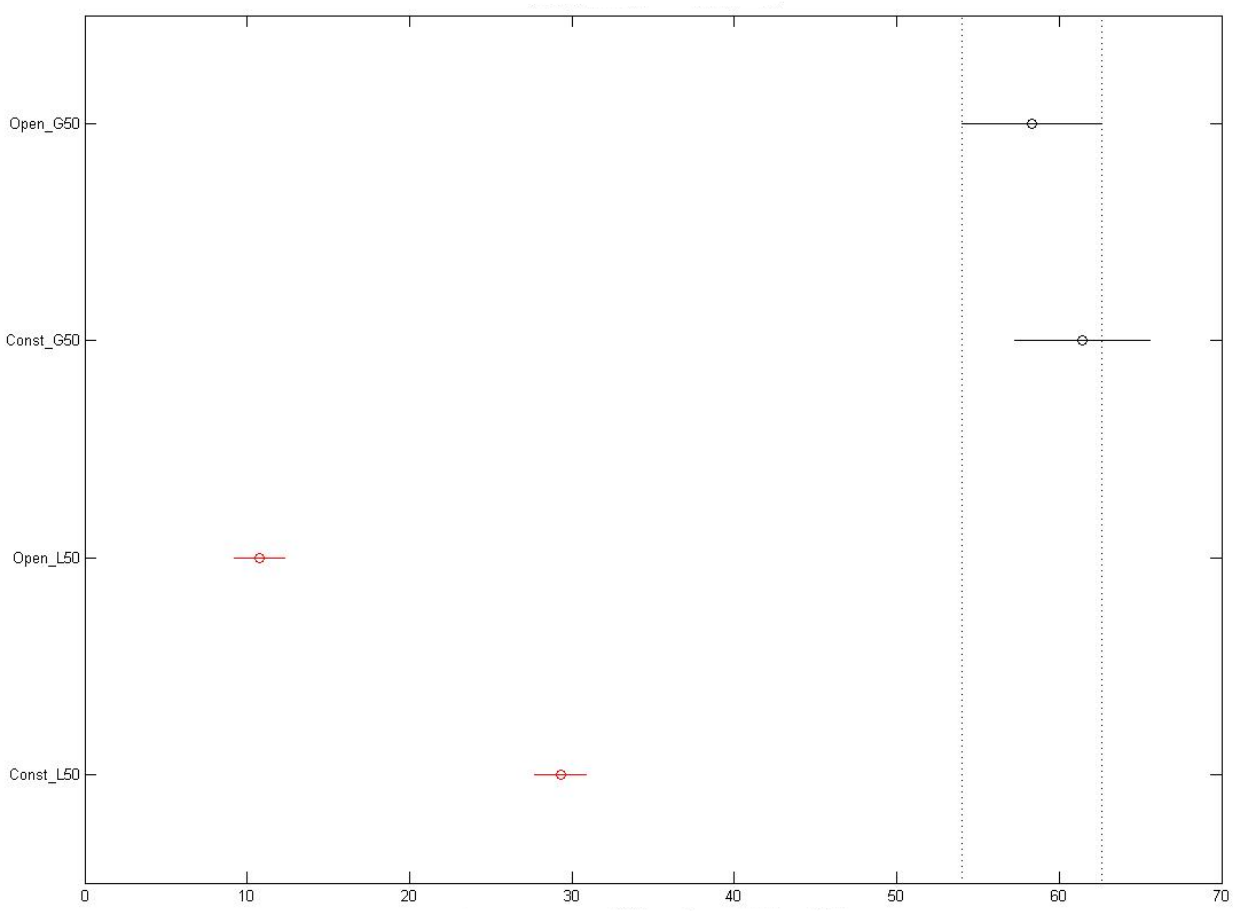

ANOVA Table

Source	SS	df	MS	F	Prob>F
Groups	1.78538e+006	3	595126.9	301.89	0
Error	1.54553e+007	7840	1971.3		
Total	1.72406e+007	7843			

Figure 35. ANOVA results for main effect and interaction between the shoulder breadth within the open, and constrained scenarios for shoulder abduction/adduction. The X-axis is the anatomical mean angular displacements.

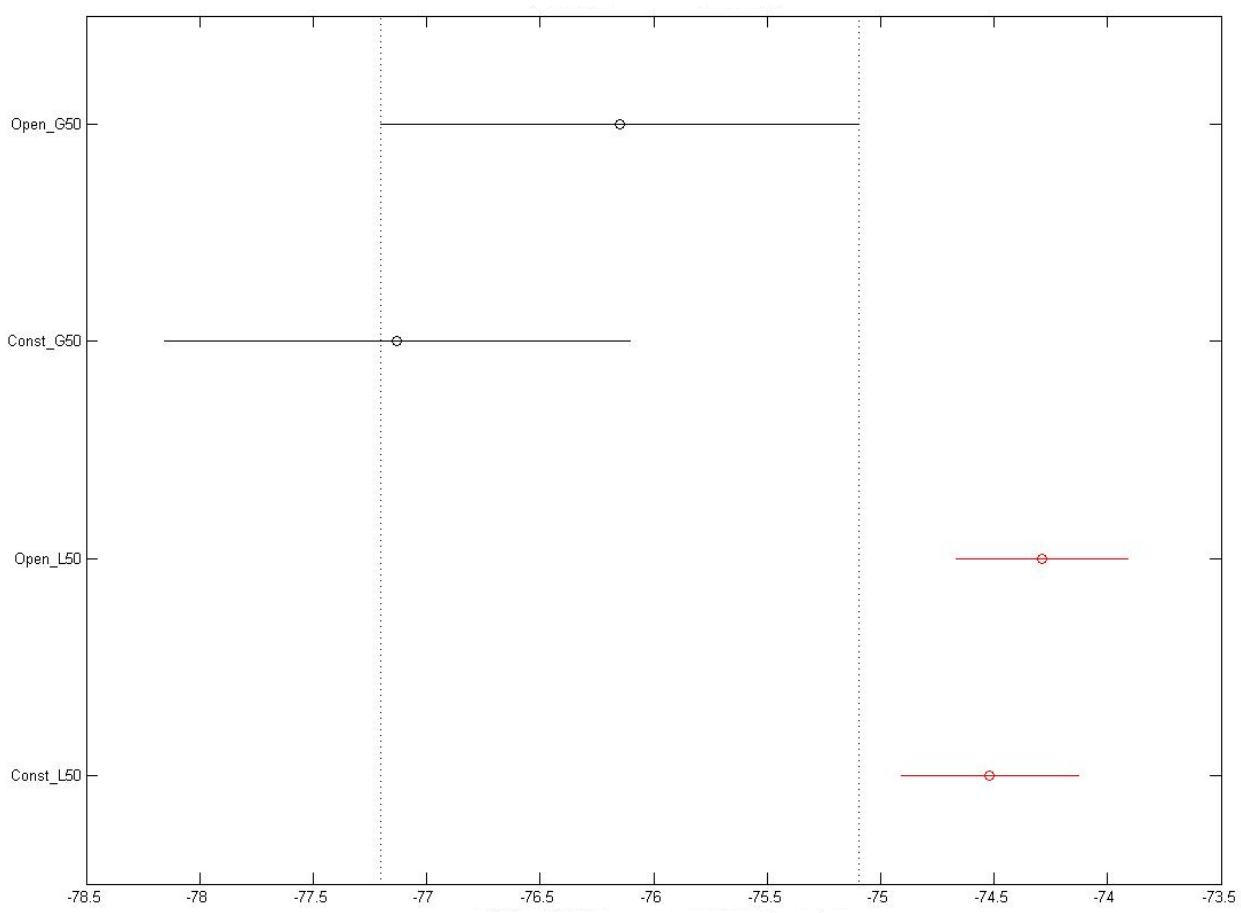

ANOVA Table

Source	SS	df	MS	F	Prob>F
Groups	3938.3	3	1312.76	11.09	2.93842e-007
Error	928409.7	7840	118.42		
Total	932348	7843			

Figure 36. ANOVA results for main effect and interaction between the shoulder breadth within the open, and constrained scenarios for shoulder flexion/extension. The X-axis is the anatomical mean angular displacements.

The results show clear statistical differences between the group with arm length and shoulder breadths greater than the 50th percentile male and the group with arm length and shoulder breadths less than the 50th percentile male. In several instances the open and constrained cycles for the group greater than the 50th percentile male show no differences within the group (Figures 32, 33, 35, and 36) and in the other cases all four conditions (open > 50, constrained > 50, open <

50, and constrained < 50) were different (Figures 31 and 34). Figures 31 and 34 reflect elbow flexion/extension. Depending on the total shoulder component approach, the slaving principal of the elbow would follow suit based on self-organization, and lead to statistically different means for the elbow flexion/extension in the four conditions.

4.3 Surface Electromyography (sEMG)

4.3.1 Maximum Voluntary Contraction (MVC)

Diagrammatically portrayed in Figure 37 and 38 is a MVC sample of Participant 4's 1 Hz open-cycle and constrained-cycle, respectively, where the summative results do not show a great effort with respect to MVC seen in Tables 17 through 20. Normal markers for MVC exertions are typically set to 85% of MVC, or at least a threshold over 50% MVC. The majority of the participant's MVC's were well below the 50% threshold for motor unit synchronization in muscle recruitment, aside from female pectoralis major's activity seen in Table 18. Female pectoralis performance traveled above the 50% mark for all the stimuli cycles in the open and constrained scenarios based on the mean and standard deviation. Assessing the maximum and minimum kinematic threshold results in Tables 11B, 11C, 13B, 13C, 15B, and 15C, female participants had less elbow flexion than their male counterparts. Additionally, the angular velocities of the female participants are higher than their male counterparts in shoulder abduction and adduction as seen in Table 14. Since medial and lateral movement is assisted by the pectoralis, a longer lever arm may cause greater MVC's in muscle recruitment. In considering trunk rotations as a potential instigator to the pectoralis recruitment, the muscles involved for a trunk rotation are not predicated on the pectoralis muscle but rather the external and internal oblique muscles. From an accuracy

perspective, rotating the trunk rather than moving the upper extremity enacts more moving parts, which results in a higher chance of end-effector inaccuracies. This is similar to Marteniuk et al. (1987) for the pointing and grabbing task, where, with more environmental movement constraints, the slower the execution became. From an optimal movement perspective, the addition of more moving parts increases the chances for greater fatigue. To assess just an upper extremity movement in the context of this dissertation, the slaving principal is a critical parameter to optimal movement, where the torso and legs become a slave to the functions of the upper extremity. Thus, the small values in total displacements of CoG shift, as seen in Table 25.

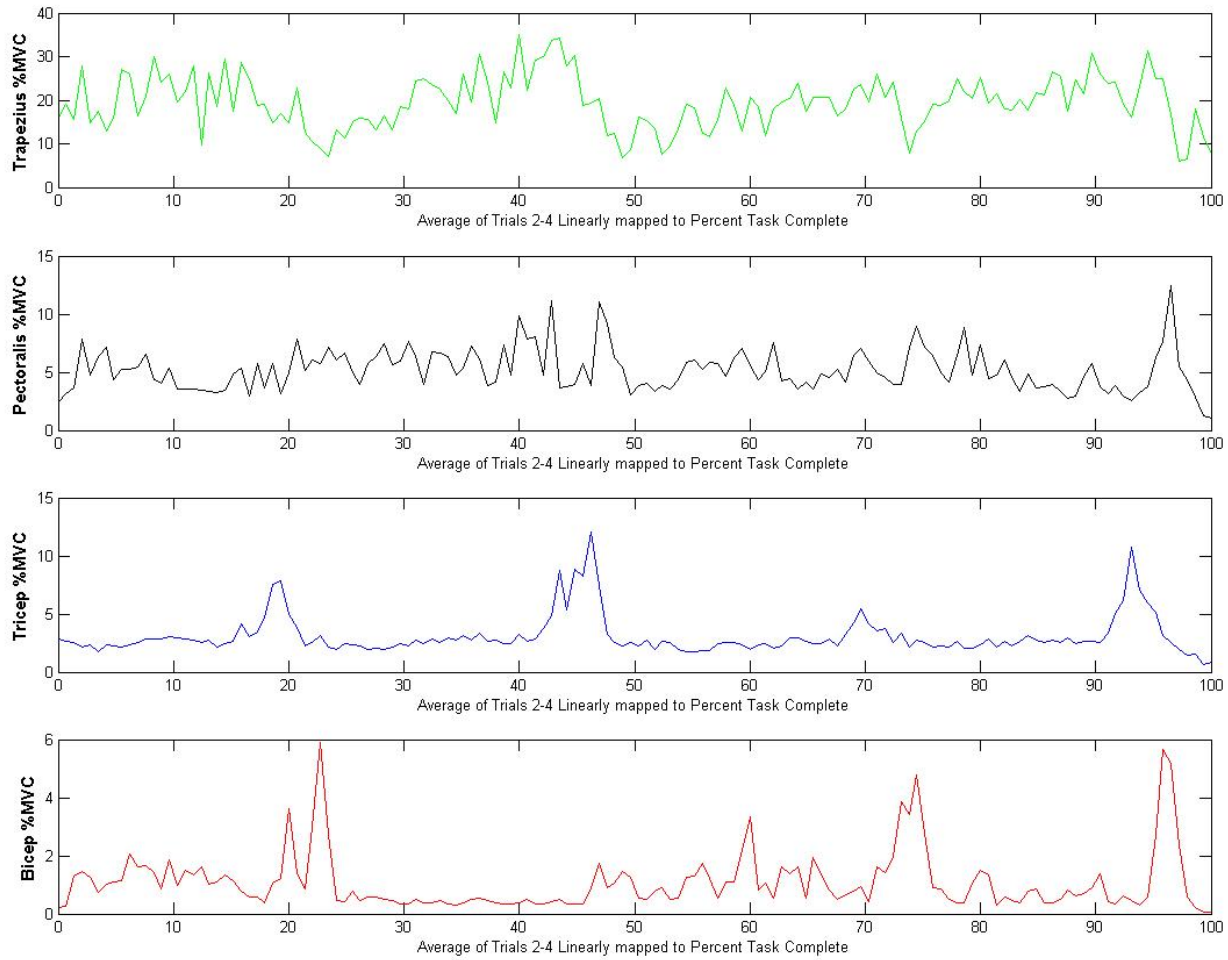

Figure 37. Maximum Voluntary Contraction for participant 4's 1 Hz open-cycle for the four sEMG locations.

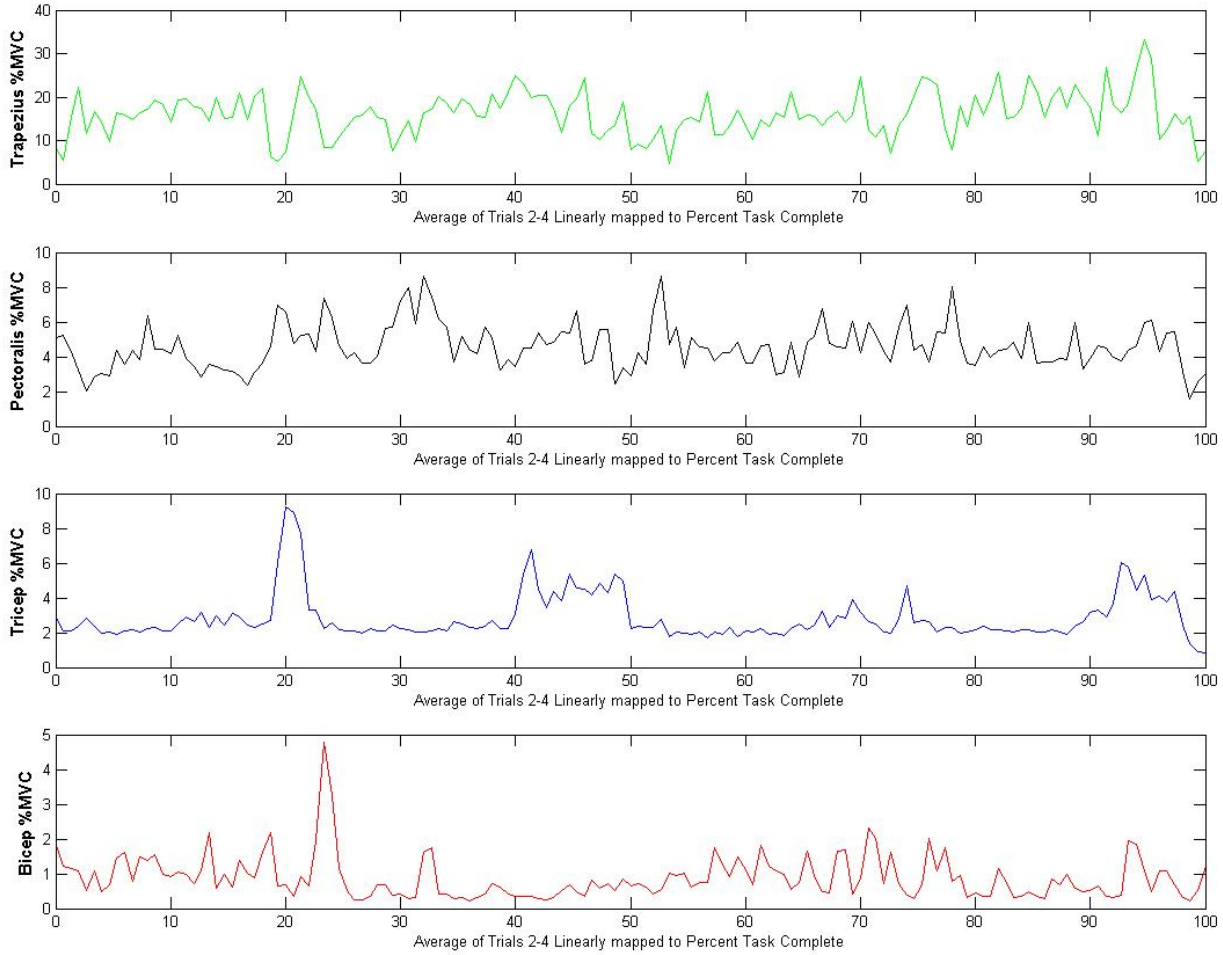

Figure 38. Maximum Voluntary Contraction for participant 4's 1 Hz constrained-cycle for the four sEMG locations.

Table 17. Summative tables for trapezius maximum voluntary contraction for all the participants in the experiment. The white highlight is the open scenario, the green is the open-adjusted scenario, and the blue is the constrained scenario.

MVC	%Trapezius-0Hz Mean (SD)	%Trapezius-1Hz Mean (SD)	%Trapezius-1.3Hz Mean (SD)	%Trapezius-1.7Hz Mean (SD)	%Trapezius-2Hz Mean (SD)	%Trapezius-2.7Hz Mean (SD)
Everyone	24.91 (5.69)	22.99 (3.85)	24.68 (3.83)	27.04 (4.65)	25.60 (5.67)	25.24 (6.37)
Male	25.01 (2.03)	22.85 (1.91)	25.08 (2.19)	28.75 (2.71)	25.25 (2.62)	25.63 (3.03)
Female	24.81 (7.78)	23.12 (5.10)	24.28 (4.96)	25.33 (5.99)	25.94 (7.58)	24.85 (8.49)
< 50th Male	20.44 (6.36)	19.42 (4.10)	19.44 (4.18)	24.51 (5.52)	21.53 (6.02)	20.35 (6.96)
> 50th Male	24.38 (4.14)	21.44 (3.93)	24.49 (4.24)	23.81 (3.87)	23.89 (4.00)	24.01 (4.27)
P3, P6, & P10	14.74 (1.04)	20.78 (1.02)	21.40 (0.64)	21.25 (1.06)	21.34 (1.03)	21.82 (1.79)
Everyone	24.77 (6.13)	22.64 (3.62)	24.34 (4.00)	24.59 (5.04)	21.78 (5.58)	25.64 (6.83)
Male	24.65 (1.77)	23.75 (1.98)	24.69 (1.67)	24.59 (2.13)	17.74 (2.02)	25.82 (3.24)
Female	24.88 (8.49)	21.52 (4.72)	23.99 (5.41)	24.59 (6.80)	25.82 (7.62)	25.46 (9.10)
< 50th Male	25.68 (7.45)	23.41 (4.27)	24.93 (4.67)	25.05 (5.88)	20.42 (6.47)	26.87 (8.14)
> 50th Male	23.40 (3.26)	22.33 (3.32)	23.12 (3.11)	23.44 (3.20)	23.40 (3.39)	23.78 (3.74)

Table 18. Summative tables for pectoralis maximum voluntary contraction for all the participants in the experiment. The white highlight is the open scenario, the green is the open-adjusted scenario, and the blue is the constrained scenario.

MVC	%Pectoralis-0Hz Mean (SD)	%Pectoralis-1Hz Mean (SD)	%Pectoralis-1.3Hz Mean (SD)	%Pectoralis-1.7Hz Mean (SD)	%Pectoralis-2Hz Mean (SD)	%Pectoralis-2.7Hz Mean (SD)
Everyone	20.47 (18.54)	18.71 (14.41)	24.83 (28.19)	31.35 (22.39)	33.31 (12.52)	33.94 (59.58)
Male	8.13 (3.20)	6.56 (3.83)	8.08 (3.25)	28.98 (22.07)	9.69 (4.48)	11.50 (5.56)
Female	32.81 (26.03)	30.86 (20.01)	41.57 (39.73)	33.71 (22.71)	56.92 (17.13)	56.37 (84.07)
< 50th Male	18.88 (6.61)	18.62 (4.47)	18.74 (4.46)	36.98 (20.54)	20.46 (6.71)	20.11 (7.74)
> 50th Male	14.52 (6.43)	10.48 (6.04)	13.05 (5.29)	14.37 (6.73)	16.25 (8.25)	18.59 (8.14)
P3, P6, & P10	13.72 (2.92)	10.84 (2.37)	13.56 (3.07)	13.92 (3.06)	16.23 (3.59)	19.32 (5.49)
Everyone	24.51 (19.97)	20.80 (16.03)	23.61 (17.06)	22.64 (20.25)	18.83 (16.39)	25.82 (39.31)
Male	9.30 (3.97)	8.18 (3.38)	8.85 (3.39)	9.48 (3.92)	8.33 (4.48)	12.20 (6.24)
Female	39.71 (27.96)	33.41 (22.41)	38.37 (23.89)	35.81 (28.37)	29.32 (22.75)	39.44 (55.24)
< 50th Male	30.86 (25.18)	27.50 (20.48)	30.79 (21.60)	28.03 (25.57)	19.69 (20.09)	29.80 (50.10)
> 50th Male	14.97 (6.76)	11.71 (4.63)	13.03 (5.34)	14.44 (6.81)	16.85 (7.52)	18.45 (8.81)

Table 19. Summative tables for triceps maximum voluntary contraction for all the participants in the experiment. The white highlight is the open scenario, the green is the open-adjusted scenario, and the blue is the constrained scenario.

MVC	%Tricep-0Hz Mean (SD)	%Tricep-1Hz Mean (SD)	%Tricep-1.3Hz Mean (SD)	%Tricep-1.7Hz Mean (SD)	%Tricep-2Hz Mean (SD)	%Tricep-2.7Hz Mean (SD)
Everyone	4.47 (1.64)	3.87 (1.34)	4.39 (1.46)	4.69 (1.26)	4.94 (1.26)	5.39 (1.64)
Male	2.69 (0.45)	2.51 (0.47)	2.60 (0.38)	3.36 (0.67)	3.06 (0.68)	3.87 (1.38)
Female	6.25 (2.28)	5.22 (1.84)	6.19 (2.02)	6.02 (1.65)	6.82 (1.64)	6.91 (1.86)
< 50th Male	3.37 (1.12)	2.91 (1.02)	3.24 (1.14)	3.90 (1.15)	4.11 (0.91)	4.52 (1.61)
> 50th Male	6.13 (2.20)	5.31 (1.71)	6.12 (1.83)	5.89 (1.41)	6.19 (1.64)	6.71 (1.69)
P3, P6, & P10	2.67 (0.31)	2.45 (0.24)	2.66 (0.28)	2.73 (0.29)	2.98 (0.32)	3.57 (0.62)
Everyone	4.28 (2.19)	3.79 (1.01)	4.24 (1.52)	4.29 (1.30)	4.36 (1.53)	5.35 (1.71)
Male	2.60 (0.38)	2.53 (0.44)	2.64 (0.39)	2.72 (0.42)	2.46 (0.63)	3.84 (1.10)
Female	5.96 (3.08)	5.05 (1.36)	5.84 (2.12)	5.87 (1.80)	6.26 (2.06)	6.86 (2.16)
< 50th Male	3.12 (2.48)	2.93 (0.83)	3.05 (1.06)	3.29 (1.34)	2.95 (1.35)	4.30 (1.61)
> 50th Male	6.03 (1.67)	5.93 (1.68)	5.94 (1.66)	5.99 (1.65)	6.21 (1.73)	6.58 (1.80)

Table 20. Summative tables for biceps maximum voluntary contraction for all the participants in the experiment. The white highlight is the open scenario, the green is the open-adjusted scenario, and the blue is the constrained scenario.

MVC	%Bicep-0Hz Mean (SD)	%Bicep-1Hz Mean (SD)	%Bicep-1.3Hz Mean (SD)	%Bicep-1.7Hz Mean (SD)	%Bicep-2Hz Mean (SD)	%Bicep-2.7Hz Mean (SD)
Everyone	3.29 (1.69)	2.86 (1.51)	3.35 (1.95)	3.19 (1.84)	3.74 (2.15)	4.31 (2.16)
Male	2.27 (0.91)	1.93 (0.76)	2.32 (1.09)	1.73 (0.60)	2.59 (1.18)	3.09 (1.24)
Female	4.31 (2.20)	3.79 (1.99)	4.37 (2.54)	4.64 (2.53)	4.89 (2.79)	5.53 (2.79)
< 50th Male	3.63 (1.97)	3.32 (1.74)	3.87 (2.40)	3.33 (2.10)	4.13 (2.53)	4.69 (2.46)
> 50th Male	2.77 (1.14)	2.22 (1.06)	2.54 (0.94)	2.84 (1.22)	2.98 (1.26)	3.31 (1.19)
P3, P6, & P10	2.62 (0.70)	1.94 (0.39)	2.35 (0.61)	2.49 (0.68)	2.67 (0.74)	3.32 (0.84)
Everyone	3.19 (1.62)	2.92 (1.41)	3.20 (1.63)	3.47 (1.76)	2.97 (1.66)	4.36 (2.51)
Male	2.23 (0.97)	2.08 (0.80)	2.20 (0.93)	2.45 (1.20)	1.35 (0.44)	3.12 (1.78)
Female	4.16 (2.07)	3.75 (1.83)	4.21 (2.10)	4.49 (2.19)	4.59 (2.31)	5.60 (3.06)
< 50th Male	3.58 (1.98)	3.45 (1.70)	3.59 (1.92)	3.76 (2.07)	2.86 (1.92)	4.61 (2.84)
> 50th Male	2.61 (0.82)	2.26 (0.91)	2.63 (1.03)	2.88 (1.11)	2.98 (1.09)	3.44 (1.48)

Table 21. Two-way ANOVA results for MVC between the male and female open and constrained scenarios. The yellow highlight show a significant difference based on $p < 0.05$.

ANOVA-% MVC Trapezius						
Source of Variation	*SS*	*df*	*MS*	*F*	*P-value*	*F crit*
Scenarios	29.66275	3	9.887583	0.053803	0.983461	2.699393
Stimuli	108.6936	5	21.73871	0.11829	0.988059	2.309202
Interaction	129.1972	15	8.613146	0.046868	1	1.7718
Within	17642.41	96	183.7752			
Total	17909.97	119				
ANOVA-% MVC Pectoralis						
Source of Variation	*SS*	*df*	*MS*	*F*	*P-value*	*F crit*
Scenarios	24364.07	3	8121.357	6.341275	0.000572	2.699393
Stimuli	1287.536	5	257.5072	0.201065	0.961296	2.309202
Interaction	4475.048	15	298.3365	0.232946	0.998654	1.7718
Within	122948.5	96	1280.714			
Total	153075.2	119				
ANOVA-% MVC Tricep						
Source of Variation	*SS*	*df*	*MS*	*F*	*P-value*	*F crit*
Scenario	298.7763	3	99.59211	6.429128	0.000516	2.699393
Stimuli	26.82272	5	5.364545	0.346306	0.883475	2.309202
Interaction	4.426772	15	0.295118	0.019051	1	1.7718
Within	1487.113	96	15.49077			
Total	1817.139	119				
ANOVA-% MVC Bicep						
Source of Variation	*SS*	*df*	*MS*	*F*	*P-value*	*F crit*
Scenario	139.0039	3	46.33464	6.293542	0.000606	2.699393
Stimuli	24.56968	5	4.913937	0.66745	0.649044	2.309202
Interaction	3.354246	15	0.223616	0.030373	1	1.7718
Within	706.7762	96	7.362253			
Total	873.7041	119				

Tables 17 through 20 provide a summary of participant's MVC performance separated by 'everyone' or all 10 participants, 'Male', 'Female', '<50th Male' or less than 50th percentile male, '>50th Male' or greater than 50th percentile male. This is done for each scenario: open (white highlight), open-adjusted (green highlight), and constrained (blue highlight). Table 21 shows the results of a two-way ANOVA of all the MVC's for each participant with respect to the

open and constrained scenarios. The significant differences were only seen for the pectoralis, triceps, and biceps MVC's, with respect to the scenarios. This again points to arm length differences, as the pectoralis, triceps, and biceps are engaged in moving the arm anteriorly and medial in the frontal plane of the body. Additionally, the efficient use of shortening the lever arm at the elbow played a big role in biceps and triceps activation and pectoralis recruitment, especially if the lever remained longer than optimum. Also, based on self-reports, the participants are able to perform the pointing task without the need of additional muscle conditioning.

4.3.2 Power Spectral Density

Figures 39 and 40 are organized with respect to the muscle groups as in Figures 37 and 38. Figures 39 and 40 are plots of the entire 5 trial cycle with vertical marks to delineate trials 2, 3, and 4. In Figures 39 and 40, which correspond to the 1 Hz open-cycle and 1 Hz constrained-cycle, there are no marked shifts from higher Type II frequencies to lower Type I for trials 2, 3, and 4. In fact, the majority of the frequencies jump back and forth from Type I to Type II, with respect to the muscle. Similar results followed for the other 9 participants. If a shift were to occur, then the result would be a fixation at the Type I muscle recruitment and not a shift up, then down, and then up again. This is a sign of upper extremity use as a result of the motor control algorithm, which is specific to a participant. In assessing MVC and spectral shift, there were no shifts in the median and mean frequencies, as seen in Tables C72 and C73 in Appendix C; however, the frequency results do point to a method of quantifying how participants recruit Type I and Type II muscles for a goal directed movement.

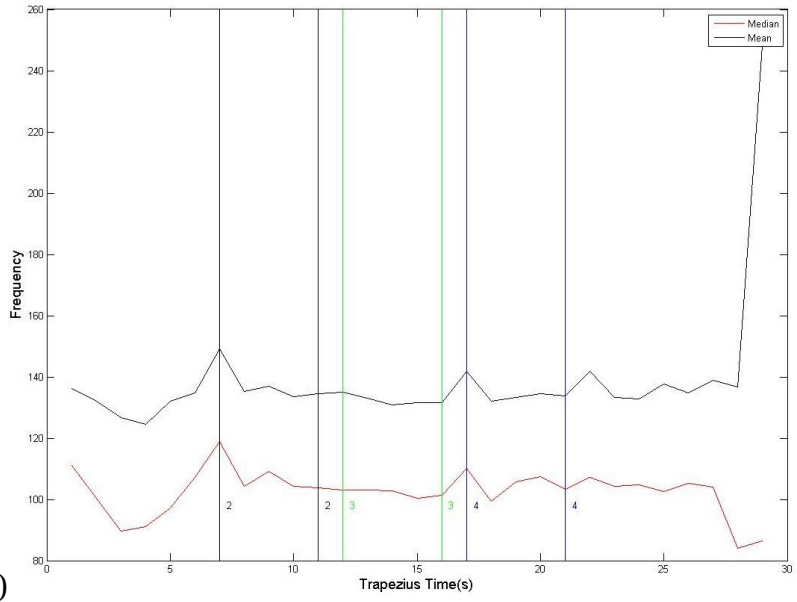
Median
Mean
Frequency
Trapezius Time(s)
2
2
3
3
4
4

A)

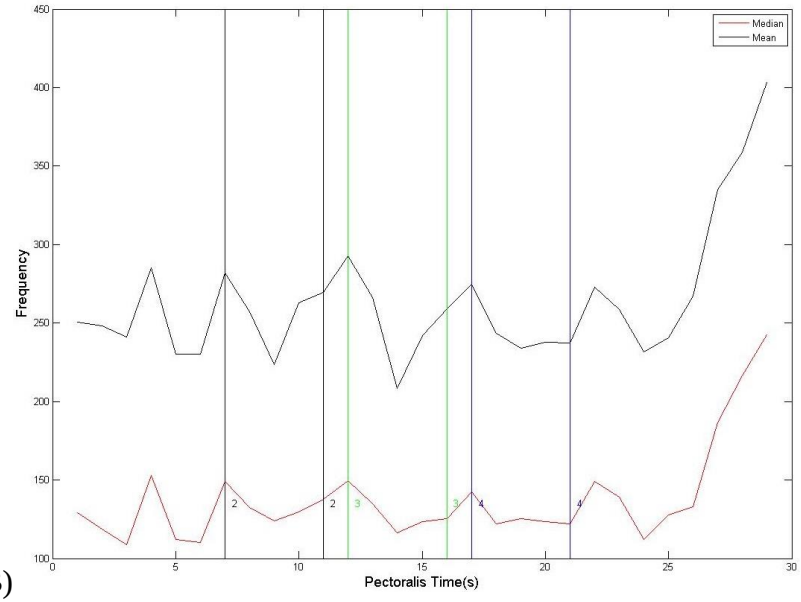
Median
Mean
Frequency
Pectoralis Time(s)
2
2
3
3
4
4

B)

C)

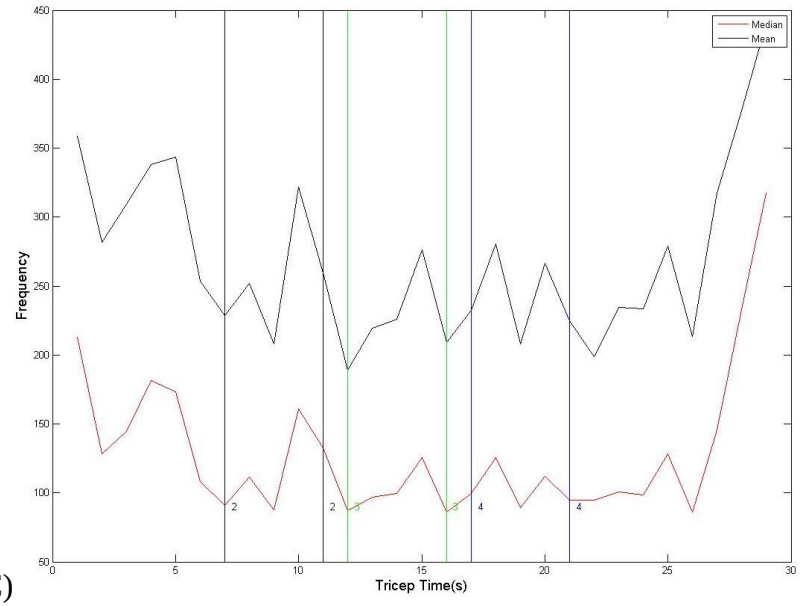

D)

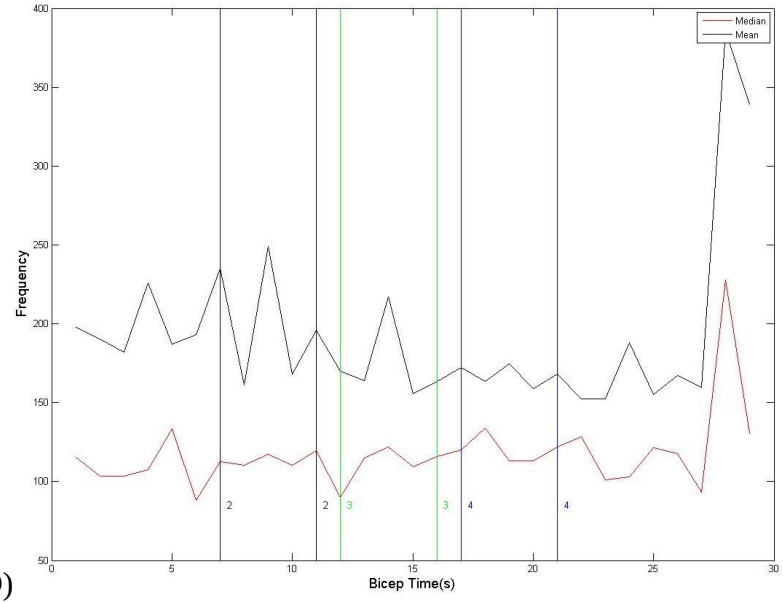

Figure 39. Frequency Spectrum for participant 4's 1 Hz open-cycle for the four sEMG locations. A) Median and mean shift for trapezius. B) A) Median and mean shift for Pectoralis. C) Median and mean shift for triceps brachii. D) Median and mean shift for biceps brachii.

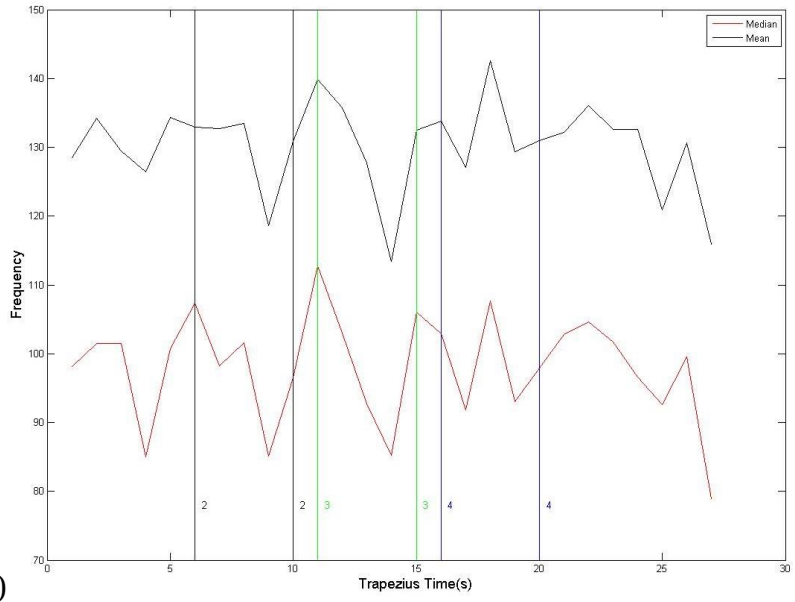
Median
Mean
Frequency
Trapezius Time(s)
2
2
3
3
4
4

A)

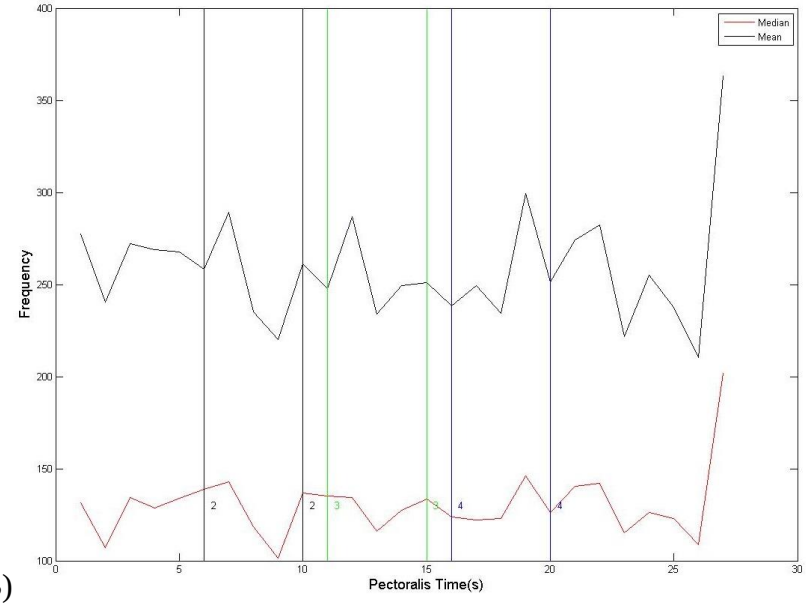
Median
Mean
Frequency
Pectoralis Time(s)
2
2
3
3
4
4

B)

C)

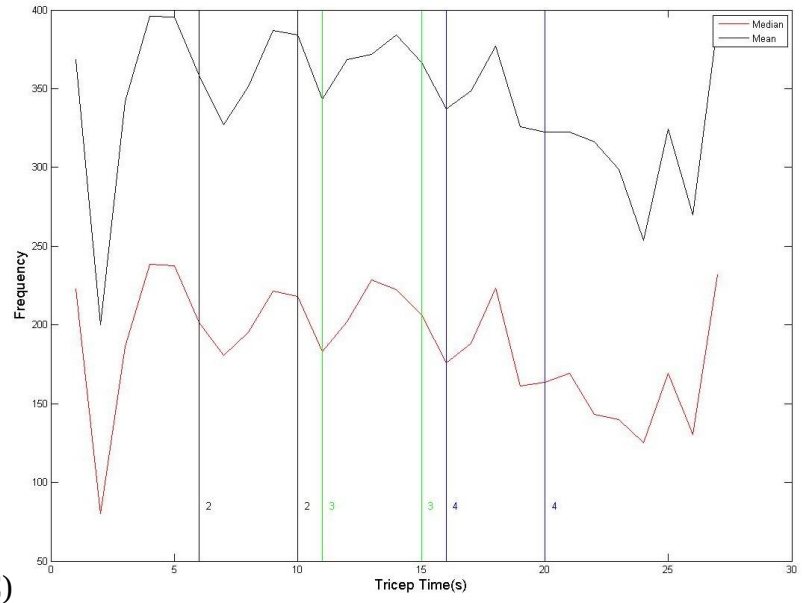

D)

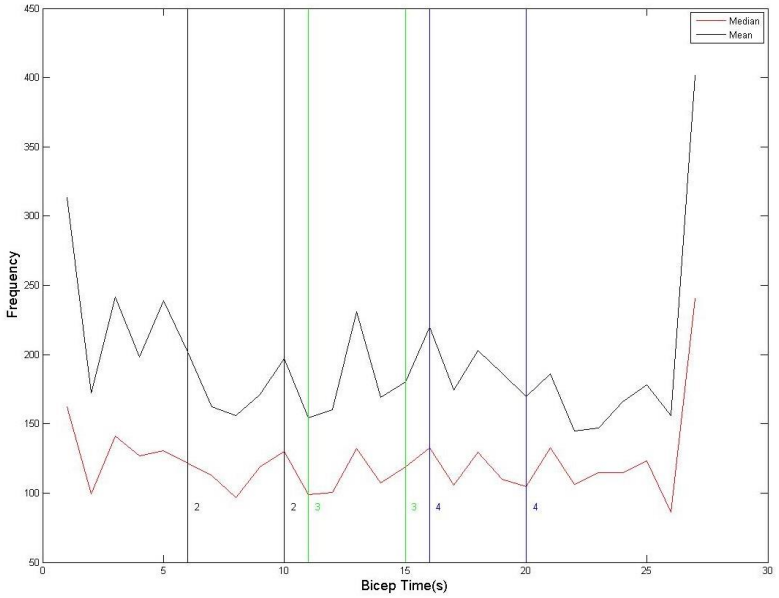

Figure 40. Frequency Spectrum for participant 4's 1 Hz constrained-cycle for the four sEMG locations. A) Median and mean shift for trapezius. B) A) Median and mean shift for Pectoralis. C) Median and mean shift for triceps brachii. D) Median and mean shift for biceps brachii.

Table 22. Two-way ANOVA results for median spectral data between the male and female open and constrained scenarios. The yellow highlight show a significant difference based on $p < 0.05$.

ANOVA-Median Frequency Trapezius						
Source of Variation	*SS*	*df*	*MS*	*F*	*P-value*	*F crit*
Scenario	11680.48	3	3893.495	4.928317	0.003158	2.699393
Stimulus	970.9583	5	194.1917	0.245804	0.940966	2.309202
Interaction	946.8455	15	63.12303	0.0799	0.999999	1.7718
Within	75842.42	96	790.0252			
Total	89440.71	119				
ANOVA-Median Frequency Pectoralis						
Source of Variation	*SS*	*df*	*MS*	*F*	*P-value*	*F crit*
Scenario	4490.442	3	1496.814	1.364501	0.258313	2.699393
Stimulus	3071.058	5	614.2116	0.559917	0.730433	2.309202
Interaction	1054.567	15	70.30448	0.06409	1	1.7718
Within	105309	96	1096.968			
Total	113925	119				
ANOVA-Median Frequency Tricep						
Source of Variation	*SS*	*df*	*MS*	*F*	*P-value*	*F crit*
Scenario	105613.9	3	35204.62	30.75281	<0.001	2.699393
Stimulus	16074.07	5	3214.814	2.808283	0.020674	2.309202
Interaction	2700.021	15	180.0014	0.157239	0.999877	1.7718
Within	109897.1	96	1144.761			
Total	234285	119				
ANOVA-Median Frequency Bicep						
Source of Variation	*SS*	*df*	*MS*	*F*	*P-value*	*F crit*
Scenario	40203.33	3	13401.11	14.41888	<0.001	2.699393
Stimulus	3381.76	5	676.3519	0.727719	0.60432	2.309202
Interaction	3328.106	15	221.8737	0.238724	0.998448	1.7718
Within	89223.76	96	929.4141			
Total	136137	119				

Tables C72 and C73 provide the results of the median spectral data for each participant separated by gender. The color coding is similar to the MVC section described earlier. Table 22 is a two-way ANOVA of the median results and there is statistical significance in the trapezius scenario, triceps scenario, and stimulus, and biceps scenario. Since the

premise of the analysis of median frequency shift was to conclude fatigue, the tables (Table C72 and C73) do not reflect a definitive shift; therefore, there are differences between males and females but only in the types of muscles they recruit based on how their motor control system uses their right upper extremity.

Table 23. Two-way ANOVA results for mean spectral data between the male and female open and constrained scenarios. The yellow highlight show a significant difference based on $p < 0.05$.

ANOVA-Mean Frequency Trapezius						
Source of Variation	*SS*	*df*	*MS*	*F*	*P-value*	*F crit*
Scenario	102560.8	3	34186.92	12.84505	<0.001	2.699393
Stimulus	3650.274	5	730.0548	0.274303	0.926171	2.309202
Interaction	1334.118	15	88.94118	0.033418	1	1.7718
Within	255502.8	96	2661.487			
Total	363047.9	119				
ANOVA-Mean Frequency Pectoralis						
Source of Variation	*SS*	*df*	*MS*	*F*	*P-value*	*F crit*
Scenario	2404.27	3	801.4235	0.241492	0.867191	2.699393
Stimulus	7005.456	5	1401.091	0.422189	0.832241	2.309202
Interaction	2523.243	15	168.2162	0.050688	1	1.7718
Within	318589.2	96	3318.638			
Total	330522.2	119				
ANOVA-Mean Frequency Tricep						
Source of Variation	*SS*	*df*	*MS*	*F*	*P-value*	*F crit*
Scenario	150957.3	3	50319.11	34.03481	<0.001	2.699393
Stimulus	21579.21	5	4315.841	2.919146	0.01696	2.309202
Interaction	2595.302	15	173.0202	0.117027	0.999982	1.7718
Within	141932.2	96	1478.46			
Total	317064	119				
ANOVA-Mean Frequency Bicep						
Source of Variation	*SS*	*df*	*MS*	*F*	*P-value*	*F crit*
Scenario	171615.2	3	57205.08	17.47656	<0.001	2.699393
Stimulus	7627.352	5	1525.47	0.466042	0.80066	2.309202
Interaction	2448.279	15	163.2186	0.049864	1	1.7718
Within	314231.6	96	3273.245			
Total	495922.4	119				

Similar to the median frequency section, Tables C74 and C75 provide mean frequency results. Table 23 is the result of a two-way ANOVA, where there is statistical significance with the trapezius scenario, triceps scenario and stimulus, and the biceps scenario. This again reflects

more of how the motor control system recruits muscle fibers rather than any fatiguing conclusions.

4.4 Center of Gravity (CoG) Postural Shift

Figures 41 and 42 show a sample result for Participant 4's 1 Hz for the open-cycle and constrained-cycles, respectively. Figures 41A and 42A reflects the shift in CoG of the participant during the 2, 3, and 4 trials of the 1 Hz cycle. Figures 41B and 42B show the CoG shift as a result of acceleration. Additionally, the green and black lines show ±1 and ±2 standard deviations of acceleration for the specific 1 Hz cycle, with up to ±2 standard deviations identifies the potential acceleration range for this particular participant.

A)

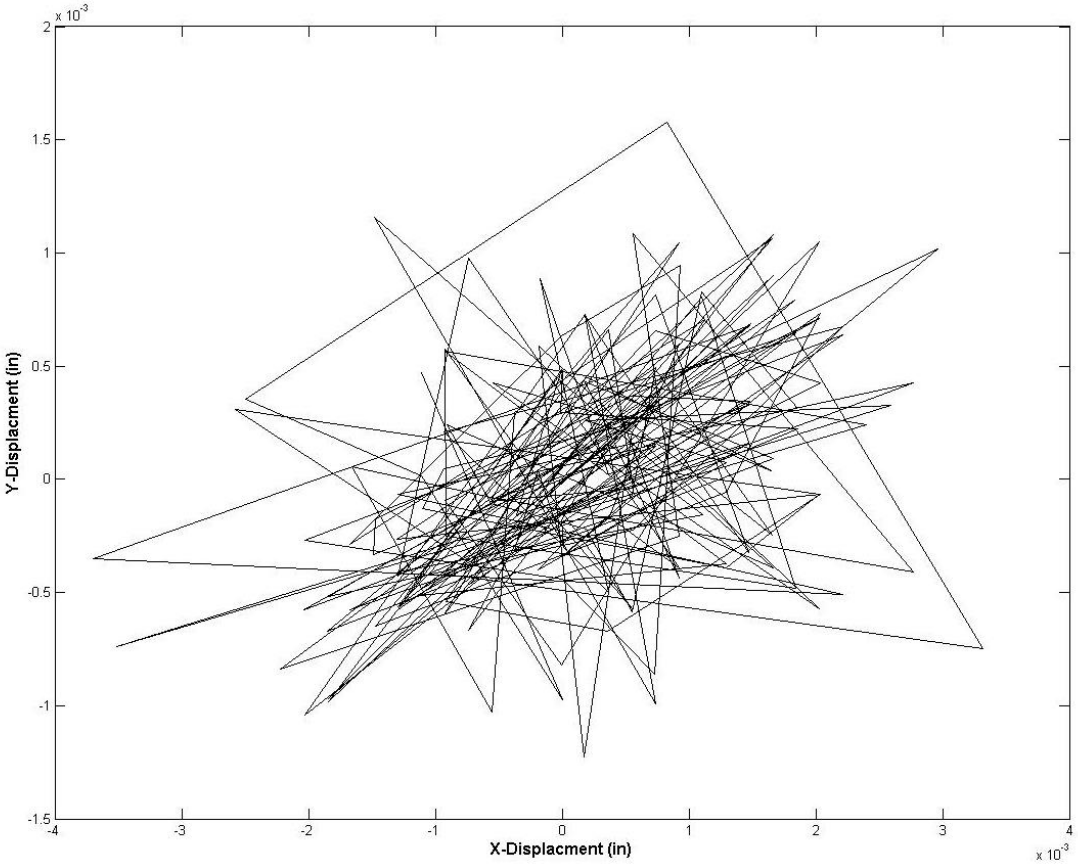
x 10^-3
2
1.5
1
0.5
0
-0.5
-1
-1.5
Y-Displacment (in)
-4
-3
-2
-1
0
1
2
3
4
X-Displacment (in)
x 10^-3

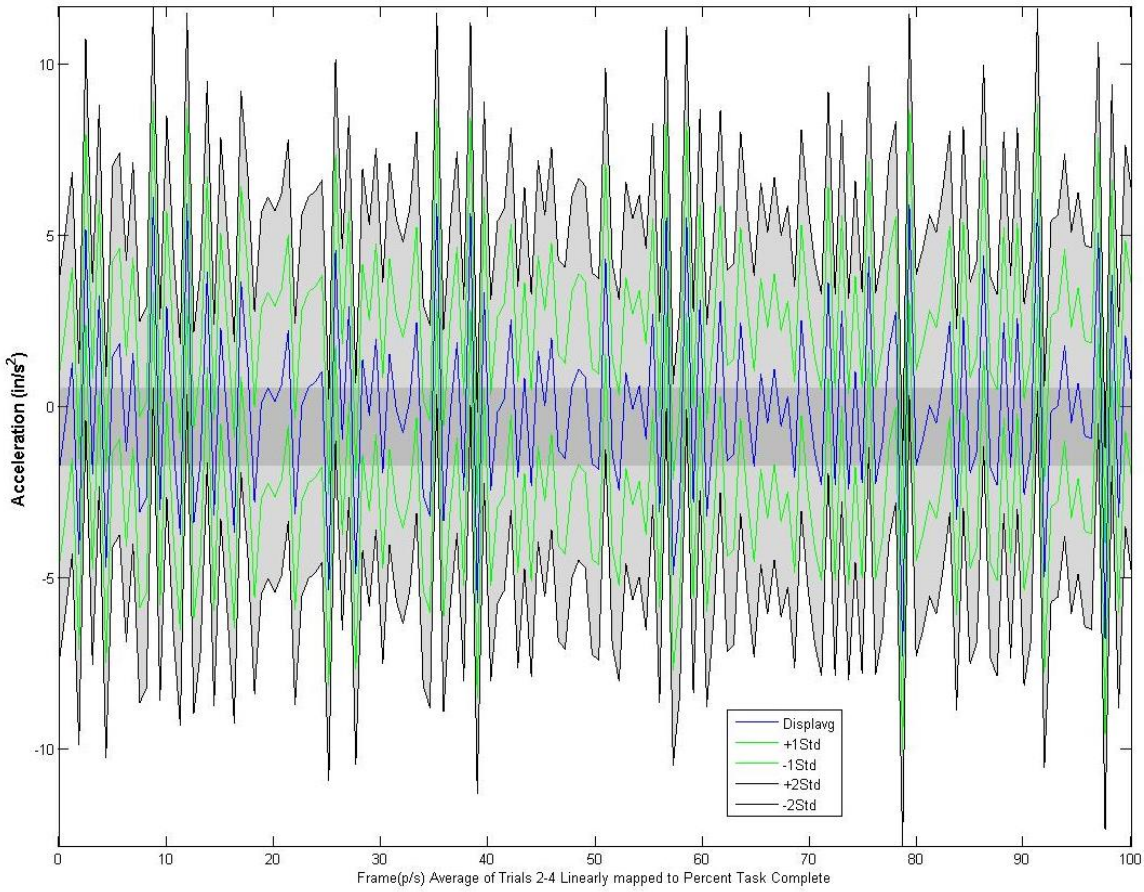

B)

Figure 41. CoG shift for participant 4's 1 Hz open-cycle. A) Body sway movement (in) B) Acceleration (in/s^2) of the movement in A.

A.

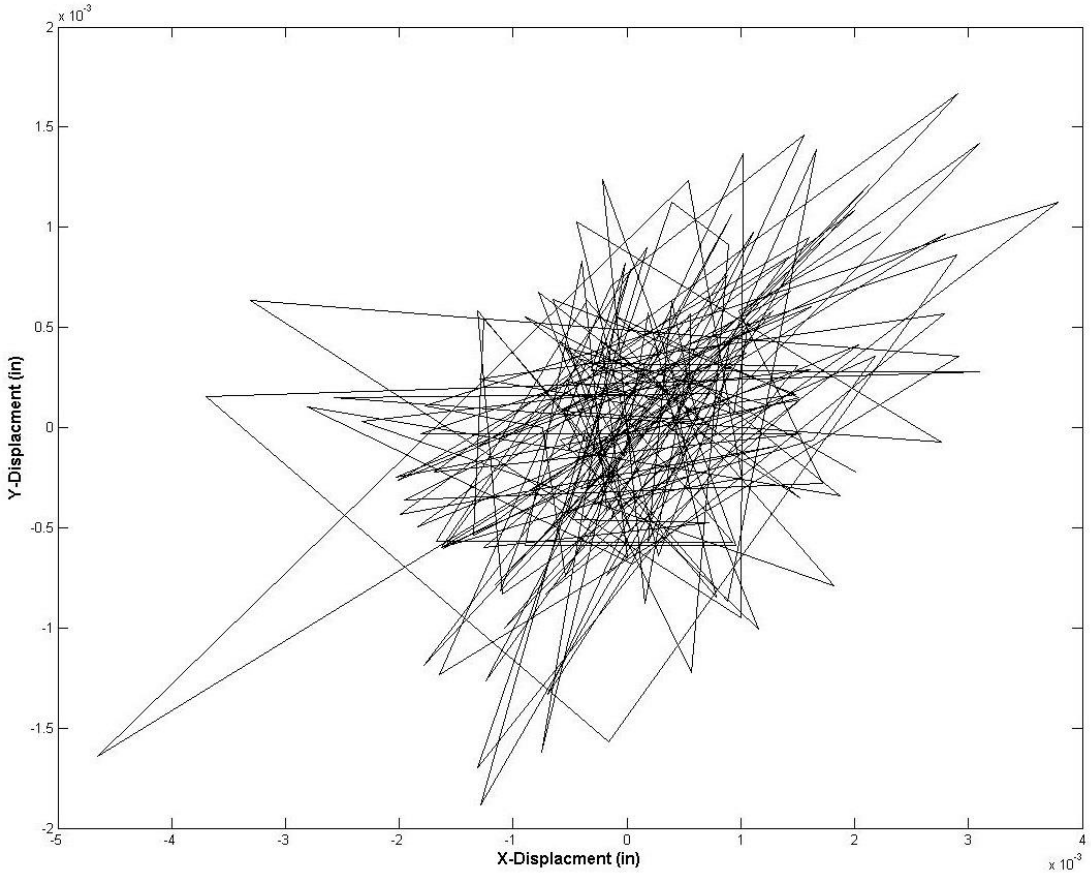
x 10^-3
2
1.5
1
0.5
0
-0.5
-1
-1.5
-2
Y-Displacment (in)
-5
-4
-3
-2
-1
0
1
2
3
4
X-Displacment (in)
x 10^-3

B.

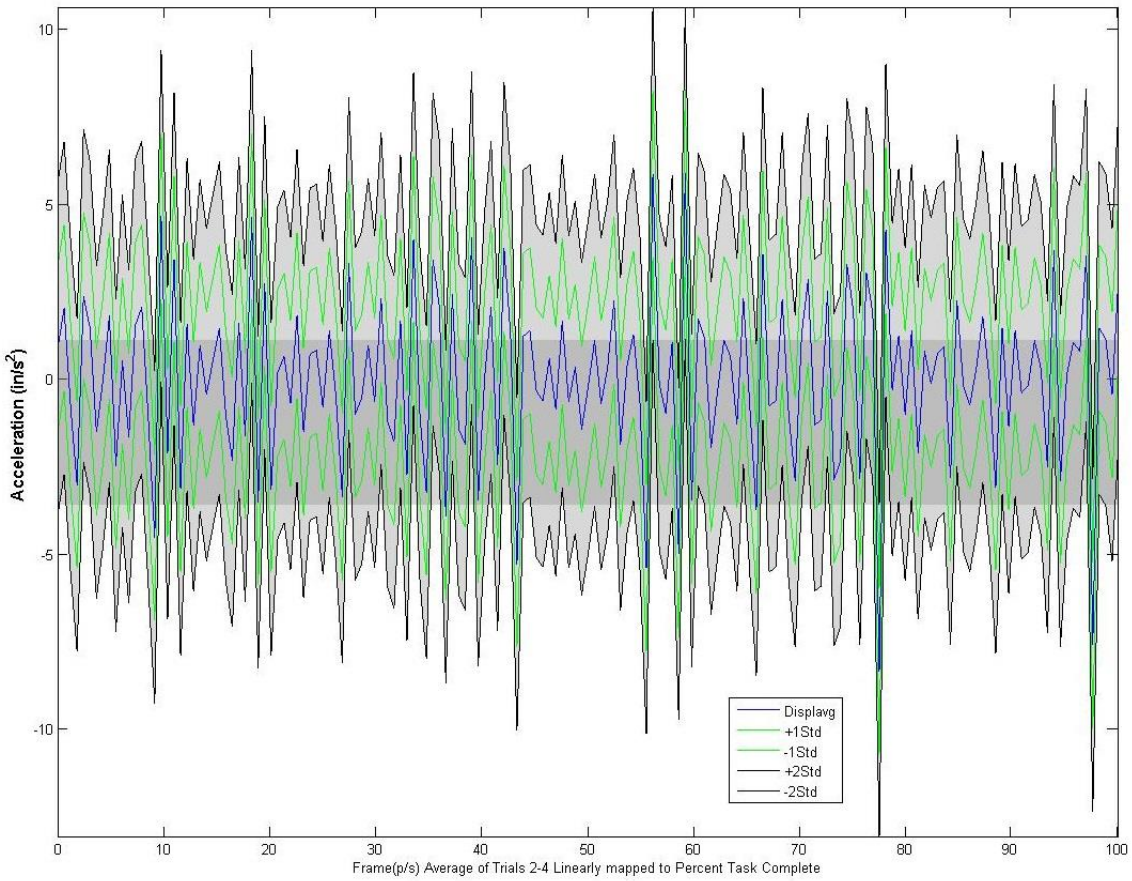

Figure 42. CoG shift for participant 4's 1 Hz constrained-cycle. A) Body sway movement (in) B) Acceleration (in/s^2) of the movement in A.

Table 24. Summative tables for total displacement in CoG shift (in) for all the participants in the experiment. The white highlight is the open scenario, the green is the open-adjusted scenario, and the blue is the constrained scenario.

CoG	Total Displacement-0Hz (SD)	Total Displacement-1Hz (SD)	Total Displacement-1.3Hz (SD)	Total Displacement-1.7Hz (SD)	Total Displacement-2Hz (SD)	Total Displacement-2.7Hz (SD)
Everyone	0.14 (0.04)	0.20 (0.02)	0.14 (0.02)	0.12 (0.02)	0.10 (0.02)	0.09 (0.03)
Male	0.12 (0.04)	0.17 (0.01)	0.13 (0.01)	0.11 (0.01)	0.09 (0.01)	0.07 (0.02)
Female	0.16 (0.03)	0.22 (0.02)	0.15 (0.01)	0.14 (0.03)	0.11 (0.03)	0.10 (0.02)
< 50th Male	0.16 (0.04)	0.21 (0.03)	0.15 (0.01)	0.13 (0.03)	0.11 (0.02)	0.09 (0.02)
> 50th Male	0.11 (0.03)	0.18 (0.02)	0.14 (0.02)	0.11 (0.01)	0.09 (0.01)	0.08 (0.04)
P3, P6, & P10	0.12 (0.04)	0.18 (0.01)	0.14 (0.01)	0.11 (0.01)	0.08 (0.01)	0.07 (0.02)
Everyone	0.15 (0.04)	0.19 (0.03)	0.15 (0.02)	0.12 (0.02)	0.10 (0.04)	0.09 (0.03)
Male	0.13 (0.04)	0.17 (0.02)	0.13 (0.01)	0.11 (0.01)	0.08 (0.04)	0.08 (0.02)
Female	0.16 (0.03)	0.22 (0.02)	0.16 (0.02)	0.13 (0.02)	0.12 (0.03)	0.10 (0.03)
< 50th Male	0.17 (0.03)	0.20 (0.03)	0.16 (0.02)	0.13 (0.02)	0.10 (0.05)	0.10 (0.03)
> 50th Male	0.11 (0.03)	0.18 (0.02)	0.13 (0.01)	0.11 (0.01)	0.10 (0.01)	0.08 (0.03)

Table 25. Two-way ANOVA results for total force displacement (in) of CoG data between the male and female open and constrained scenarios. The yellow highlight show a significant difference based on $p < 0.05$.

ANOVA-Total Displacement Force						
Source of Variation	*SS*	*df*	*MS*	*F*	*P-value*	*F crit*
Scenario	0.025927	3	0.008642	15.78488	<0.001	2.699393
Stimulus	0.142737	5	0.028547	52.14125	<0.001	2.309202
Interaction	0.002723	15	0.000182	0.331608	0.990567477	1.7718
Within	0.05256	96	0.000548			
Total	0.223947	119				

Table 26. Two-way ANOVA results for force acceleration (in/s^2) of CoG data between the male and female open and constrained scenarios. The yellow highlight show a significant difference based on $p < 0.05$.

ANOVA-Acceleration Force						
Source of Variation	*SS*	*df*	*MS*	*F*	*P-value*	*F crit*
Scenario	6.13482	3	2.04494	7.065486	<0.001	2.699393
Stimulus	0.99137	5	0.198274	0.685058	0.635873057	2.309202
Interaction	2.76973	15	0.184649	0.637981	0.836584789	1.7718
Within	27.78496	96	0.289427			
Total	37.68088	119				

Table 24 is the summative data for Tables C76 and C77, where Tables C76 and C77 are the results of total CoG displacement per stimulus grouped by male and female, respectively. Tables C78 and C79 are the results of acceleration of CoG displacement grouped by male and female. Table C78 and C79 have some negative acceleration means that denote the quadrants of the force plate and, based on the stimulus run, participants were either more on the balls of their feet (positive) or on their heels (negative). This movement phenomena is a compensatory device to remain balanced when performing an upper extremity movement. As a result, Table 25 shows a two-way ANOVA of total CoG displacement, where scenario and stimulus are statistically significant. Table 26 is similar to Table 25 except that it shows the results for CoG acceleration. In Table 26, the scenario or open and constrained comparison between males and females is statistically significant. This all makes sense in that an individual's control of their upper extremity, with regard to how they accommodate for movement, is dissipated differently. If an individual is of a larger anthropometry, which is usually the male population, then the motor control strategy is dependent on muscle distribution and physical size. However, if an individual is of a smaller anthropometry, which is usually female, then the motor control strategy would be

different and there may be more total movement to perform the same task, as seen in Tables 24. Additionally, adipose tissue distribution may have an effect on CoG shifts depending on where the major deposits reside.

In all, the modalities and results provide a robust holistic view in painting a clear picture of upper extremity movement. Every measurement modality delineated in this dissertation encompasses a method to quantify a specific component of biomechanical information in an upper extremity movement.

4.5 Self-Reported Surveys

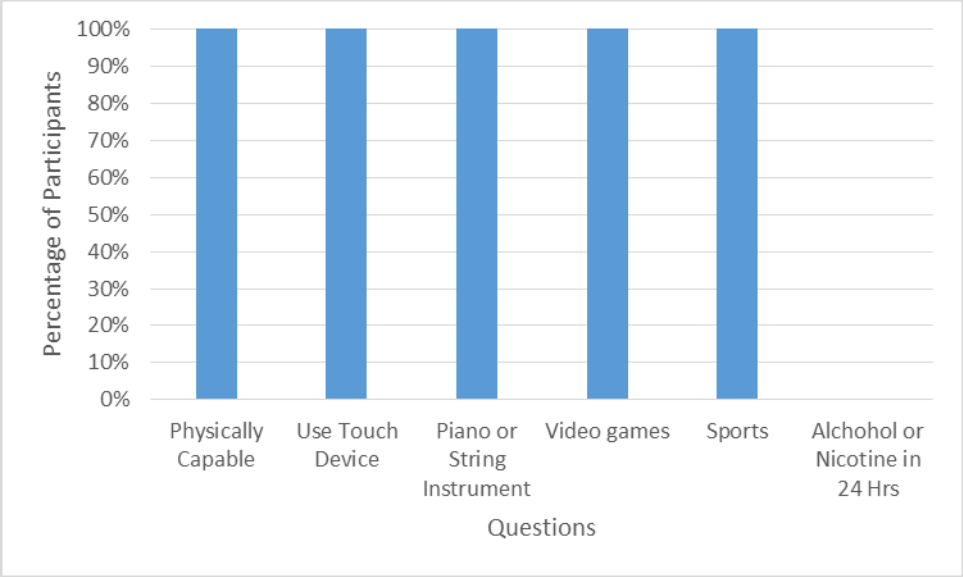

Figure 43. Self-report results for the pre-survey questionnaire (Appendix A)

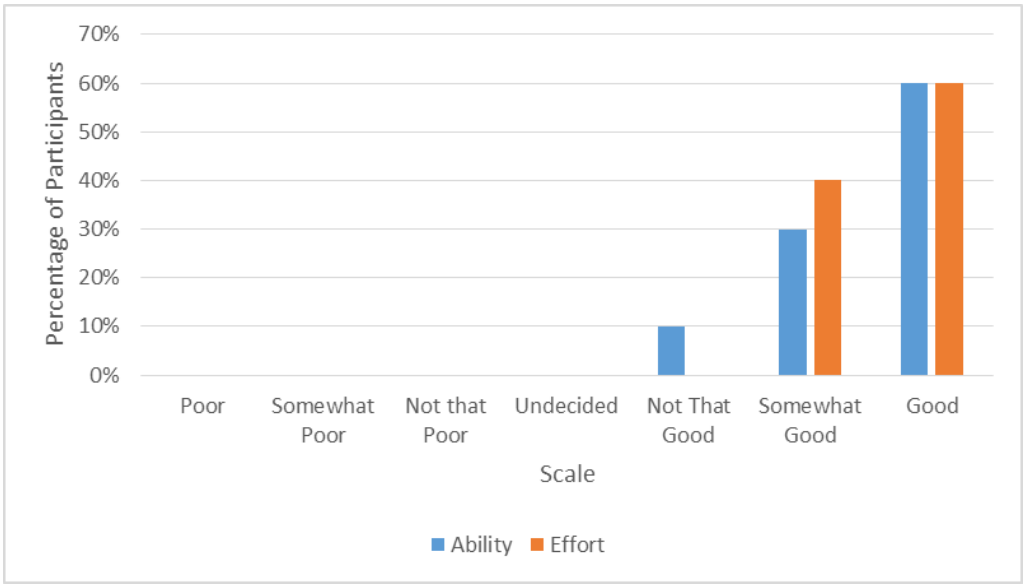

Figure 44. Self-report results for the post-survey questionnaire on the participant's performance (Appendix A)

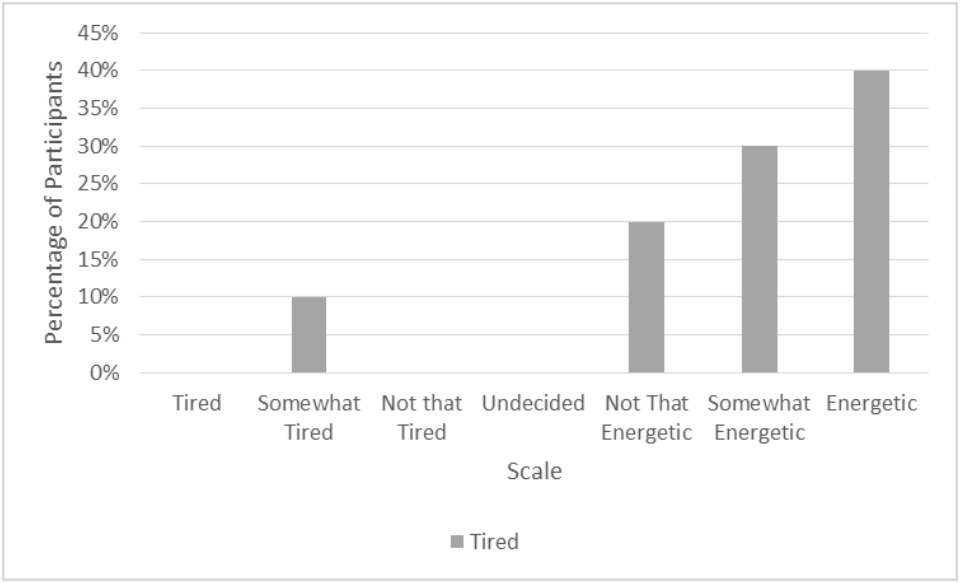

Figure 45. Self-report results for the post-survey questionnaire on the participant's post physiological state (Appendix A)

The results from the self-reported surveys, seen in Figure 43, reflects the criteria delineated in the design section of this dissertation. Figure 44 shows that the majority of participants (60%) thought their ability and effort was good. Only 10% of the participants thought their ability was not that good, while 40% and 30% thought they were somewhat good in effort and ability, respectively. In essence, the participants report that they were trying to be successful in performing the experiment at their utmost ability. Figure 45 provides a self-report on fatigue, where 40% were energetic, 30% were somewhat energetic, 20% were not that energetic, and 10% were somewhat tired. However, the objective power spectral results did not reflect fatigue for all 10 participants. The subjective results may be a function of the focus to perform the task as opposed to physical muscle fatigue during the task.

5. Discussion

5.1 Design Considerations

The results provide a holistic view of right upper extremity performance and the method can be expounded to both upper extremities in a pointing task or to a grabbing task. The essence of the simple technique to quantify biomechanical information is that other tasks can be captured with only a change to the touchscreen. More specifically, if it is a grabbing task, then only a change from the touchscreen to a cup or tool is required to model dexterity. Additionally, the measurement modalities are portable enough that comparisons can be made aboard naval vessels; therefore, comparisons can be made within the controlled laboratory environment and the uncontrolled naval environment. This is particularly important when the vessel is out to sea and potential results can yield valuable insight into appropriate and efficient design modifications.

From a design perspective, the term *golden section* in human anatomy is a result of the anatomical length variation between two connected parts. The most important characteristic of the *golden section* is that it is a proportion which harmonizes the design of two disparate items (i.e., the human and the interface) (Gielo-Perczak, 2001). The *golden section* can be expressed as B: C = C: (B+C), which describes the relationship between two asymmetrical parts. This same expression has been applied to human anthropometry at varied levels (i.e., the forearm, hand, and the phalanges of the hand) by Gielo-Perczak (2001). Figure 46 shows an example of the *golden section* proportion attributed to the forearm and hand of the human upper extremity. Humans tend to drive for symmetry in many of the products that are designed, while nature suggests that asymmetry is truly a harmonizing factor (Figure 46).

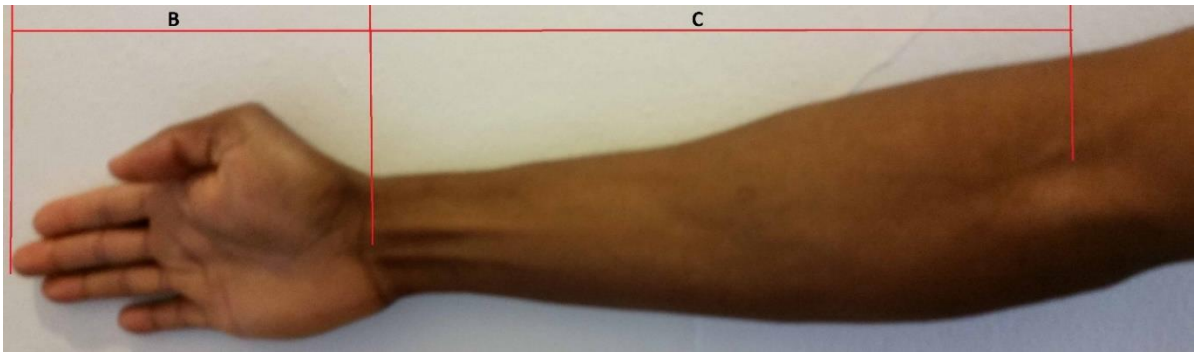

Figure 46. A paradigm of the *golden section*, where C/B = (B+C)/C

Table 27. Shows characteristic measurements of the upper extremity with respect to the *'golden section'* ratio

	Anthropometric Categories	P1-F	P2-F	P3-M	P4-F	P5-M	P6-F	P7-M	P8-F	P9-M	P10-M
a	Arm(Acromion to Lateral Epicondyle) (in)	12.1	12.2	13.8	12.7	13.8	12.2	13.2	13.6	13.4	13.9
b	Forearm (Lateral Epicondyle to Ulna)(in)	9.0	8.9	10.2	9.5	10.0	9.4	9.5	10.4	10.5	10.0
c	Right Hand Size (mm to in conversion)	7.6	7.0	7.5	7.5	7.1	6.9	7.6	8.3	7.6	7.8
	Golden Section: ((b+c)+a)/(b+c) = 1.618	1.7	1.8	1.8	1.7	1.8	1.7	1.8	1.7	1.7	1.8
	Golden Section: (a+b)/a = 1.618	1.7	1.7	1.7	1.7	1.7	1.8	1.7	1.8	1.8	1.7
	Golden Section: (b+c)/b = 1.618	1.8	1.8	1.7	1.8	1.7	1.7	1.8	1.8	1.7	1.8
d	Torso to Screen Distance: NB_Open	16.9	18.1	16.8	15.7	15.7	16.9	15.8	18.0	16.3	16.3
	Torso to Screen Distance Std.: NB_Open	2.2	2.0	1.5	1.8	2.2	1.9	2.0	2.5	1.8	3.5
e	Total Arm length	28.7	28.1	31.5	29.7	31.0	28.5	30.3	32.3	31.6	31.6
	Golden Section: e/d = 0.618	0.588	0.644	0.534	0.529	0.508	0.594	0.522	0.558	0.515	0.514
d	Torso to Screen Distance: NB_Constrained	15.6	15.5	15.9	15.0	15.3	15.7	16.1	17.7	17.6	17.3
	Torso to Screen Distance Std.: NB_Constrained	3.1	2.8	2.5	2.3	1.6	1.9	2.1	1.7	3.3	5.1
e	Total Arm length	28.7	28.1	31.5	29.7	31.0	28.5	30.3	32.3	31.6	31.6
	Golden Section: e/d = 0.618	0.544	0.553	0.506	0.505	0.496	0.550	0.531	0.549	0.559	0.545

In assessing the *golden section* with respect to the anthropometries within this study, an interesting proportion was found. The ratios highlighted in yellow do not meet the 0.618 value; however, in engaging the screen, the ratio between the torso and the screen aims to maintain the ratio of the total arm length, as seen in Table 27, where the most notable value is the ratio of arm length with body position to the screen. The results of a t-test assuming unequal variances yielded no significant difference ($p = 0.305$) between the *golden section* results for arm length and torso distance from the screen (yellow highlighted categories). This might suggest that the participants are interacting in a manner to try and maintain their natural arm length proportion as they interact with the screen. The interplay of the arm proportion and the shoulder breadth with respect to proportional optimization is a hard line to follow. The statistical significance of arm length, with respect to abduction/adduction, suggests that it is not only the fore aft movement in the frontal plane of the arm away from the torso but the medio-lateral movements in the sagittal plane as well. Therefore, design consideration cannot be based on one singular dimension, which is commonly stature. The consideration needs to be based on the multi-dimensionality of the human physique. In the case of a goal directed pointing movement, arm length and shoulder breadth, and screen placement with respect to the environment space, in addition to stature, should be considered.

Additionally, prolonged periods of accelerated movements are seen as a detriment to the musculoskeletal system, where, for example, greater angular accelerations and decelerations around the shoulder during a work task can create large moments within the glenohumeral joint that can lead to overuse, and thus, may result in a work-related musculoskeletal disorder (WMSD), worker pain, and poor performance (Punnett and Wegman, 2004). While less joint movement may promote a more optimal movement trajectory, the level of variation in anthropometry makes it more of a subjective optimization. With a watch cycle shift from 18 hours to 24 hours, the potential for WMSD is elevated (Young et al., 2015; Larter, 2016). By recalling Participant 10's self-report on moving their torso in the constrained environment, the body did adapt but that additional movement dissipated. In doing so, there could be potential moments generated in other areas of the body to facilitate the adaptation. This occurred in an ideal non-sea state environment but, in a sea state environment, results could be markedly pronounced. Design considerations may provide the greatest means to objectively optimize movement trajectories and, from this study, design considerations should include screen size, screen height of the deck, and user proximity to the screen.

5.2 Strengths and Weaknesses to the Technique

Uncertainty is the bedrock which is fundamental to the strengths and weaknesses of any research effort. (To quote one of my associate advisors, Dr. John Bennett, "There is a certainty to uncertainty".) In properly understanding the insidious nature of uncertainty in the current research, weaknesses manifest and in so doing mitigation strategies must be taken. There are several points that provided some level of uncertainty, with one such point as the analysis of the

movement trials. To reduce the movement uncertainty associated with each stimulus pattern, the first and last trials were discarded (DiStefano et al., 2009). This was an effort to reduce the effects of movement preparation and movement suspension that may have occurred during the first trial and last trial, thereby providing a more accurate reading of end-effector performance.

In addition, validation of joint displacements provided insight into the inherent error in the planar projection method. Peterson (1999) knew the limitations of joint angle projections onto the anatomical planes, where the error estimate was within ±3 degrees; however, the uncertainty associated with human error has been estimated to be about ±5 degrees and the uncertainty associated with a manual goniometer is estimated to be about ±1 degree. If the square root of the sum of the squares for human error and goniometer measurement error is taken, the error comes out to be 5.1 degrees (Tantawy, 2012). Considering the largest error based off of the test sequences, kinematic displacements were well within the movement parameters for an upper extremity pointing movement. Since the movement dynamics fall below the largest error of the planar projections, the proposed measurement method is more accurate and timely than a manual human goniometric measurement and more efficient and understandable than the other proposed measurement methods. Additional error manifested itself in other ways, such as anatomical uncertainty due to marker placement, size, and reflectivity (clean or dirty - may add a degree or two of error); however, the total error is still within ±5 degrees (Peterson, 1999). Further factors include, movement of the marker or shake due to skin movement, disappearance of the marker, noise can be due to editing mistakes by the computer and/or user within the Motive software (Peterson, 1999; Cappozzo et al., 2005; Chiari et al., 2005; Leardini et al., 2005). Interpolation of missing markers during long periods of marker absence is invalid and manual estimation must be made based on other markers in close proximity (Peterson, 1999; Cappozzo et al., 2005;

Chiari et al., 2005; Leardini et al., 2005). Differences in a participants approach to carrying out the task could cause marker disappearance. Strategically placing OEMC cameras and using several cameras for the measurement minimized disappearances as a result of participant motor behavior (Peterson, 1999). The environment (e.g., glare from a light fixture or sun light or other shining objects in the space) can also add potential artifacts. Additionally, reflection of a camera placed in such a way that other cameras see its infrared light emittance may add additional artifact. Mitigation strategies built into the Motive software utilizes a masking feature; however, the masked area are similar to a blind spot in your retina and markers could potentially be dropped. A mitigation strategy was to arrange and rearrange the system until the least amount of masking was utilized. In addition, using a higher resolution by tracking in millimeters helped to avoid greater errors.

With Euler/Cardan angles and quaternions being computationally arduous, planar projections present a simpler method and the errors are known a posteriori (Coates and Peterson, 2007). Furthermore, Gimbal Lock becomes a nonissue. As a result, the clinician is afforded an intuitive view into motor movement as it would occur during a goal directed pointing movement from an end-effector proprioceptive vantage point. The planar projection method decomposes an upper extremity goal directed movement into its component parts (i.e., flexion/extension, abduction/adduction, etc.) and these decompositions affords the clinician to aid the patient in correcting short falls and optimizing overall motor performance.

From a sEMG perspective, placing the electrode on a superficial muscle belly avoids interference signals from among other muscles in the area; therefore, trying to pinpoint smaller muscle groups with sEMG may induce crosstalk. This study focused on large superficial muscle groups with very little in the way of smaller muscle groups such as the forearm. Additionally, consistent

sensor placement is critical, especially in performing MVC. Placing the sensor at the beginning of the experiment and conducting all of the cycles for the entire experiment within a continuous block of time mitigates errors in placement, especially if a participant was to return on a different day to finish the experiment. When a muscle fatigues, there is a frequency shift from high to low frequencies; however, fatigue measures may not be valid if the MVC level for the muscle is below 10% of MVC (Redfern, 1992). Lastly, in obtaining MVC results, it is imperative to train the participant on how to actuate their maximum voluntary contraction without the additions of props or immovable devices (i.e., a wall or the floor). As part of the training, biofeedback should be provided to the participant as a way for the participant to gauge their effort (Solomonow, 1999). This dissertation's simple approach to quantify biomechanical information during an upper extremity goal directed movement task accounted for the prior weakness in an effort to validate this simple method.

Lastly, the use of a custom-made force plate using uniaxial loadcells reduces the ability to assess torques due to shifting or rotations in the torso due to the upper extremity movement. Additionally, the custom made force plate had a smaller measurement area than commercial of the shelf units. This required the experiment to control where the participants could stand to capture accurate measurements (Figure 16). In controlling stance location, the experiment forced participants to stand with their feet approximately shoulder width apart. This has a pro and con: pro in that it controlled how all participants engaged the screen thus reducing a confounding variable and con in that participants may naturally stand a little bit differently instead of both feet astride, where they may favor one foot by having it forward of the other. If this environment were shifted to a sea-state, then participants may vary their stance based on the boat's conditions

and the duration the participant spends standing. All this can easily be accounted for by swapping this custom force plate for a multi-axial commercial unit.

5.3 Strengths and Weaknesses of the Overall Approach

The major strength of the overall approach was comprehensive in nature and enables the validation of assertions made by participants on self-reports (i.e., Participant 10). Additionally, the technique can be expanded to assess both dominant and non-dominant upper extremities. This would require an additional four sEMG sensors and nine retro-reflective markers for the non-dominant upper extremity. The OEMC, sEMG, and force plate systems are easily scalable and the approach is sea-state portable, where no additional changes are required for a sea-state comparison.

The major weakness of the approach was not integrating the use of electroencephalography (EEG). The use of EEG would have provided the cognitive signals that are a result of an event-related potential. An event-related potential is measureable cognitive activity that is a result of a motor event, for the case of this dissertation. As comprehensive as the current approach is, EEG was the only missing modality to address how the muscles receive their signal to contract or relax. Due to time and monetary constraints, EEG was not feasible; however, the modality can be integrated without an exorbitant amount of effort and would require using the appropriate sensor unit that can be hardware triggered.

Using wireless sensors could potentially help to reduce any performance deficits, where the participant focuses on the unnatural state of being connected and measured. This has a tendency to indirectly alter the participant's relaxed cognitive state, thereby causing potential performance

anxiety. It should be noted that, from the pre-survey self-repots, nine participants reported feeling carefree and one felt anxious; however, with a larger pool of participants, the results could be mixed. Wireless sensors are more unencumbering and provide a more natural feel as the participants performs an upper extremity movement. Additionally, the level of realism of the constrained environment could have been improved with the use of better materials instead of a black cloth and PVC piping. The addition of reduced lighting to simulate a darker maritime environment, the smell (e.g., hydraulic fluid), and white noise in the form of machinery sounds, would have provided a higher level of realism and could have potentially influenced upper extremity performance outcomes.

Lastly, including different variations on the touch procedure, and/or variations on touchscreen size, and/or using a sitting versus a standing posture, could have an influence on upper extremity performance. This is due to the performance requirements that either, or all, of these conditions place on the participant. Changing the touch procedure may cause a participant to use their upper extremity in a manner that they are not accustomed. If the procedure has a participant moving from right to left or from the bottom to the top, this may alter parameters that participants could grow accustomed to. Additionally, the same effect can occur with the location of the targets on the screen. For example, using multiple smaller touchscreens with single targets would allow for movements to be adjusted as much or as little as desired by the experimenter. Furthermore, such placements could be over the participants head, to their side, or below their waist. If the procedure was varied and the various smaller screens increased the movement range, then adding a sitting posture would also add in the effect of torso differences across participants. When a participant operates a touchscreen in a standing posture, the confounding

nature of human asymmetry is reduced since shoulder breadth, arm length, and stature are the anthropometric confounders. If the posture were to shift to a sitting posture, a fourth confounder, torso length, is added. This is due to the fact that two human beings can be six feet tall and in a standing posture no real difference can be discerned, but in a sitting posture, one could have longer legs and a shorter torso and the other could have shorter legs and a longer torso. More specifically, with two participants at the same standing height but varying sitting heights, the participant with the longer torso would be taller than the participant with the shorter torso. Accounting for procedure, screen, and posture variation, might add additional fidelity to upper extremity performance.

6. Conclusion

The two main objectives behind this dissertation were to: 1) create a simple technique to quantify biomechanical information in an upper extremity goal directed movement task and 2) validate the technique by assessing upper extremity movement patterns of right-hand dominant participants with respect to anthropometry. The method developed in this dissertation integrated the use of anatomical planer projections from opto-electronic motion capture data, an isochronal stimulus from a metronome (to pace participants), a touchscreen procedural pattern for end-effector terminal end points, surface electromyography, and a force plate. The anatomical planer projections were broken down into the upper extremity's movement components of flexion, extension, abduction, and adduction, where angular displacements and velocities were calculated. Figure 47 conceptualizes the essence of the technique developed in this dissertation. Figure 47A shows the three angular displacement components of an upper extremity pointing

task mapped to 100% task complete for Participant 4's third trial of the 1 Hz open cycle. Additionally, the percent MVC from the sEMG is displayed for each of the trapezius, pectoralis, triceps, and biceps. Furthermore, the CoG postural shifts based on the upper extremity movement is graphed with respect to acceleration (in/s^2). Within the conceptual framework are the individual targets touched (vertical red lines), and the end effector terminal end points for each target (Figure 47B). Figure 47 provides a holistic picture of how the shoulder, elbow, and second digit worked in unison to perform an upper extremity pointing movement in a non-sea state environment. Additionally, surface electromyography was used to assess maximum voluntary contractions and frequency shifts in muscle recruitment from power spectral density analysis. This all provided a means to understand muscle recruitment and activation based on how each individual's upper extremity motor control adapted to the environmental constraints. Lastly, the force plate was used to assess CoG shifts as a result of the upper extremity movement. The second objective assessed the validity of the measurement technique by focusing on design considerations with respect to anthropometry. This objective had three sub-topics associated with anthropometric design. First, using standard height or stature as a design specification alone was not a predictive vehicle to drive the design to optimality. Stature, shoulder breadth, and arm length in the context of an end-effector upper extremity pointing task were necessary in articulating how the design could be optimized. Second, naval program managers should not have such a large sample of anthropometries with which to design. Rather, a narrower sample of anthropometries yields easier design optimization, especially with the use of legacy equipment and cost constraints. Last, there are individual differences in how people perform a task, yet alone there are differences in how a person performs the same task on different occasions. If retraining is not part of the overall design acquisition cost, then some

level of design adjustability needs to be considered, so the operator can personalize the task and therefore optimize their task execution. The last two topics kind of go hand in hand, if an operator performs the same task differently as a result of the lack of environmental affordance, it would be very difficult to design for a large demographic of people. The variance between participants is a variable that would drive the acquisition cost very high in trying to account for the large design range. During a paced movement of 1 Hz, 1.3 Hz, 1.7 Hz, 2.0 Hz, and 2.7 Hz, some participants still performed the task faster than others. While during none paced movements or 0 Hz, participants were all over the time spectrum for completing the same task. These results may be predictive of a greater error rate in more critical tasks. Instead, narrowing the demographic design range appropriates the design moneys more effectively. Additionally, providing design affordances such as equipment adjustability and alternate input methods (i.e., gesture based input, trackball, voice command) in-conjunction with a narrower design range, truly affords design optimization.

Figure 47 is a performance benchmark for operators. These benchmarks allow for performance comparisons over time for operators performing various tasks. This is quintessential when you have operational events where you have frequent opportunity for error. Understanding the operators performance based on the conceptual framework affords individual optimizations to reduce noncritical errors. This is similar to what professional sports teams and concert conductors execute on their performers. However, in the event of a catastrophe or critical error, personalized training becomes more of the salient parameter, rather than individual design optimizations. Furthermore, the conceptual framework complements the concept of personalized training, since the framework is a performance benchmark for an individual operator. The result is less time in training and more training efficiency.

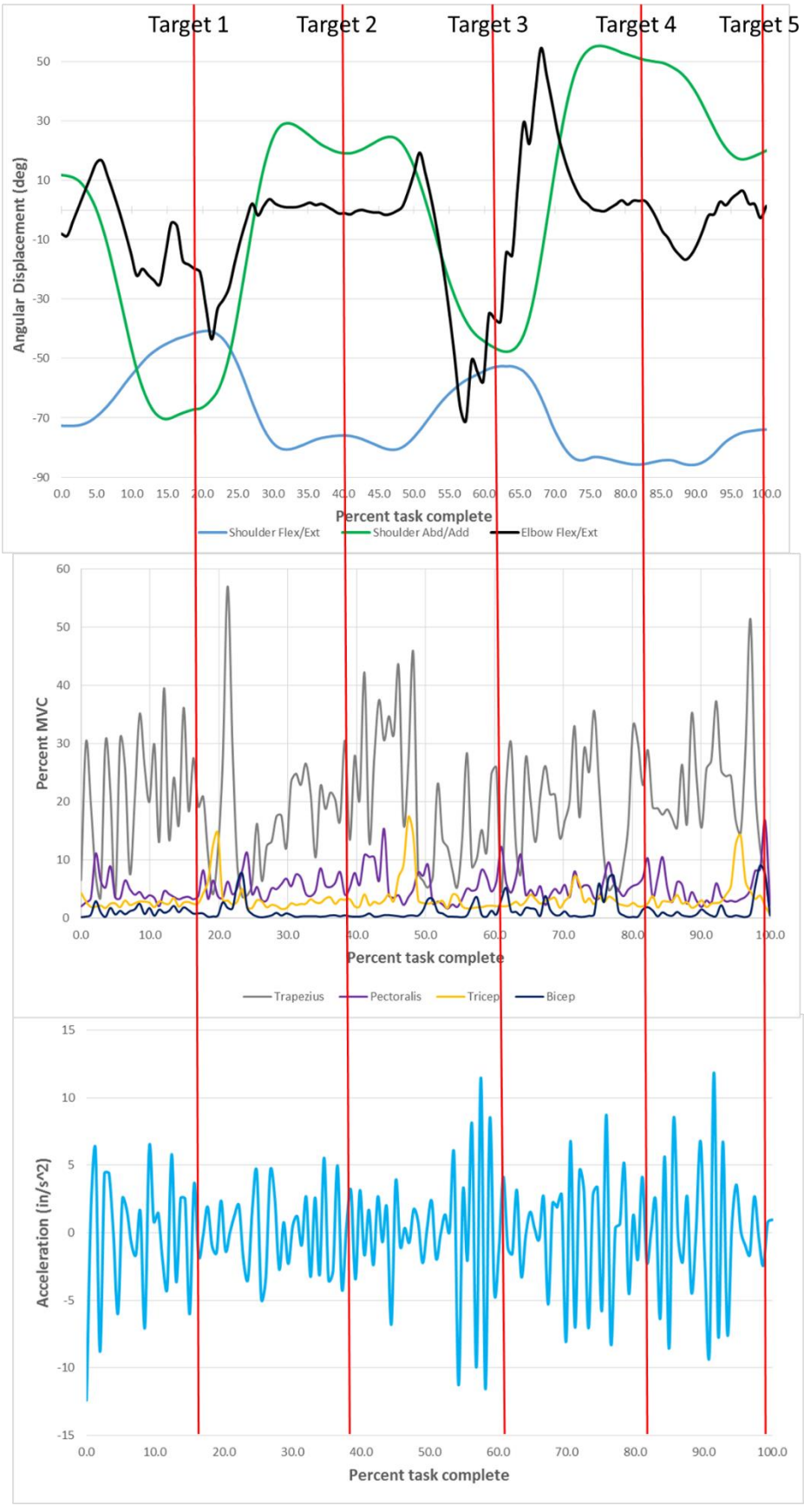
Target 1
Target 2
Target 3
Target 4
Target 5
Angular Displacement (deg)
Percent task complete
Shoulder Flex/Ext
Shoulder Abd/Add
Elbow Flex/Ext
Percent MVC
Percent task complete
Trapezius
Pectoralis
Tricep
Bicep
Acceleration (in/s^2)
Percent task complete

A)

B)

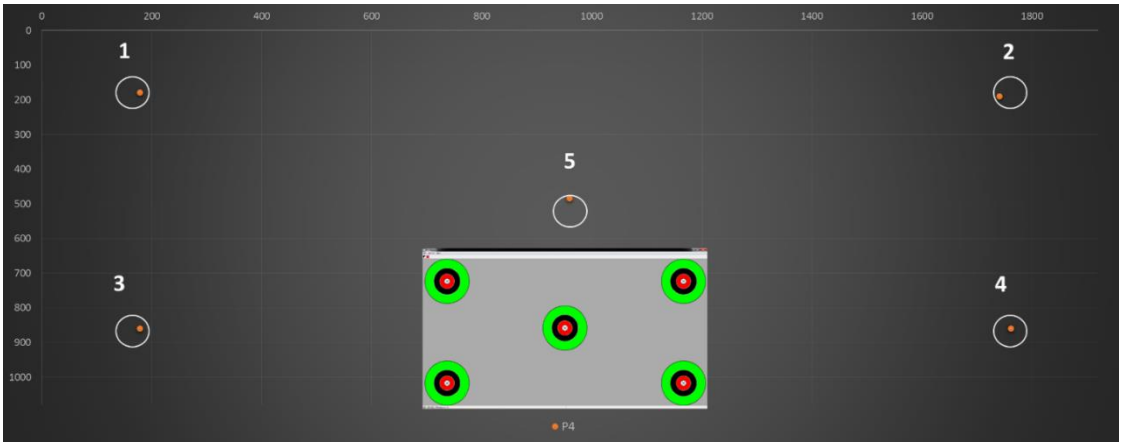

Figure 47. A) A conceptual framework portraying the complete movement of the upper extremity for trial 3 of the 1 Hz open cycle for participant 4 with the 5 target locations. The blue line is shoulder flexion/extension, the green is shoulder abduction/adduction, and the black is elbow flexion/extension. The second graph displays the sEMG percent MVC values for the trapezius (grey), pectoralis (purple), triceps (yellow), and biceps (dark blue). The third graph shows the CoG postural shift acceleration (in/s^2). B) A graph which represents the end-effector terminal touch points based on the movement in 'A'.

This dissertation defines a research method to provide further insight into measuring goal directed end-effector proprioceptive biomechanics from an anthropometric perspective in a non-sea state environment (Figure 47). Additionally, this experiment provides a quantitative method to capture the ecological approach to perception and action (Newell, 1991) as a subset to help investigate what Latash et al. (2010) described as the next frontier in motor control research – "To create a formal description, operating with exactly defined variables, of the physical and physiological processes that make coordinated voluntary movement possible". Therefore, the following denotes the steps in performing a goal directed movement and the measurement modalities which capture said movement:

I. Movement Preparation (5 Static visual target & pattern of movement)

II. Movement initiation and timing (Auditory stimulus)

III. Muscle activation (sEMG)

IV. Joint movement (Optoelectronic Motion Capture System)

V. Postural adjustment (Force plate: CoG)

VI. Accuracy of end-effector terminal touch point (Touchscreen X- pixel, Y-pixel locations)

As a result, the technique can be expanded to comparing both upper extremities in a sea state environment. Further, the technique can focus more on reaction time assessments if the need exists. The technique developed can not only assess design with respect to anthropometry, but the technique can be leveraged by clinicians for retraining the upper extremity after surgery. A pointing task is a simple movement that addresses an intent by the participant to move to a target. Pointing is a precursor to a more complex task like grasping, thus the technique herein can retrain a fundamental principal of movement. Lastly, the technique developed can also be expanded to the assessment of upper extremity prosthetics. The conceptual framework in Figure 47 provides a holistic view of an upper extremity movement. A comparison between a natural upper extremity and prosthetic upper extremity in a fundamental movement such a pointing task can aid clinicians in fine tuning the parameters necessary for more efficient human performance.

Efforts to understand goal directed motor movement efficiency in the context of human performance is vital in modeling and predicting potential outcomes to shipboard naval damage control procedures. More importantly, understanding anthropometric variations in natural goal directed motor movement provides broader insight, from a biomechanical perspective, for naval system designers, especially since goal directed movements, with respect to kinematics, requires a higher level of acuity.

7. References

Adamo, D.E., Martin, B.J., Brown, S.H. (2007). Age-related differences in upper limb proprioceptive acuity. Percept Mot Skills, 2007, 104, 1297-1309.

Adams, J.A. (1968). Response feedback and learning. Psychological Bulletin, 70, 486-504.

Adams, J.A. (1971). A closed-loop theory of motor learning. Journal of Motor Behavior, 3, (2): 111-149.

Adams, J.S., and Xhignesse, L.V. (1960). Some determinants of two-dimensional visual tracking behavior. Journal of Experimental Psychology, 60, 391-403.

ADULTDATA: The Handbook of Adult Anthropometrics and Strength Measurements—Data for Design Safety, Institute for Occupational Ergonomics, University of Nottingham, UK, 1998.

Alty, S.R., Georgakis, A. (2011). Mean Frequency Estimation of Surface EMG Signals Using FilterBank Methods. 19th European Signal Processing Conference, ISSN: 2076-1465, 1387- 1390.

Annett, M. (1985). Left, Right, Hand and Brain: The Right Shift Theory. Erlbaum, London.

ASTM Standard F 1166-07, (2007), "Standard Practice for Human Engineering Design for Marine Systems, Equipment, and Facilities". ASTM International, West Conshohocken, PA, 2007.

Bernstein, N. (1967). The coordination and regulation of movement. London: Pergamon.

Bonnet, V., Mazza, C., Fraisse, P., Cappozzo, A. (2013). Real-time estimate of body kinematics during a planar squat task using a single inertial measurement unit. IEEE Transactions on Biomedical Engineering, vol. 60, 7, 1920-1926.

Bellemare, F., Woods, J.J., Johansson, R., Bigland-Ritchie, B. (1983). Motor-Unit Discharge Rates in Maximal Voluntary Contractions of Three Human Muscles. Journal of Neurophysiology, 50, 6:1380-1392.

Callahan, S. (2003). Navy Celebrates 25 Years of Women at Sea. Retrieved from http://www.msc.navy.mil/sealift/2003/december/women.htm.

Cappozzo, A., Croce, U.D., Leardini, A., Chiari, L. (2005). Human movement analysis using stereophotogrammetry Part 1: theoretical background. Gait and Posture vol. 21,186-196.

Carson, R.G., Elliott, D., Goodman, D., Thyer, L., Chua, R., Roy, E.A. (1993). The role of impulse variability in manual-aiming asymmetries. Psychol Res 55,291-298.

Chao, E.Y.S. (1980). Justification of triaxial goniometer for the measurement of joint rotation. Journal of Biomechanics, 13, 989-1006.

Chiari, L., Croce, U.D., Leardini, A., Cappozzo, A. (2005). Human movement analysis using stereophotogrammetry Part 2: Instrumental errors. Gait and Posture vol. 21:197-211.

Chowaniec, M.J., Peterson, D.R. (2007). Dynamic loading of the shoulder during the Codman exercise. Proc 33rd Northeast Bioeng Conf, Stony Brook, NY, 5-6.

Coates, J.O., Peterson, D.R. (2007). Using a simplified marker configuration to determine Cardan angles of shoulder orientation. Proc 33rd Northeast Bioeng Conf, Stony Brook, NY, 7-8.

Cohen, J. (1988). Statistical power analysis for the behavioral sciences (2nd ed.). Hillsdale, NJ: Lawrence Earlbaum Associates.

Delignieres, D., Torre, K. (2009). Fractal dynamics of human gait: a reassessment of the 1996 data of Hausdorff et al., Journal of Applied Physiology 106, 1272–1279.

Dickinson, J. (1976). Proprioceptive Control of Human Movement. Princeton Book Company, Publisher, Princeton, NJ.

DiStefano, L.J., Blackburn, J.T., Marshall, S.W., Padua, D.A. (2009). Gluteal muscle activation during common therapeutic exercises. Journal of Orthopedic & Sports Physical Therapy, vol. 39, 532-540.

Eagleman, D.M., Sejnowski, T.J. (2007). Motion Signals Bias Localization Judgements: A Unified Explanation for the Flash-lag, Flash-drag, and Flash-jump, and Frolich Illusions. Journal of Vision, 7 (4): 3, 1-12.

Ellis, M.J. (1969). Control dynamics and timing a discrete motor response. Journal of Motor Behavior, 1, 119-134.

Enoka, R. M. (1994). Neuromechanical basis of kinesiology (Ed. 2). Champaign, Ill: Human Kinetics, pp. 166-170.

Faul, F., Erdfelder, E., Lang, A.-G., Buchner, A. (2007). G*Power 3: A flexible statistical power analysis program for the social, behavioral, and biomedical sciences. Behavior Research Methods, 39, 175-191.

Faul, F., Erdfelder, E., Buchner, A., Lang, A.-G. (2009). Statistical power analyses using G*Power 3.1: Tests for correlation and regression analyses. Behavior Research Methods, 41, 1149-1160.

Fitts, P.M. (1954). The information capacity of the human motor system in controlling the amplitude of movement. Journal of Experimental Psychology, 47, 381-391.

Frank, T.D., Peper, C.E., Daffertshofer, A., Beek, P.J. (2006). Variability of Brain Activity During Rhythmic Unimanual Finger Movements. In K. Davids, S. Bennett, & K. Newell (Eds.), Movement System Variability (271-304). IL: Human Kinetics.

Gazzola, V., Keysers, C. (2009). The observation and execution of actions share motor and somatosensory voxels in all tested subjects: single-subject analyses of unsmoothed fMRI data. Cereb Cortex 19 (6): 1239–1255.

Keysers, C., Kaas, J.; Gazzola, V. (2010). Somatosensation in Social Cognition. Nature Reviews Neuroscience 11 (6): 417–28.

Ghez, C., Gordon, J., Ghilardi, M.F. (1995). Impairments of reaching movements in patients without proprioception. II Effects of visual information on accuracy. J Neurophysiol 73, 361-372.

Ghez, C., Sainburg, R. (1995). Proprioceptive control of interjoint coordination. Can J Physiol Pharmacol 73, 273-284.

Gibbs, C.B., Logan, O. (1965). Tests of the functions of proprioception and interaction of senses. Perceptual and motor skills, 20, 433-442.

Gielo-Perczak, K. (2001). The *golden section* as a harmonizing feature of human dimensions and workplace design. Theor. Issues in Ergon. Sci., 2 (4):, 336 -351.

Gilbert, A.N., Wysocki, C.J. (1992). Hand preference and age in the United States. Neuropsychologia 30 (7), 601–608.

Goble, D.J., Brown, S.H. (2007). Task-dependent asymmetries in the utilization of proprioceptive feedback for goal-directed movement. Exp Brain Res, 180,693-704.

Goble, D.J., Brown, S.H. (2009). Upper Limb Asymmetries in the Matching of Proprioceptive verses Visual Targets. J Neurophysiol.

Goble, D.J., Brown, S.H. (2008). The biological and behavioral basis of upper limb asymmetries in sensorimotor performance. Neurosci Biobehav Rev., 2008, 32 (3), 598-610.

Goble, D.J., Lewis, C.A. Brown, S.H. (2006). Upper limb asymmetries in the utilization of proprioceptive feedback. Exp Brain Res, 168, 307-311.

Goble, D.J., Lewis, C.A., Hurvitz, E.A., Brown, S.H. (2005). Development of upper limb proprioceptive accuracy in children and adolescents. Hum Mov Sci, 24(2) 155-170.

Grose, J.E. (1967). Timing control in finger, arm, and whole body movements. Research Quarterly, 38, 10-21.

Gur, R.C., Richard, J., Calkins, M.E., Chiavacci, R., Hansen, J.A., Bilker, W.B., Loughead, J., Connolly, J.J., Qui, H., Mentch, F.D., Abou-Sleiman, P.M., Hakonarson, H., and Gur, R.E (2012). Age group and sex differences in performance on a computerized neurocognitive battery in children age 8-21. Neuropsychology, 26(2), 251–265; doi:10.1037/a0026712.

Haken, H. (1977). Synergetics. An Introduction. Springer-Verlag, Berlin-Heidelberg-New York. XII, 325 S., 125 Abb., DM 72.—.

Hall, J.F. (1966). The psychology of learning. Philadelphia: J.B. Lippincott Company.

Hausdorff, J.M., Purdon, P.L., Peng, C.K., Ladin, Z., Wei, J.Y. et al. (1996). Fractal Dynamics of human gait: stability of long-range correlations in stride interval fluctuations. Journal of Applied Physiology 80, 1448–1457.

Howard, I.P., Templeton, W.B. (1966). Human spatial orientation. New York: Wiley.

Hu, B., Ning, X. (2016a). Cervical Spine Biomechanics and Task Performance During Touchscreen Computer Operations. International Journal of Industrial Ergonomics, 56, 41-50.

Hu, B., Ning, X. (2016b). Effects of Touch Screen Interface Parameters on User Task Performance. Proceedings of the Human Factors and Ergonomic Society 2016 Annual Meeting, 820-824.

Huang, M.H. (2009). Age differences in the control of posture and movement during standing reach. Ph.D. Dissertation. The University of Michigan.

Ingalhalikar, M., Smith, A., Parker, D., Satterthwaite, T.D., Elliott, M.A., Ruparel, K., Hakonarson, H., Gur, R.E., Gur, R.C., and Verma, R. (2013). Sex differences in the structural Connectome of the human brain. PNAS Early Edition.

Kaya, D. (2014). Proprioception: The Forgotten Sixth Sense, Chapter Proprioception and Gender. Published by OMICS Group eBooks, Foster City, CA, USA.

Keele, S.W. (1981). Behavioral analysis of movement. In: Brooks, V.B., ed. Handbook of physiology. I: The nervous system vol2. Motor Control, Part 2. Baltimore: Williams & Wilkins, 1391-1414.

Ko, H. (2000). Open Systems Advanced Workstation Transition Report. SSC San Diego TR-1822.

Kroemer, K.H.E. Fitting the Human: Introductions to Ergonomics. CRC press, 6th edition, 2006.

Kuiken, T.A., Li, G., Lock, B.A, Lipschutz, R.D., Miller, L.A, Stubblefield, K.A., Englehart, K.B (2009). Targeted Muscle Reinnervation for Real-time Myoelectric Control of multifunction artificial arms. JAMA, 301(6): 619–628.

Kupfermann, I. (1991). Learning and Memory. In: Kandel, E.R., Schwartz, J.H, Jessell, T.M, eds. Principles of neuroscience. 3rd ed. New York: Elsevier, 997-1008.

Larter, D.B. (2016). This 'life-changing' shift has made submariners much happier. Retrieved from https://www.navytimes.com/articles/this-life-changing-shift-has-made-submariners-much-happier.

Latash, M.L., Mindy, L.F., Sholz, J.P., Schoner, G. (2010). Motor Control Theories and Their Applications. Medicina (Kaunas); 46(6): 382-392.

Leardini, A., Chiari, L., Croce, U.D., Cappozzo, A. (2005). Human movement analysis using stereophotogrammetry Part 3: Soft tissue artifact assessment and compensation. Gait and Posture vol. 21, 212-225.

Mahan, A.L. (1890). The Influence of Sea Power upon History: 1660-1783. Cambridge, MA, University Press: John Wilson and Son.

Marteniuk, R.G., Mackenzie, C.L., Jeannerod, M. et al. (1987). Constraints on human arm movement trajectories. Can J. Psychol; 41,365-368.

Moran, C.W. (2011). Revolutionizing Prosthetics 2009 Modular Prosthetic Limb–Body Interface: Overview of the Prosthetic Socket Development. Johns Hopkins APL Technical Digest, Volume 30, Issue 3, pp. 240–249.

Morrison, S., Hong, S.L., and Newell, K.M. (2011). Similarity in the dynamics of contralateral motor overflow through increasing frequency of movement in a single limb. Exp.Brain Res., 213, 4, 403-414.

Newell, K.M. (1991). Motor Skill Acquisition. Annu Rev Psychol; 42,213-237.

PeopleSize (2008). Open Ergonomics Ltd, Leicestershire, UK.

O'Brien, M. (2015). "Will a robotic arm ever have the full functionality of a human limb"? PBS News Hour, available at: http://www.pbs.org/newshour/bb/will-artificial-arm-ever-full-functionality-human-limb/.

Oldfield, R.C., (1971). The assessment and analysis of handedness: the Edinburgh inventory. Neuropsychologia 9 (1), 97–113.

Peterson, D.R. A Method for Quantifying the Biodynamics of Abnormal Distal Upper Extremity Function: Application to Computer Keyboard Typing. Ph.D. Dissertation. University of Connecticut, 1999.

Peterson, D.R., Bronzino, J.D. (2015). Biomechanics Principles and Applications. CRC Press. Boca Raton, FL.

Peterson, D.R., Cherniack, M.G. (2001a). Vibration, grip force, muscle activity, and upper extremity movement of a manual hammering task. Proc 9th Intl Conf on Hand-Arm Vibration, Nancy, France.

Peterson, D.R., Cherniack, M.G. (2001b). Repetitive impacts from manual hammering: Physiological effects on the hand-arm system. Canadian Acoustics, 12-13.

Peterson, D.R., Seils, D., Tantawy, T., Kueck, A., Roberts, M.K.E. (2012). Novel method for comprehensively assessing the biomechanical risks associated with the use of minimally-invasive surgical instruments. Proc Soc Am Gastroint Endosc Surg, San Diego, CA, 207.

Punnett, L., Wegman, D.H. (2004). Work-related musculoskeletal disorders: the epidemiologic evidence and the debate. Journal of Electromyography and Kinesiology, 14, 13-23.

Redfern, M. (1992). Functional Muscle: Effects on Electromyography Output. In G.L. Soderberg (Ed.), Selected Topics in Surface Electromyography for Use in the Occupational Setting: Expert Perspectives (pp. 104 – 120). Cincinnati: National Institute for Occupational Safety and Health.

Ribeiro, F., Oliveira, J. (2011). Factors influencing proprioception: what do they reveal? In: Klika V (ed.), Biomechanics in Applications. InTech Croatia.

Rothwell, J.C., Traub, M.M., Day, B.I. et al. (1982). Manual Motor Performance in a Deafferented Man. Brain 105, 515-542.

Roy, E.A., Elliott, D. (1989). Manual Asymmetries in Aimed Movements. The Quarterly Journal of Experimental Psychology, 4/A (3) 501-516.

Sainburg, R.L., Ghilardi, M.F., Poizner, H., Ghez, C. (1995). Control of limb dynamics in normal subjects and patients without proprioception. J Neurophysiol 73, 820-835.

Sato, N., Nakajima, K. (2011). Effects of Touch Screen Response Time on Psychological State and Task Performance. P. Campos et al. (Eds.): INTERACT 2011, Part IV, LNCS 6949, pp. 507–510.

Schmidt, L., Depper, L., Kerkhoff, G. (2013). Effects of age, sex and arm on the precision of arm position sense-left-arm superiority in healthy right-handers. Front Hum Neurosci 7, 915.

Schmidt, R.A. (1975). A Schema Theory of Discrete Motor Skill Learning. Psychol Rev; 82,225-260.

Seils, D.R., (2012). A Comprehensive Methodology for Assessing Biomechanical Risks Associated with Hand Tool use: Applied to Laparoscopic Surgical Instruments. Masters Thesis. Paper 282.

Sejdic´, E., Fu, Y., Pak, A., Fairley, J.A., Chau, T. (2012). The effects of rhythmic sensory cues on the temporal dynamics of human gait. PLoS ONE 7(8): e43104.

Sherrington, C.S. (1906). The Integrative Action of the Nervous System. New Haven: Yale University Press.

Shumway-Cook, A., Woollacott, M.H. Motor Control: Theory and Practical Applications. Maryland: Lippincott Williams & Wilkins, Second Edition 2001. Print.

Smith, J.L (1969). Kinesthesis: a model for movement feedback. In R.C. Brown and B.J. Cratty (Eds.), new perspectives of man in action. Englewood Cliffs: Prentice-Hall Inc.

Sobolev, A. (2015). Cross Product. http://stackoverflow.com/questions/32146434/determinant-method-vs-cross-product-area-of-a-triangle.

Solomonow, M. (1999). Standards for Reporting EMG Data. Jounral of Electromyography and Kinesiology, 9, 410 – 412.

Stroobant, N., Vingerhoets, G. (2000). Transcranial Doppler Ultrasonography Monitoring of Cerebral Hemodynamics during Performance of Cognitive Tasks: A Review. Neuropsychology Review, 10, 213-231.

Taub, E., Berman, A.J. (1968). Movement and Learning in the Absence of Sensory Feedback. In: Freedman, S.J., ed. The Neurophysiology of Spatially Oriented Behavior. Homewood, NJ: Dorsey, 173-192.

Tantawy, T.A. (2012). Determining upper extremity posture using a simplified marker configuration for biomechanical risk evaluation during tool use. Master's Theses. Paper 273.

Terrier, P., Deriaz, O. (2011). Kinematic variability, fractal dynamics and local dynamic stability of treadmill walking. Journal of NeuroEngineering and Rehabilitation, 8:12.

Tupling, S.J., Pierrynowski, M.R. (1987). Use of cardan angles to locate rigid bodies in three dimensional space. Medical and Biological Engineering and Computing. 26, 527-532.

Von Holst, E. (1954). Relation between the central Nervous System and the peripheral organs. Br J Anim Behav 2, 89-94.

Woltring, H.J. (1994). 3-D Attitude representation of human joints: A standardization Proposal. Journal of Biomechanics, 27.12: 1399-1414.

Woodworth, R.S. (1899). Accuracy of voluntary movement. Psychological review, monograph supplement, 3, 13.

Wu, C., Stefanescu, R.A, Martel, D.T. (2015). Listening to another sense: somatosensory integration in the auditory system. Cell Tissue Research, 361, 233-250.

Young, C.R., Jones, G.E., Figueiro, M.G., Soutiere, S.E., Keller, M.W., Richardson, A.M., Lehmann, B.J., Rea, M.S. (2015). At-Sea Trial of 24-h-Based Submarine Watchstanding Schedules with High and Low Correlated Color Temperature Light Sources. J Biol Rhythms., 30, 144-154.